Passivation of III-N materials of the GaN type

Sabria Benrabah

N°d'ordre NNT : 2021LYSE1310

THESE de DOCTORAT DE L'UNIVERSITE DE LYON
opérée au sein de
l'Université Claude Bernard Lyon 1

Ecole Doctorale N° 206
Chimie (Chimie, Procédés, Environnement)

Spécialité de doctorat : Chimie des matériaux semi-conducteurs

Soutenue publiquement le 09/12/2021, par :
Sabria Benrabah

Passivation des matériaux III-N de type GaN

Devant le jury composé de :

Léonard Didier, Professeur des Universités, Université Lyon 1	**Président**
Besland Marie-Paule, Directrice de recherche CNRS	**Rapporteure**
Cordier Yvon, Directeur de recherche CRHEA-CNRS	**Rapporteur**
Robert-Goumet Christine,	**Examinatrice**
Maitre de conférences, Université de Clermont Ferrand	
Yvon Arnaud, Ingénieur, ST Microelectronics	**Examinateur**
Thieuleux Chloé,	**Directrice de thèse**
Directrice de recherche CNRS, Université de Lyon 1	
Charles Matthew, Ingénieur CEA-LETI	**Encadrant**
Bassem Salem, Chargé de recherche, LTM-CNRS	**Encadrant**
Besson Pascal, Ingénieur, ST Microelectronics	**Invité**

Remerciements

Ces travaux n'auraient pas été possible sans les conseils et l'aide de plusieurs personnes, qui d'une manière ou d'une autre, ont contribué et apporté leur aide précieuse à la réalisation de ce projet.

En premier lieu, je tiens à remercier mes encadrants, Matthew Charles et Bassem Salem pour leurs conseils, leurs recommandations et leur extraordinaire patience, ainsi que leurs encouragements au cours de cette thèse. J'adresse également un immense merci à Pascal Besson avec qui j'ai beaucoup appris de sa longue expérience du domaine. Je souhaite également remercier Marie-Christine Roure qui a encadré ma première année de thèse et a su me guider dans mes premiers pas dans ce projet. J'adresse également mes remerciements à Chloé Thieuleux, ma directrice de thèse, qui m'a conseillé tout au long de mes travaux.

En second lieu, je souhaite remercier Marie-Paule Besland ainsi que Yvon Cordier d'avoir accepté d'être les rapporteurs. Je remercie également Christine Robert-Goumet ainsi que Arnaud Yvon qui m'ont fait l'honneur d'examiner ma thèse. J'adresse mes sincères remerciements au Professeur Didier Léonard d'avoir accepté de présider la commission d'examen.

Ces travaux ont été réalisé avec la collaboration de nombreuses personnes que je tiens à remercier pour leur contribution, en particulier Pablo Acosta Alba, Eugénie Martinez, Christophe Lecouvey et Denis Mariolle.

Je remercie également l'équipe du LTM pour leur accueil et leur bonne humeur. Je tiens à remercier tout particulièrement Bernard Pelissier, Maxime Legallais et Sébastien Labau qui m'ont été d'une grande d'aide pour tout ce qui est caractérisations XPS. Ils ont toujours été disponible et à l'écoute de mes nombreuses questions.

Je suis reconnaissante à tous les membres du laboratoire CP2M de Lyon pour leur accueil chaleureux. Je tiens à remercier Vincent Dardun, Isis N'dala Louika et Laurent Veyre pour leur très grande disponibilité qui m'avoir permis de mener à bien mes travaux.

Je tiens également à remercier l'intégralité du SSURF pour leur bienveillance et leur enthousiasme qui m'ont été précieuses au cours de ces trois années. Une pensée particulière aux « précaires » du SSURF que j'ai rencontré au cours de ma thèse, et les bons moments partagés au bureau 418. Je remercie Joël Kanyandekwe pour le temps qu'il m'a accordé pour répondre à mes nombreuses questions autour du GaN, ainsi que pour ses nombreuses discussions autour du thé, des voyages, de la montagne et des Etats-Unis.

Un grand merci à mes amis et tout particulièrement Hicham, Carine et Jérôme qui ont été là dans les moments difficiles.

Merci à Anissa, qui, à plusieurs milliers de kilomètres, m'a apporté un soutien sans failles. Merci à elle d'avoir été une amie si précieuse au cours de ces dernières années.

Enfin, les mots me manquent pour exprimer ma gratitude envers les membres de ma famille. Je remercie mes parents, mon frère et ma sœur qui m'ont toujours soutenu et ont su me redonner le sourire. Je remercie également ma tante Khadra pour son immense soutien ainsi que mes oncles Refas et Habib qui m'ont donné le goût pour la science.

Pour tout cela, merci.

Table of contents

LIST OF ACRONYMS

AFM	Atomic Force Microscopy
ALE	Atomic Layer Etching
B.E	Binding Energy
EDX	Electronic Dispersive X-ray
FOM	Figure Of Merit
FTIR	Fourier Transform Infra-Red
FWHM	Full Width at Half Maximum
HEMT	High Electron Mobility Transistor
HVPE	Hydride Vapor Phase Epitaxy
ICP-RIE	Inductive Coupled Plasma Reactive Ion Etching
LASER	Light Amplification by Stimulated Emission of Radiation
MIS	Metal Insulator Semiconductor
MOCVD	Metal Organic Chemical Vapor Deposition
MOSFET	Metal Oxide Semiconductor Field Effect Transistor
pAR-XPS	parallel Angle Resolved X-ray Photoelectron Spectroscopy
RMS	Root Mean Square
RT	Room Temperature
RTP	Rapid Thermal Processing
SCCM	Standard cubic centimetres per minutes
SEM	Scanning Electron Microscopy
TEM	Transmission Electron Microscopy
XRR	X-ray Diffraction
XRD	X-ray Reflectivity

Contributions on experiments or analyses

AFM (serval months H2SO4:H2O2 treatments)	Denis Mariolle	CEA-LETI
AFM (RTP initial works on as-grown GaN)	Thomas Kaltsounis	CEA-LETI
C-V measurements	Pedro Fernandes Paes Pinto Rocha	CEA-LETI
Dry-etching steps on wafers	Simon Ruel	CEA-LETI
EDX	Gauthier Lefèvre	LTM
H_3PO_4 wet treatments	Pascal Besson	CEA-LETI
LASER anneals	Pablo Acosta Alba	CEA-LETI
RTP	Bassem Salem	LTM
SEM on wafers	Pablo Acosta Alba	CEA-LETI
SEM on powders	Laurent Veyre	CP2M
TEM/EDX	David Cooper	CEA-LETI
XPS on powders	Eugénie Martinez	CEA-LETI
XRD on powders	Nicolas Vaxelaire	CEA-LETI
XRR	Matthieu Lafossas Matthew Charles	CEA LETI

General introduction

To meet demands for the development of new products in the fields of power electronic convertors for electric cars, solar panels, wind turbines, and new LED-based lightening technologies or RF components, research has focused on direct wide bandgap materials, including Gallium Nitride (GaN). GaN has attracted significant interest due to its exceptional properties for next-generation power electronic devices. With a high saturation velocity and a high operating voltage, GaN-based devices can operate at high frequency and with excellent efficiency, making GaN a material of choice in power applications.

However, the development of III-N materials is still immature, especially in terms of quality control of the various interfaces within the devices. The presence of high density of interfaces states can be the cause of device malfunctions. Therefore, understanding and controlling the surface of GaN is a challenge for possible future industrial integration. Today, there is no suitable and effective standard surface preparation of GaN.

In order to investigate this problem, this PhD project was carried out in a collaboration between CEA-LETI (Grenoble), LTM (Grenoble) and CP2M laboratories (Catalysis, Polymerisation, Process and Materials, Lyon). The main objectives of this project are, first, to understand the surface chemistry following various surface preparations, and second, to set up the configuration of surface bonds. Therefore, this PhD project focused on the preparation and characterisation of the extreme surface of GaN after various chemical and physical treatments.

The first chapter of this work is divided into two major parts. The first deals with GaN growth and general details of GaN properties. Then, a typical HEMT structure is presented in order to illustrate where the GaN surface treatments may influence the electrical properties such as current leakage, for instance. The second part is a non-exhaustive review of several investigations based on wet treatments performed on GaN, mainly acids or bases.

The second chapter presents the characterisation techniques used during this PhD project, mainly focused on surface characterisation techniques looking at surface chemistry and surface morphology. The surface chemistry was investigated *via* parallel Angle Resolved X-ray Photoelectron Spectroscopy (pAR-XPS) for which detailed explanations are given. Then Atomic Force Microscopy (AFM) was used for surface morphology investigations. Other techniques such as Fourier Transform Infra Red (FTIR), to determine the chemical composition of GaN, X-ray Reflectivity (XRR), to measure thin films on a substrate and X-ray Diffraction

(XRD) to determine structural information are also briefly presented. Finally, the Current-Voltage (C-V) measurement method, used to evaluate the electrical properties is described.

The third chapter focuses on an experimental systematic review. The first part shows a systematic study of the impact of wet chemical etchants encountered in the microelectronic industry, performed on our GaN on silicon wafers. The pAR-XPS analyses, which give the atomic percentage of oxygen and an estimation of the equivalent oxide thickness after each treatment, are presented. The second part of this chapter presents the systematic study, in the same conditions as conducted on GaN wafers, on GaN powders under ambient and inert atmosphere.

In the fourth chapter, we investigate the destabilisation of the Ga-N surface bonds *via* dry techniques. This study focuses on as-grown and dry-etched GaN wafers. Indeed, as the as-grown surface gives the basis of the study and comparisons with literature precedents, using dry-etched surface allows the study to be performed in conditions closer to those found during transistor fabrication. In a first section, an investigation on the influence of the number of shots under inert and oxidative atmosphere on the surface chemistry and morphology after nanosecond LASER anneals is presented. Then, with the idea of developing "digital etching", investigations on Rapid Thermal Processing (RTP) anneals are presented in a second section. Digital etching is a two-step technique that involves repeated loops of surface oxidation and etching to accurately control the etch thickness. For this study, this technique is investigated to obtain an atomically clean, and ideally passivated surface, *via* the formation of Ga-S (or another atom) surface bonds.

In the fifth chapter, we investigate the destabilisation of the Ga-N surface bonds of GaN wafers *via* wet treatments. Two high boiling point etchants are presented: H_2SO_4:H_2O_2 mixture and H_3PO_4. The first part focuses on the impact of repeated immersions of GaN wafers into H_2SO_4:H_2O_2 solutions on the surface morphology and chemistry, as well as XRR measurements to investigate the etchant properties. The evolution of the surface morphology over time is also presented. In a second part, the influence of H_3PO_4 wet treatment on as-grown GaN and dry-etched GaN is shown. The impact of the treatment time on the surface chemistry and morphology are presented, and etched thickness is assessed by XRR. Finally, electrical characterisations of capacitors created using this wet treatment followed by dielectric deposition are given. The relationship between surface chemistry, surface morphology and the electrical measurement is discussed.

We finish the manuscript with a conclusion section highlighting key results and perspectives for future work.

Chapter I - State of the art and context

I.1. GaN in power electronics

I.1.1 Overview

III-N or III-nitrides refer to the set of compound semiconductors composed of InGaN, GaN and AlGaN with application in many fields. The most established applications for III-nitrides are optoelectronics with the emergence of GaN-based Light Emitting Diodes (LED) in the 1990s. Novel devices in power and RF electronics have also gained major attention during the last decade and other applications such as spintronic, sensors, photovoltaic panels [1] and nuclear detections [2] are under extensive research as well.

I.1.2 GaN in power electronics

In today's societies, electronic devices are fully included in our everyday life. The history of electronics would be hard to imagine without the development of silicon materials. Power electronic is the technology that refers principally to energy conversion. The main components in this field are diodes and transistors. Currently the semiconductor market for power electronics is dominated by silicon-based devices.

Whether it is for computers, domestic appliances, transportation or industry, the need of energy is constantly increasing and silicon has reached its limits. Furthermore, facing our environmental issues, the demand for electric energy is becoming critical. This high demand has led researchers to consider wide bandgap materials for improved conversion efficiency.

In particular, Silicon Carbide (SiC) and III-N materials have gained a significant interest. These wide bandgap materials have remarkable properties that surpass those of silicon. For example, GaN MOSFET can operate at a wider temperature range, which tends to reduce leakage current and to reduce power consumption [3]. While Si-based devices degrade at temperature above 150°C, GaN MOSFET could reach 250°C [4] . Another interesting property due to its bandgap feature is the higher power per unit size, which allows the production of smaller devices and ease of manufacturing. These advantages should in turn result in more efficient energy conversion and lower production costs.

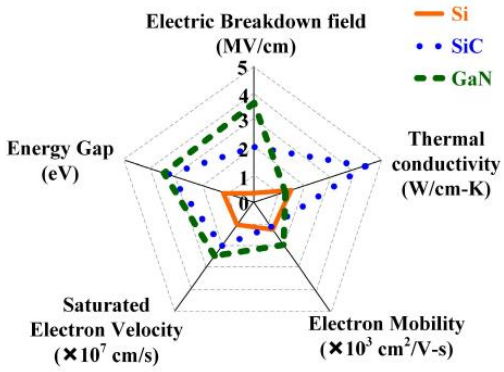

Figure 1. Comparison of Si, SiC and GaN properties [5]

Figure 1 compares Si, SiC and GaN properties for power applications. Even though SiC has remarkable features with wider range temperatures, GaN presents superior properties making it one of the most promising candidates. Indeed, as GaN has a higher saturation velocity and a higher electron mobility it gives to the material high frequency. Moreover, its higher electric breakdown field and its higher band gap allow higher operating voltage, and higher efficiency (Figure 1). Furthermore, SiC devices are exclusively built on native substrates, which are expensive, while high performance GaN devices can be fabricated on non-native substrates such as silicon or sapphire. In particular, GaN grown on Si substrate allows a significant cost reduction by enabling the use of 200 mm diameter wafers versus typically 150 mm diameter for SiC wafers, in addition to lower substrate cost.

A common method to benchmark different semiconductor materials for power electronic applications are Figure Of Merits (FOM). This parameter indicates a certain value in which the higher the value, the better the performances. One of the first FOM reported in the literature is the Johnson's Figure Of Merits [6] and is defined as follows :

$$\mathrm{JFOM} = \left(\frac{E_c V_{sat}}{2\pi}\right) \qquad \text{I-1}$$

Where:

- E_c is the breakdown electric field,
- V_{sat} is the saturation electron velocity.

JFOM defines the suitability of materials for high power at high frequency applications. According to equation I.1 and knowing that wide bandgap materials have high breakdown electric field, in hetero-structure electronic devices, these materials give higher velocity saturation, therefore they are suitable for high power at high frequency applications.

Another interesting FOM is the Baliga FOM (BFOM) which defines the ultimate performance of field effect transistors (FET) at low frequency power switching application. At low frequency, conduction losses are dominant. In other words, BFOM defines the parameter to minimize the conduction losses in FETs for a given surface area [7]. BFOM can be written as follows:

$$\mathrm{BFOM} = \epsilon_r \, \mu E_c^3 \qquad \text{I-2}$$

Where:

- ϵ_r is the dielectric constant,
- μ is the mobility of the carriers,
- E_c is the critical electric field.

In the case of high frequency applications, switching losses are dominant. Baliga High Frequency FOM (BHFFOM) takes into account these losses [7]:

$$\mathrm{BHFFOM} = \frac{\mu E_c^2 V_G^{0.5}}{2 V_B^{1.5}} \qquad \text{I-3}$$

Where:

- V_G is the gate drive voltage,
- V_B is the breakdown voltage required.

From equation. I.3 it can thus be deduced that devices with extremely high breakdown voltage are typically not suitable for high frequency operations. More specific FOM, such as Keyes FOM (KFOM), have also been introduced. KFOM takes into account thermal conductivity and thus highlights thermal limitations to transistors' switching behaviour in integrated circuits [7].

$$\mathrm{KFOM} = \lambda \left(\frac{c V_{sat}}{4\pi\epsilon_r} \right)^{0.5} \qquad \text{I-4}$$

Where:

- λ is the thermal conductivity,
- c is the speed of light.

Table 1 summarizes the FOM values for some of the competitive semiconductor materials candidates in power electronics. These values are referred to those of Silicon.

Figure Of Merit	Si	GaN	GaAs	SiC
JFOM	1	270-480	2	324-400
BFOM	1	17-34	13	6-12
BHFFOM	1	86-172	10	57-76
KFOM	1	1.4	0.4	4.5-4.8

Table 1.Figure of Merit of wide bandgap semiconductor materials in power electronics [1]

It can be seen that GaN is an excellent candidate for high power and high frequency applications. Although SiC presents a better KFOM than GaN, its saturation velocity and on-resistance limit its use in high frequency power applications.

I.1.2.1. GaN in other applications: optoelectronics

Another field where GaN is commonly used is that of optoelectronics. This refers to electronic devices and systems that generate, detect and control light. Although the light emitting diode (LED) is a 100 years old technology, there was a lack of reliable, high performance blue light emitting devices until the early 90's. The first GaN-based UV and blue spectral band LED was reported in 1992 by Isamu Akasaki and Hiroshi Amano with p-n homo-junction LED [1]. From that moment, GaN has opened the way to white LED. Unlike conventional light sources, GaN-based white LEDs can exhibit efficiency of up to 300 lm/W against 15-100 lm/W for conventional light sources. The high efficiency of GaN-based white LEDs is not their only remarkable property as they also show extremely long life, a quick response and above all, they are non-toxic (mercury-phosphorus- and arsenide-free).

Here, we described only two fields of applications for GaN-based materials even if they start to attract attention for applications in spintronics [8].

I.2. GaN properties

I.2.1 Crystalline structure

III-N materials can be grown with various crystalline structures: zinc blende, rock salt, and wurtzite. The Rock salt structure possesses two cubic sub-lattices. The zinc blende

configuration is obtained in some circumstances on cubic substrates such as SiC, Si, or GaAs along the [011] plane. Zinc blende and wurtzite structures are shown in Figure 2. In the zinc blende crystalline structure, (Figure 2(a)), each cubic cell has four atoms of group III and four N atoms. The wurtzite crystalline structure (Figure 2(b)) contains two intercepting hexagonal closed packed sub-lattices. Each hexagonal unit cell includes six atoms of each type and each III atoms is coordinated by four N atoms. In the same way, each N atom is surrounded by four III atoms.

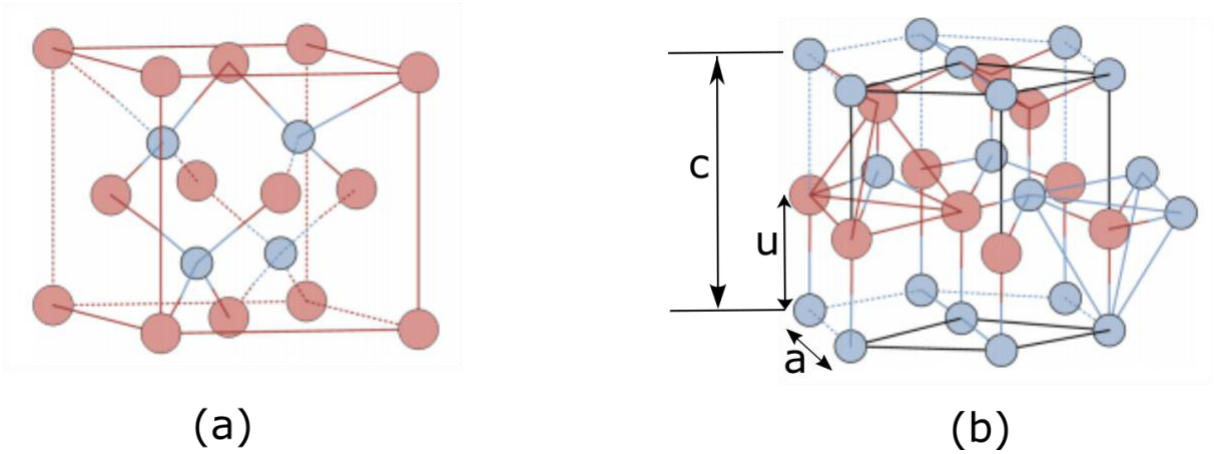

Figure 2. Crystalline structure of (a) zinc-blende and (b) wurtzite of III-N materials [9]

The wurtzite crystalline structure is defined by two lattice constants: a and c. The side length of the hexagonal base corresponds to a, and c refers to the height of the cell. A third lattice parameter, defined by u=1/c, characterizes the anion-cation bond length along the c-axis. Under ambient conditions, wurtzite is the most thermodynamically stable crystalline structure and therefore the most common configuration. Thus, further descriptions will only concern the wurtzite crystalline structure.

A close look of the unit cell reveals that the structure is asymmetric along the c-axis. Indeed, the [0001] and [000$\bar{1}$] directions are different depending on whether the tetrahedrons base is composed of gallium or nitrogen atoms. This indicates anisotropic crystals and is also referred to as polarity. Therefore, we talk about Ga polarity [0001] or N polarity [000$\bar{1}$], and sometimes Ga-face or N-face layers. It should be noted that Ga-face and N-face refer only to the polarity, and do not refer to the final atoms on the surface of the layers. In addition to the

polar planes, i.e. (0001), also named c-plane, and the $(000\bar{1})$ plane, there are two types of planes: semi-polar and non-polar.

In the next paragraph, we will describe some of the effects of these different polarisations.

I.2.2 Spontaneous and piezoelectric polarisations

I.2.2.1. Spontaneous polarisation

Without any exterior mechanical constraints, the GaN crystalline structure presents a spontaneous polarisation. In order to describe this phenomenon, it is necessary to take into account the influence of some parameters and properties of the crystalline structure. First, let consider the length bond between anions and cations, noted u, and the lattice parameter ratio c/a. In an ideal wurtzite structure, each one equals:

$$u = {}^{3}/_{8} = 0.375 \quad \text{I-5}$$

$${}^{c}/_{a} = \sqrt{{}^{8}/_{3}} = 1.633 \quad \text{I-6}$$

Table 2 summarizes these parameters and the spontaneous polarisation P_{sp} value for GaN, AlN and InN. We can see that when compared with the ideal wurtzite structure, the values differ from GaN and InN parameters values and even more for AlN, which results into a more pronounced polarisation.

III-N	c/a	u	P_{sp} ($C.m^{-2}$)
GaN	1.634	0.376	-0.029
AlN	1.619	0.380	-0.081
InN	1.627	0.377	-0.032

Table 2. c/a, u, and P_{sp} values for GaN, AlN, and InN

As mentioned previously, the GaN wurtzite structure is asymmetric along the c-axis. The non-coincident barycentre gives GaN its polarisation effects. Since the tetrahedrons within the crystal are irregular, the ionic bond length strongly varies. The spontaneous polarisation is thus composed of non-symmetric pairs of Ga-N which induce a larger concentration of outer

electron shells near N atoms. Consequently, each Ga-N pair contributes to a dipole moment. Considering the whole GaN structure, the result is a succession of dipoles oriented along the (0001) axis, which corresponds to the growth orientation and an electric field is present and oriented in the opposite direction (Figure 3).

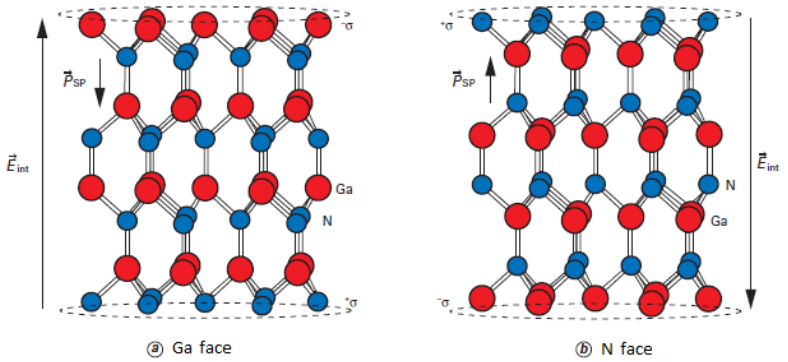

Figure 3. Spontaneous polarisation and charge distribution within the wurtzite GaN structure [10]

Depending to the polarity, i.e. Ga face or N face, the spontaneous polarisation is different and can be explained as follows. In the Ga-face case, the Ga atoms are surrounded by four N atoms, three of them being within the same crystallographic plane that is perpendicular to the c-axis (Figure 4).

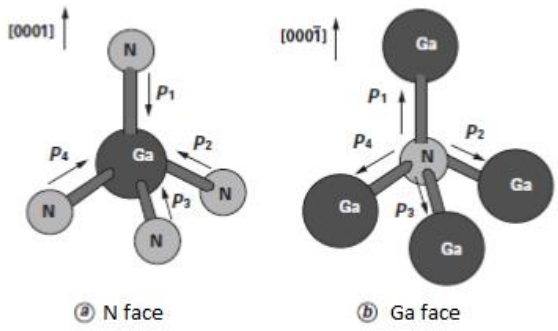

Figure 4. Dipole moment distribution [10]

Therefore, the resultant vector is equal to:

$$\overrightarrow{P_R} = \overrightarrow{P_2} + \overrightarrow{P_3} + \overrightarrow{P_4} \qquad \text{I-7}$$

The fourth N atoms is within the c-axis and its dipole moment is oriented in the opposite direction of the resulting moment. Therefore, within a relaxed structure, this results in a spontaneous polarisation $\overrightarrow{P_{sp}}$ which is oriented along the c-axis:

$$\left|\overrightarrow{P_1}\right| > \left|\overrightarrow{P_R}\right| \quad \text{I-8}$$

$$\left|\overrightarrow{P_{SP}}\right| = \left|\overrightarrow{P_1}\right| - \left|\overrightarrow{P_R}\right| \quad \text{I-9}$$

For N-faced GaN, the eq. I.9 becomes:

$$\left|\overrightarrow{P_{SP}}\right| = \left|\overrightarrow{P_R}\right| - \left|\overrightarrow{P_1}\right| \quad \text{I-10}$$

Wurtzite GaN presents on both side, Ga-face and N-face, the same density of fixed charges but with opposite sign. The wurtzite GaN is by definition naturally polarised along the c-axis without the application of external excitation.

I.2.2.2. Piezoelectric polarisation

Piezoelectricity is the ability of a material to produce a dipole electrical charge as a result of a mechanical stress applied to it. The existence of an internal electric dipole created by the separation of the centre of gravity of the positive charges from the negative charges under an external mechanical constraint causes a direct polarisation piezoelectric effect. Conversely, the application of an external electric field causes a mechanical deformation of the material which creates a polarisation called indirect polarisation effect. These phenomena are reversible. In the case of GaN semiconductors, the mechanical constraints result typically from the epitaxial growth of layers such as between GaN and AlGaN which have a lattice mismatch. Depending on whether the previous layer has larger or smaller lattice constant, the material will be under tension or compression. The piezoelectric polarisation P_{sp} can be written as:

$$P_{sp} = 2\left(\frac{a - a_0}{a_0}\right)\left(e_{31} - e_{33}\frac{c_{13}}{c_{33}}\right) \quad \text{I-11}$$

Where:

- a_0 is the lattice parameter without mechanical constraints,
- a is the lattice constant of the material under applied stress,
- e_{31} and e_{33} are piezoelectric constants,

- c_{31} and c_{33} are elastic constants.

To summarise, GaN is a wide gap material with spontaneous polarisation and piezoelectric polarisation when mechanical stress is applied. Combined with great thermal stability, its properties make it suitable for high voltage and high temperature applications.

I.3. AlGaN/GaN HEMT: High Electron Mobility Transistor

I.3.1 Polarisation effect in the hetero-structure

HEMT structure is based on two layers with different bandgaps and polarisation fields grown on top of one another. Consequently, a discontinuity in the polarisation field is created resulting in a potential well, as shown in Figure 5.

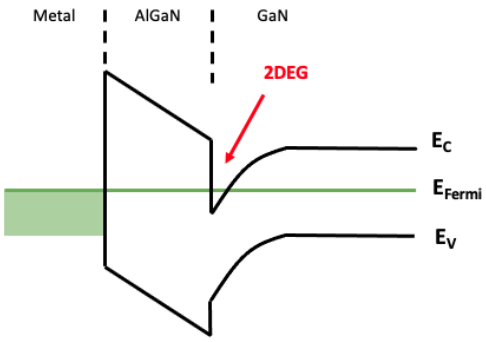

Figure 5. AlGaN/GaN band diagram

This well results in a high charge density and increases the electron mobility leading to the formation of a two-dimensional electron gas (2DEG). In GaN-based transistors, a hetero-structure is grown to form the 2DEG, where the material with the larger bandgap is usually AlGaN, and represents the barrier. The underlying GaN constitutes the channel where the 2DEG is formed. Due to the electronic affinity difference between the two materials, AlGaN electrons have a lower potential energy than GaN electrons. Thus, the electrons will migrate from AlGaN to GaN which induces a depletion zone at the AlGaN's side and an accumulation of electrons at the AlGaN/GaN interface until thermodynamic equilibrium is reached. Once in equilibrium, a discontinuity in the conduction band appears at the AlGaN/GaN interface creating a potential well on the GaN side (Figure 5).

There is no doping in the barrier layer (AlGaN) since both spontaneous and piezoelectric polarisations induce an electric field to create the 2DEG. The electron concentration can reach very high level, up to $2x10^{13}$ cm^{-2}.

I.3.2 HEMT: basic structure

From the 2DEG created in the AlGaN/GaN hetero-structure, HEMT devices are typically fabricated with three metallic elements: two Ohmic contacts and one gate (Figure 6). The two Ohmic contacts are the source and the drain and are located on each side of the transistor allowing the connection with the electric channel. Electrons leave the source, and get to the drain, through the channel. The gate is located between the source and the drain and allows current modulation.

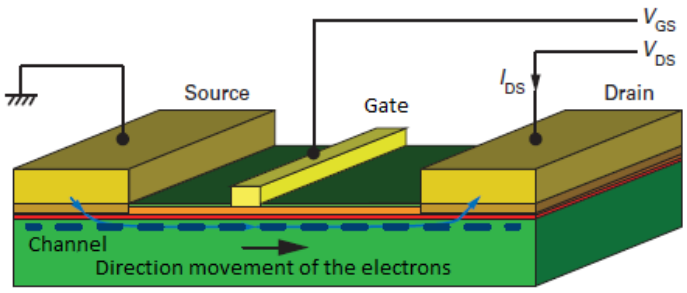

Figure 6. HEMT typical structure [11]

The formation of the contact requires dry etching process, typically high energetic plasma treatments that induce considerable surface damages. The removal of such damages is usually performed *via* wet etching. The impact of the wet etching treatments on GaN will be detailed in section I.5.

I.4. Elaboration

As mentioned above, GaN based semiconductors are commonly grown by hetero-epitaxy due to the very high cost of bulk materials. Indeed, bulk GaN is very difficult to obtain. To synthetize bulk, single crystal of GaN, high melting temperature above 2200°C and high pressure of about 6 GPa are necessary [12]. Considering those extreme conditions and the small sized wafer obtained it is hard to consider industrial applications. An alternative is to start the growth from non-native substrates and grow very thick layers of GaN that have high quality and support themselves. These substrates are referred to as “freestanding GaN” and they are grown onto wafers up to 100 mm in diameter. However, this process is long, expensive, and

poorly optimised, and all the widespread applications of GaN-based devices are grown by hetero-epitaxy in large applications. Hetero-epitaxy consists of growing GaN on a foreign substrate. Several methods exist such as, Molecular Beam Epitaxy (MBE), or Metal Organic Chemical Vapor Deposition (MOCVD). In addition, several substrates have been studied and are commercialized for GaN, in particular sapphire for LED production.

I.4.1 Substrate choices

In the absence of GaN bulk substrates, researchers have turned to the possibility of growing GaN on foreign substrates. The substrate is used as the basis of the growth process. For HEMT manufacturing, substrates must fulfil specific criteria such as good crystalline quality, large diameter, cheapness and a good thermal conductivity to avoid self-heating of the device. Furthermore, the substrate has to be stable toward the high growth temperature. Other physical parameters have to be considered such as the differences in lattice parameters and thermal dilatation coefficients. HEMTs are currently manufactured on Silicon Carbide (SiC), typically for high frequency devices, where the high thermal conductivity and excellent electrical insulating properties are critical, and Silicon (111) for higher power and lower frequency devices. The following table summarises the physical properties of the main substrates encountered in the literature.

	Lattice parameter a (Å)	Lattice mismatch with GaN (%)	Thermal conductivity κ ($W.cm^{-1}.K^{-1}$)	Thermal dilatation coefficient $\frac{\Delta a}{a}$ ($x10^{-6}.K^{-1}$)
GaN	3.19	0	1.3	5.6
6H-SiC	3.08	-3.4	4.9	4.2
Sapphire	2.75	-16	0.4	7.5
Si (111)	3.84	+17	1.5	3.6

Table 3. Physical properties of different substrates

The first good quality GaN grown on sapphire was fabricated in 1986 by Amano *et al.* [13] and the first GaN based blue LEDs were grown on sapphire substrates. Due to its low thermal conductivity, GaN/Sapphire is not an appropriate deal for high frequency power applications, but this kind of hetero-epitaxy is extremely common for optoelectronic devices such as LEDs where the transparency of sapphire can also help for the fabrication of devices.

In contrast, SiC has many advantages as a substrate. Indeed, it exhibits a very low lattice mismatch with respect to GaN and consequently the dislocation density is relatively low.

Furthermore, it has an excellent thermal conductivity and can be produced with low electrical conductivity which makes it perfect for high frequency power application. However, its price remains very high (1400 euros per 100 mm [10]).

Finally, Si (111) is one of the most attractive substrates for GaN based devices for power applications. It offers the possibility of obtaining a good quality material and has interesting physical properties. Despite its very large difference of thermal dilatation coefficient (about 54%) and a 17% lattice mismatch with GaN, Si benefits from a high technological maturity. However, these problems have been overcome using specific growth strategies for power HEMT devices up to 650V, and so from an industrial point of view, Si is a good candidate since wafers can reach 300 mm and are produced with low prices (about 60 euros for a 200 mm wafer).

I.4.2 Epitaxy

Epitaxy refers to the deposition of thin single layers onto a substrate while maintaining a crystalline order in these layers imposed by the substrate. Epitaxy is also a process used for growing stacks of layers one up the other, while keeping crystalline structure.

Historically, the first GaN growth was small crystals synthesized by reacting gallium in a flow of ammonia at the University of Chicago in 1932 [14]. At that time, the researchers noticed GaN's well-known inertness and thermal stability. They also observed that GaN sublimates at 800°C in dihydrogen (H_2). In the 1960's and 1970's, the first GaN synthesized by Hydride Vapor Phase Epitaxy (HVPE) was reported by Ejder *et al.*, using NH_3 and metallic gallium [15].

In the late 1960's, Manasevit *et al.* developed the first Metal Organic Chemical Vapor Deposition (MOCVD) growth of GaN using Trimethylgallium (TMGa) at 950°C – 975°C on a c-plane sapphire [16]. The 6µm thick GaN was obtained and found to be resistant to acids and bases but could be destroyed under H_2 at 1050°C confirming earlier observations made by Johnson in 1932 [14]. Unfortunately, the reagent impurities, the high density of defects and the roughness of the resulting GaN compromised the usefulness of this final material. One of the major breakthroughs in GaN technology was the introduction of nucleation layers. Until that time, GaN grown directly on sapphire presented hexagonal structures at their surfaces. The use of AlN as a nucleation layer was introduced by Amano *et al*. The AlN growth conditions at a temperature around 1000°C allowed the formation of an amorphous layer resulting in a smooth film of GaN [13]. This growth technique was then used by Nakamura *et al*. in 1991 [17]. They

used a GaN buffer layer grown at a lower temperature, between 450°C – 600°C, allowing a smooth surface as shown in Figure 7.

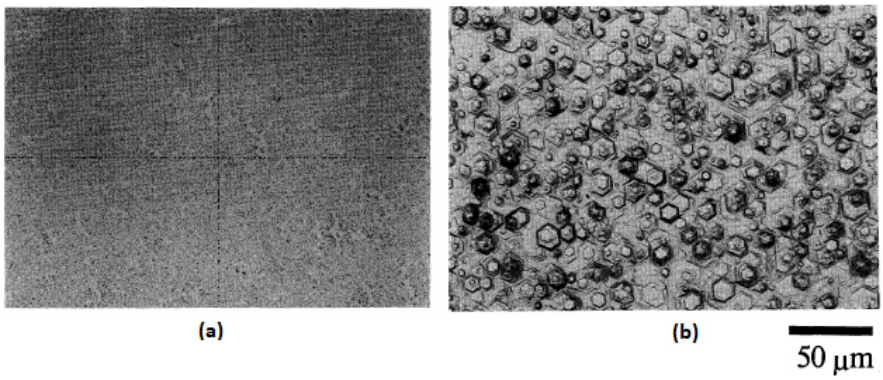

Figure 7. Interference micrographs of surface of GaN films grown on sapphire (a) with (b) without GaN buffer layer at low temperature. Micrographs reproduced from reference [17]

MOCVD, also known as MOVPE (Metal Organic Vapor Phase Epitaxy) is a specific CVD technique that uses metal organic molecules as precursors. This technique produces thin layers of good quality and is the most commonly used method in industry. The principle of the chemical vapor deposition is to deposit a solid layer from gaseous reagents on the substrate's surface. This technique is schematized in Figure 8 and can be broken down into seven steps.

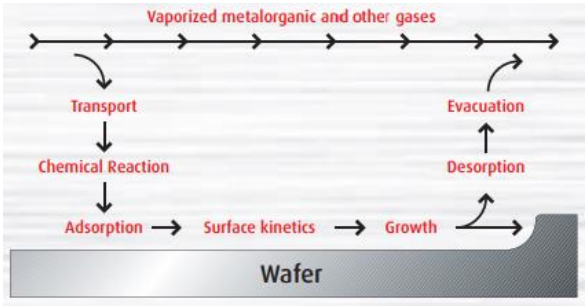

Figure 8. Principle of MOCVD (scheme from AIXTRON website)

The first step is the mass transport of the reactants in the growth chamber by a neutral gas carrier toward the surface of the substrate. Then, chemical reactions occur near the surface as well as the decomposition of the gaseous precursors. Third, the products are adsorbed onto the surface. Surface diffusion takes place followed by the formation of grain that initiates the growth. Then, by-products are taken away from the surface and finally evacuated from the

growth chamber. In the case of the MOCVD growth of GaN, the most common precursors are Triethylgallium (TEGa) or Trimethylgallium (TMGa), and ammonia as source of N.

In GaN-based HEMT devices, a typical stack of layers is shown in Figure 9. Each layer has a specific contribution.

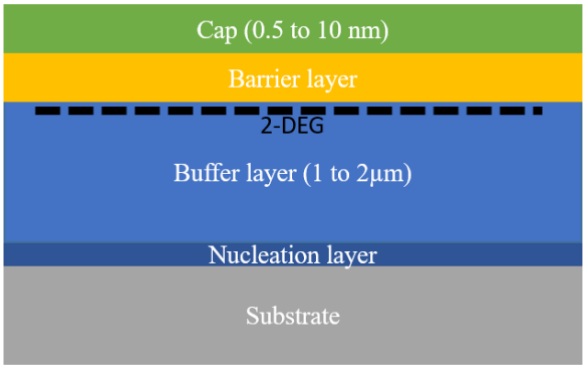

Figure 9. Typical layer stack for GaN transistors

As stated earlier, GaN is usually grown on a substrate which is often another material, like Si (111) for example. To initiate the growth of GaN on a foreign substrate, a nucleation layer is deposited above the latter. The nucleation layer is generally a layer of AlN which protects the silicon from gallium, which reacts strongly together, and provides a layer with a smaller lattice parameter than GaN. Next, different AlGaN layers and the GaN buffer layer are grown, adding compressive strain into the layers during the growth to compensate for the difference in thermal expansion during cooling. The final layer before the barrier is a high quality GaN layer with very low intrinsic doping, ensuring a high performance 2DEG formed below the barrier layer. A schematic of the growth of GaN on silicon is shown in Figure 10.

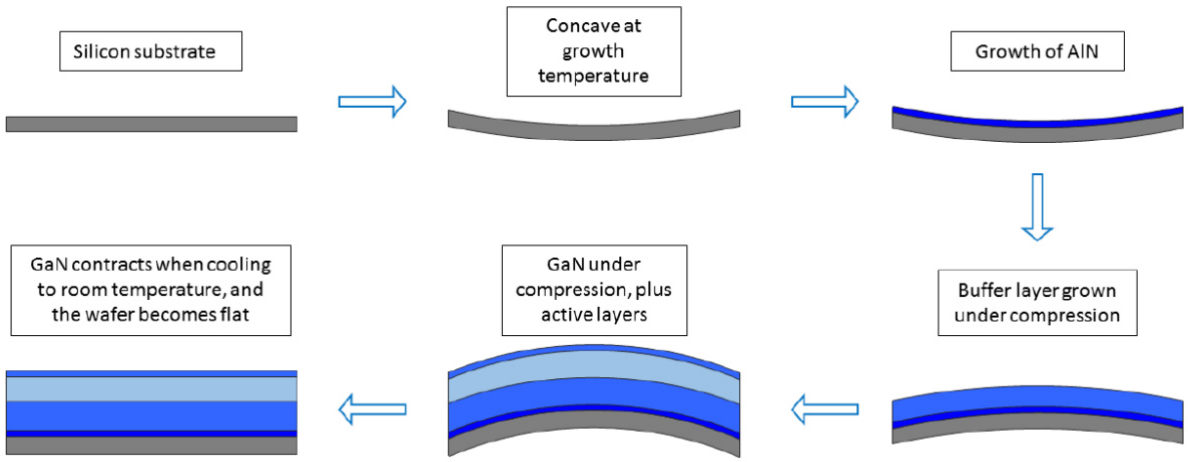

Figure 10. Schematic of GaN on silicon growth as reported in reference [18]

The barrier layer is typically formed of AlGaN and finally a cap layer is grown on top to prevent the oxidation of the barrier layer and to protect the AlGaN layer during cooling down to room temperature after growth. This capping layer is made of GaN or SiN. Such stacking layers lead to normally-ON transistors, meaning that when no voltage is applied to the gate, electrons can easily flow from the source to the drain. This configuration is undesirable for commercial power switch applications due to safety concerns, and due to incompatibility with current modules based on silicon MOS devices. Therefore, blocking the 2DEG is necessary to obtain a normally-OFF device. To obtain such properties, several post-epitaxy approaches have been investigated such as a dry etching-based recess-gate, a p-type gate, and a fluorine-based ion implantation gate. The gate-recess consists of etching the barrier layer and approaching the gate closer to the barrier/GaN interface. This method leads to a thinner barrier layer or to the removal of this barrier layer, which induces a break of the 2DEG.

The gate recess is usually performed with dry etching processes, typically using plasma. Several etching technologies are reported for plasma creation. The plasma can be yielded by either physical or chemical methods, and sometimes both, such as induced coupled plasma reactive ion etching (ICP-RIE). Such treatment has been reported to seriously damage the surface. Indeed, some studies report that, ion-induced damage affects the electrical properties [19] through the introduction of defects, disorders such as non-stoichiometric surfaces [20, 21], and oxygen contamination [22]. Thus the carrier mobility and conductivity [23] are modified and, in addition, trapping can affect the dynamic behaviour of the devices. Furthermore, dry etching processes are used at other steps of the device fabrication, such as the contact formation for example, thus multiplying their negative effects.

I.5. Chemistry of wet etching

Whether for optoelectronic or high power applications, cleaning and etching processes play a critical role in improving device efficiency for GaN base devices. In MOSFETs, the presence of contaminants such as carbon or oxygen may induce surface traps which affect the breakdown voltage and reduce the overall efficiency of the final devices. Wet etching processes are usually performed between two dry etching processes during the transistor fabrication. For example, a wet treatment is often performed after dry etching a part of the passivation layer, before the deposition of the contact or the gate. Several types of plasma etching processes have been investigated during the last few years, but as stated in the previous paragraph, plasmas generate ion-induced damages and it is often difficult to obtain smooth etch sidewalls.

The aim of wet treatment steps is thus twofold. First, the removal of all contaminants that may have been introduced after a dry etching step, like oxides, particles or carbon. Second, wet treatments can correct the surface defects induced by a dry etching process which generally leaves a high roughness and point defects such as vacancies. Consequently, wet etching is an important process that complements dry etching techniques. Indeed, wet etching should be able to repair surface damage from other processes, removing defects and leading to smoother surfaces. In addition, it is inexpensive and easy to implement in electronics fabs.

In addition to the different steps that GaN-based devices go through during fabrication, we should also note that GaN on silicon typically presents a small quantity of oxide on the surface post-epitaxy. This native oxide is of poor quality and can compromise the efficiency of the transistors. Thus, the removal of this native oxide is required. However, GaN is known for its low reactivity towards etchants [24]. Indeed, due to its wide bandgap and the high bond strength between Ga and N in the wurtzite configuration (about 8,92 eV/atoms [25]), GaN is a difficult material to etch, especially the common (0001) facet. Unlike other semiconductors like GaAs, GaN remains inert when dipped in concentrated acids or bases. Even now, there is no efficient wet etchants for (0001) planes, i.e. no chemical species were found to be able to etch GaN surfaces at a reasonable rate.

I.5.1 Wet etching mechanism

Wet etching refers to the use of liquid chemicals. The goal of wet etching in the semiconductor industry is to dissolve a target material. During the early days of semiconductor

processing, wet etching was the only way to remove a layer from a material. Water is the most commonly used solvent in the microelectronic field with advantage that most semiconductors are unaffected or dissolved at a very slow rate in water. The etching mechanism can be divided into two distinct steps. The first one is the activation of the surface layer. This step includes the diffusion of the etchant species toward the surface, and their adsorption at active sites. Then, the surface layer reacts with the chemical species present in the solution. The second step is the dissolution of the previously activated surface layer into the solution. Indeed, the activated layer reacts with the etchant species and is transformed into a product that is readily dissolved into water and diffuses away from the surface. Usually, for metals, oxidizing agents will oxidise the metal into a corresponding cation, as in the equation:

$$M + H^+ \rightarrow M^+ + H \qquad \text{I-12}$$

The dissolution step depends on various factors such as the solubility, the diffusion coefficient of the etched material, and the solvating components.

As immersion was the only technique used for wet etching process in this PhD project, we will focus on this method in the following paragraphs.

The sample to be etched is immersed in a quartz vessel for a chosen period of time and at a determined temperature. Many cleaning procedures already exist for device fabrication in the industry, and during the fabrication process of a transistor, the cleaning step generally occurs after the dry etching processes. For example, wet cleaning takes place after the removal of the photoresist in order to remove any residue.

Cleaning processes also occur before and after the gate formation and Ohmic contact deposition. Many studies on GaN cleaning procedures for devices fabrication have been performed. However, there is currently no standard method for the surface preparation of GaN.

In the next paragraph, we will discuss the studies made on GaN so far and their impact on the surface chemistry and morphology, and electric properties.

I.5.2 Conventional wet etching

Depending on the purpose of wet etching, specific chemicals are required, and wet etching may be used to remove contaminants such as native oxide, organic and inorganic compounds, particles as well as damaged layers from prior dry etching processes.

GaN and other III-nitrides are known for their strong chemical stability, and this inertness can be illustrated by their resistance to wet etching. Various chemicals are reported in the literature. For the removal of native oxide, the chemical etchants reported for III-N substrates are aqueous acids, bases and molten salts solutions, as described below.

I.5.2.1. Bases

Potassium hydroxide (KOH) is a basic solution reported to be efficient for oxide removal of GaN [26]. KOH is frequently used as a molten salt [27] and the mechanism of KOH etching on GaN has been widely commented. The efficiency of KOH strongly depends on the polarity of GaN. Indeed, several studies show that N-oriented GaN is more easily attacked by hydroxyl anions OH^- and the etching rate is higher for the N-polar surface than for the Ga-polar surface. A mechanism explaining this difference has been proposed by Li *et al.* [28] which can be divided into two steps for the N-polar surface. The first step is the attack of the OH^- ions, which initiate the formation of oxide at the surface. At this stage, KOH acts as a catalyst. The second step is the dissolution of the oxide by KOH. On Ga-polar surfaces, even before being exposed to the KOH solution, the first layer of Ga is easily accessible to hydroxide ions in solution. The oxide formed is subsequently dissolved into the solution exposing a nitrogen-terminated layer. Because of the repulsion between OH^- ions and the three occupied dangling bonds of N, the reaction is stopped.

Aqueous sodium hydroxide (NaOH) solution has also been investigated. This has been reported to slowly dissolve GaN surface at room temperature [24, 26] or upon heating at 100°C [29]. Zhou *et al.* found features suggesting etching effects and Scanning Tunnelling Microscopy (STM) images showed that concentrated NaOH at 90°C completely removed the terraces structures, and enabled the creation of surface trenches [30]. It is suggested that NaOH etches preferentially at defect points [29, 30], implying that the etching is very hard on pure (0002) surfaces.

Among the basic species reported for GaN wet etching, NH_4OH is generally used for oxide removal. The most thermodynamically stable gallium oxide is Gallium (III) oxide or Ga_2O_3 which is known to be dissolved in alkali solutions [31]. For example, XPS analyses of GaN after NH_4OH treatment reveal a decrease of the oxygen at the surface [31–34]. However, most authors report that NH_4OH is ineffective on gallium oxide if used at room temperature.

Finally, ammonium sulphide $(NH_4)_2S$ is a commonly investigated basic solution. On GaAs substrates, $(NH_4)_2S$ has shown to be an excellent oxide remover as well as a passivating

agent [35]. This passivating property is used on GaAs surfaces to prevent re-oxidation by breaking Ga-As bonds leading to Ga-S and As-S bonds. Many reports have shown an improvement of optical and electrical performances of GaAs as well as of GaN after $(NH_4)_2S$ treatment. Maruyama *et al.*, have investigated the surface chemistry of GaN before and after $(NH_4)_2S$ treatment and they have shown the removal of the native oxide, concluding that there is a formation of an S-terminated layer on GaN [36]. Huh *et al*. have compared aqueous and tert-butanol solution of $(NH_4)_2S$. They have concluded that ammonium sulphide in t-butanol resulted in a more effective passivation. They explained this trend by the fact that alcohol-based solvents have a lower dielectric constant, increasing the reactivity of S^{2-} ions. As a result, electrostatic interactions between S^{2-} ions and the surface atoms of the semiconductor are increased [37]. Another study concerning $(NH_4)_2S$ in alcohol-based solvent was performed by Kumar *et al*. and photoluminescence measurements showed a reduction of surface states induced by the introduction of sulphur species and the removal of the oxide [38]. This study is in agreement with the work of Han *et al*. who evaluated the influence of $(NH_4)_2S$ treatment prior to $HfAlO_x$ gate dielectric deposition. The treatment allowed an improvement of the charge trapping characteristics of GaN MOS devices. In addition, they observed a higher capacitance, lower hysteresis and a thinner sub GaO_x [39].

I.5.2.2. Acids

One of the most common acids encountered in the literature for oxide removal of GaN is hydrofluoric acid (HF). Two types of HF can be found: Dilute HF (DHF) and Buffer HF or Buffer Oxide Etch (BOE), which corresponds to a mix of NH_4F and HF. The latter solution has the advantage of being more stable over time since HF has the tendency to evaporate easily. HF is reported to be an efficient oxide and carbon remover [40] and furthermore, HF leads to a passivation layer of F and O atoms bonded to Ga atoms. This layer can be removed and the nitrogen-vacancies (V_N^+) recovered by in-situ N_2 plasma as illustrated in Figure 11 [41].

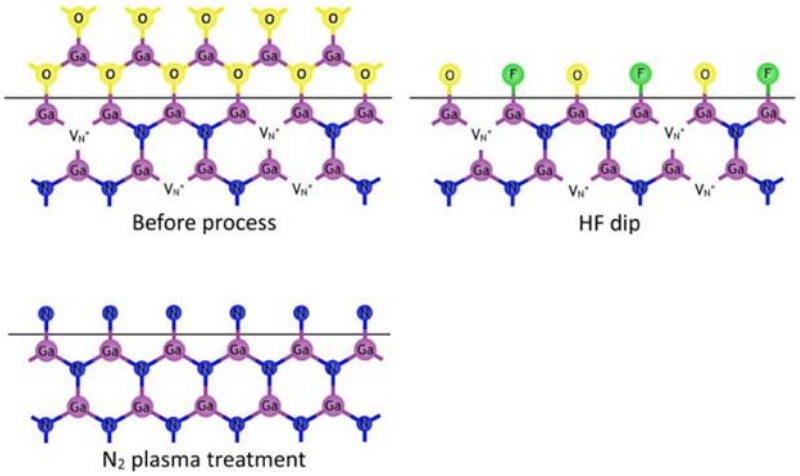

Figure 11. Chemical wet etching of HF on GaN as reported in reference [41]

In the halogen family, hydrochloric acid (HCl) has also been widely studied. Like HF, HCl is used for the removal of GaN oxide [42] and chloride ions (Cl^-) are generally found at the surface after treatment [34, 43]. It is believed that Cl^- ions preferentially bond to Ga atoms since the Ga-Cl bond strength is higher than the N-Cl bond strength. However, the binding between Cl and N is however not completely ruled out. King *et al.* have also found that oxygen coverage was inversely related to the amount of Cl detected on the surface [34]. Okada *et al.* have compared the effect of diluted HCl and boiling HCl prior to SiN deposition [42]. XPS analyses and electrical measurements revealed an increase of the drain current attributed to the oxide removal by boiling HCl. It is also important to note that, after HCl treatment, the surface remained smooth as highlighted by Zhou *et al.* [30].

Acid mixtures, such as piranha solution have been extensively reported on GaN surfaces. The piranha solution is a mixture of sulphuric acid (H_2SO_4) and hydrogen peroxide (H_2O_2) usually in a ratio of 3:1 or 4:1. Mixing H_2SO_4 and H_2O_2 leads to an exothermic reaction that can reach a temperature higher than 100°C. The reaction between H_2SO_4 and H_2O_2 produces an oxidizing agent called peroxymonosulphuric acid (H_2SO_5), also called Caro's acid, which is highly unstable. Consequently, the mixture is generally prepared right before use. Historically, Caro's acid is commonly used to remove organic residues, such as those from photoresists and some investigations on GaN reported a decrease of carbon level [44]. The authors have attributed the carbon removal to the oxidation of the hydrocarbon leading to the formation of carbonyl compounds. As the latter species are more volatile, annealing after treatment allowed their desorption. English *et al.* also reported similar results with XPS analyses showing an increase of oxygen bonded to carbon and not to gallium [45]. Furthermore, the authors reported a smoother surface after piranha solution treatment compared to that

obtained with $(NH_4)_2S$, HCl and HF for example. Hossain *et al.* also observed a smoother surface after piranha treatment as compared that yielded with $(NH_4)_2S$ and HF treatments [46]. These observations were completed by a reduced capacity-voltage hysteresis found when the piranha treatment was used before ALD Al_2O_3 deposition. The authors also highlighted the possible link between the surface morphology, the better oxide removal, the lowest carbon level and the better electrical performances. The link between the surface morphology, oxide and carbon removals, and a lower C-V hysteresis are in line with the work of Nepal *et al.* [47]. They have all concluded that the piranha solution led to a lower amount of oxide and a lower average density of trapped electron at the interface. Wang *et al* have combined first-principle calculations and XPS analyses to better understand the reactions occurring between the piranha solution and the GaN surface. Their study provides the assumption that the adsorbed hydroxyl groups on the GaN (0001) surfaces are more likely to be located near the centre of the hexagon, forming coordination with three gallium atoms, as schematised in Figure 12 [48].

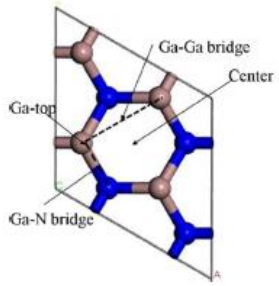

Figure 12. GaN (0001) surface top view as reported in reference [48]

While most authors reported etchant properties for piranha solution, Tsuji *et al.*, observed *via* XPS analyses an oxidizing property for the piranha solution and a better removal of the oxide by $(NH_4)_2S$ treatment [49]. However, the concentrations used in this study were not provided.

I.5.3 Selective etching

Selective etching implies that the unwanted material is removed at a higher rate than the remaining material. These kinds of chemicals are generally used for patterning [50]. For example, for electronic device fabrication, wet etching can be used to pattern a conductive oxide electrode [51]. The use of wet etching processes for patterning requires a reasonable etching rate. Indeed, etchants are selected depending on their ability to etch the target layer without attacking the underlying layer which means that the etching rate must be controlled. The

patterning of GaN has been studied by Ng *et al.* and they produced a periodically poled GaN stripe [52]. The main idea behind this concept was to generate a pre-patterned GaN by alternating Ga and N-polar regions. After dipping in KOH, the N-polar area was successfully removed without attacking the Ga-polar area. This technique allowed to generate smooth sidewalls, using a maskless patterning, as shown in Figure 13.

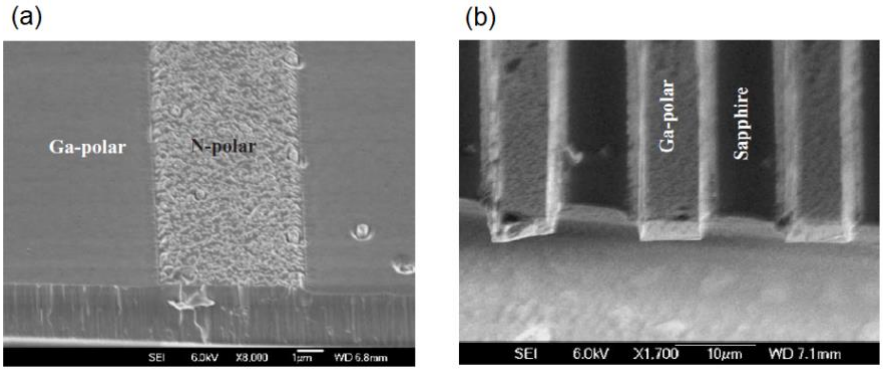

Figure 13. Scanning electron micrograph of a periodically poled GaN stripe pattern (a) before (b) after using polarity-selective chemical etch [52]

Etchants can also be used to selectively etch at defect points. Defect-selective etching has been widely investigated on GaN (0001) and the main reported etchants are hot phosphoric acid (H_3PO_4), molten KOH, and H_2SO_4/H_3PO_4 mixtures [53]. However, the depicted investigations tend to contradict one another. In some studies, the etch pit density is reported to be lower than the dislocation density as found by TEM. On the other hand, others found the etch pit density obtained with H_3PO_4 to be consistent with the dislocation densities found on AFM and TEM images [54–56].

In summary, all studies showed that Ga-polar GaN was a very hard material to etch by means of wet techniques. This highlights the fact that no standard procedures were proposed for obtaining atomically clean GaN.

I.5.4 Digital etching

Digital etching is a technique generally used to remove a layer of a fixed thickness from a material. Unlike conventional etching, this consists of a two-step process. The first step involves a chemical reaction leading to the formation of a thin layer of new molecules at the surface of the material. The second step is another chemical reaction that selectively remove the newly formed layer from the surface without affecting the unreacted material underneath. Therefore, the reactions are independent and etching occurs by sequential application of the

reagents, which allows an excellent control of the etch depth and uniformity. It is therefore, possible to extract the etch-rate per cycle with this technique. For conventional III-V materials, digital etching is mostly performed using an oxidation step followed by the removal of the obtained oxide layer [57–59]. Various techniques of digital etching have been reported on GaAs. One single cycle can include both dry and wet processes, or exclusively dry or wet processes. For example, early studies on digital etching on GaAs used reactive ion etching (RIE) to form a layer composed of $GaCl_3$ and $AsCl_3$ which was removed by Ar ions or low energy electrons [60–62]. The formation of an oxide layer by anodic oxidation followed by a wet chemical etchant has also been reported on GaAs. Fully wet digital etching has been proposed for GaAs substrates [57] where the authors tested several acids or bases for the removal of the oxide layer formed by hydrogen peroxide (H_2O_2) which was used as the oxidizing agent [63].

To the best of our knowledge, only a few papers have been devoted to the digital etching on GaN, and most of these studies have a dry process as the oxidation step. The oxidation step is often performed by plasma under oxidative atmosphere such as O_2 [64, 65], and N_2O [59, 65] and the etching is performed by wet chemical processes using solutions of HCl [59] or HF [64]. This again shows the lack of mature techniques for wet treatments on GaN.

I.6. Context of the PhD project

As stated at the beginning of this work, the need to develop and improve the efficiency of power devices is crucial. The answer to this new challenge lies on GaN-based power electronics with higher breakdown voltage, faster switching speed, and higher thermal conductivity. GaN-based transistors are anticipated to play a key role in power conversion market. Despite their promising properties, GaN-based devices still encounter issues related to their surface or interface. Indeed, to produce efficient devices, industrials must understand how materials interact along all the steps of the fabrication process. Indeed, the device processing technology includes steps such as lithography and contact formation for example. As seen in the previous paragraph, those steps include high-energy processes such as plasmas, which induce detrimental effects on the surface morphology and chemistry that affect the electrical properties.

This work takes place in the context of the cleaning and the surface finishing of GaN. It intends to understand the mechanisms that take place during the intermediate wet cleaning process, which occurs in the HEMT transistor fabrication. The aim of the PhD project is thus

to unravel the near surface chemistry, the morphology and electrical properties before and after several treatments. Unlike bulk materials, the surface feature is different due to under-saturated coordination leading to dangling bonds and contaminant adsorption such as oxygen and carbon. Those adsorbates are responsible for some issues in GaN-based transistors as they can trap charges and thus weaken the 2DEG [5]. Hence, controlling the quality of the GaN surface is key.

My work as a Ph.D. student thus dealt with the preparation and the characterisation of near surface GaN before and after different treatments. These chosen wet treatments are those classically encountered in the microelectronic industry. Some experiences also included physical treatments such as rapid thermal processing (RTP), LASER annealing, or plasma. Moreover, in order to get closer to the manufacturing conditions of HEMT transistors, dry etching processes were included to the study. The main characterisations were focused on the surface chemistry, surface topography and electrical measurements. Most of the research was carried on GaN wafers. However, in order to further explain the mechanism occurring at the liquid/GaN interface and the role played by oxygen, wet treatments were performed on a commercially available GaN powder under rigorously controlled atmosphere (under Argon) at the C2P2 laboratory (renamed CP2M laboratory in January 2021).

In the next chapter, we will explain in details the principles of the characterisation techniques used in this work and how they were used in order to analyse the chemistry composition and morphology of the surface for GaN on silicon and on GaN powder. The use of GaN powder intended to overcome the difficulty of performing some analyses such as Fourier Transform Infra-Red due to multiple layers beneath the GaN. In addition, we will describe the electrical measurements performed to understand the effect of changing surfaces on devices behaviour.

Chapter II - Experimental techniques

As stated earlier, the aim the PhD project was to remove the native oxide and passivate the GaN surface, which implied to set up the bonds of the surface. To reach this goal, several treatments were performed on GaN wafers. In order to evaluate the impact of the treatments, we systematically investigated the surface chemistry thanks to parallel Angular Resolved X-ray Photoelectron Spectroscopy (pAR-XPS). In some cases, the surface morphology was also investigated *via* Atomic Force Microscopy (AFM), the film thickness were measured *via* X-ray Reflectivity (XRR), and the electrical properties on Metal Insulator Semiconductor (MIS) capacitors *via* capacitance-voltage measurements (C-V) were investigated. Further investigations on GaN powders, such as the crystalline structure was characterised *via* X-ray Diffraction (XRD). The impact of the treatments on GaN powders were evaluated *via* Fourier Transform Infra-Red (FTIR), and XPS to overcome the characterisation difficulties related to the heteroepitaxial GaN. All these techniques are detailed in the following paragraphs.

II.1. Surface chemistry analyses by parallel Angular Resolved X-ray Photoelectron Spectroscopy (pAR-XPS)

II.1.1 Principle

XPS is a widely used characterisation technique in the field of surface science. It provides a surface sensitive measurement that gives information such as the relative atomic percentage (at. %), the chemical state and the electronic structure of elements from the top 10 nm of a material. The XPS measurement is based on photoemission. The material to be analysed is irradiated by X-rays in which an incident photon of energy hυ is absorbed by atoms of the surface, as shown in Figure 14.

The absorption of photons induces a photoemission that results in excess energy, so the atoms are in an excited state. The excess energy is then released through a relaxation process where an electron from the upper shell fills the hole. Next, two phenomena can occur. Either an X-ray photon is released, in a process called X-ray fluorescence, or a second electron is emitted, in a process called Auger electron emission.

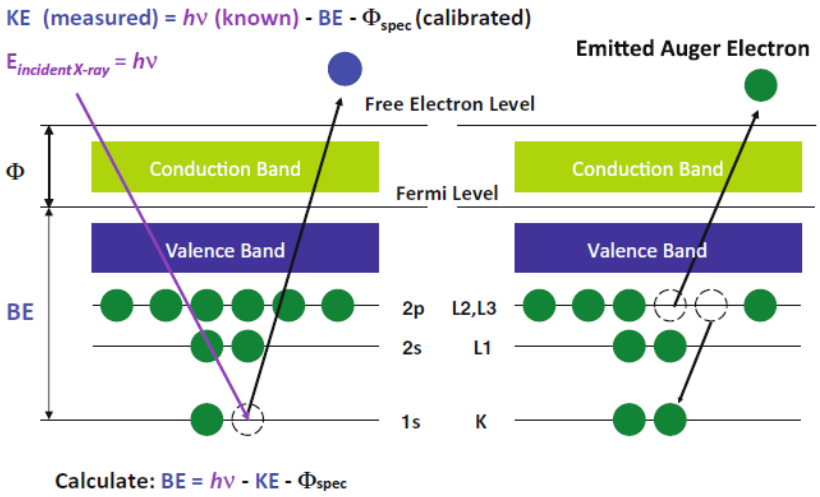

Figure 14. Photoelectron and Auger emission process as reported in the reference [66]

XPS measures the kinetic energy of the collected photoelectrons, which is equal to:

$$KE = h\upsilon - BE - \Phi_{spectrometer} \qquad \text{II-1}$$

Where:

- hυ is the energy of the incident photon,
- KE is the kinetic energy at which the photoelectrons were collected,
- BE is the binding energy of the photoelectrons,
- $\Phi_{\text{spectrometer}}$ is the work function of the spectrometer.

The kinetic energy of the photoelectron depends on the X-ray source energy. Therefore, in order to make comparisons between spectra collected from different sources, the photoemission spectra are conventionally presented as a function of the binding energy.

$$BE = h\upsilon - KE - \Phi_{spectrometer} \qquad \text{II-2}$$

In this study, the surface composition was analysed by parallel Angle Resolved X-ray Photoelectron Spectroscopy (pAR-XPS). The photo-emitted electrons were collected simultaneously over a range of 8 angles from 23.75 to 76.25°, regarding the surface normal without tilting the sample. The model used is a customised Thermo Fisher Scientific Theta 300.

The X-ray were produced from a monochromatic Al-Kα anode source at 1486 eV, with a beam size of 400 µm. The analyses were performed under Ultra High Vacuum (UHV) (10^{-9} mbar).

II.1.2 Qualitative spectra analysis

A wide scan is usually used to obtain qualitative information on a sample. For GaN, a survey scan is typically performed from 0 to 1300 eV, with an example of a spectrum shown in Figure 15.

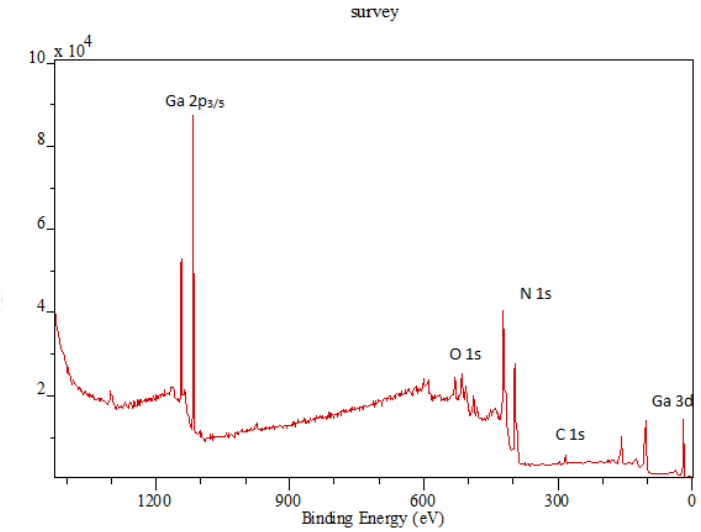

Figure 15. Typical survey spectrum of GaN

Since the kinetic energy has a different sign from the binding energy (eq. II.1), the binding energy (B.E) scale is presented with increasing energy from right to left. The spectrum presented here (Figure 15), shows core-level photoelectrons but also Auger electron peaks. Contrary to core level photoelectrons, the position of Auger electrons on the binding energy scale depends on the X-ray source energy. In the case of using an Al X-ray source, the gallium KLL Auger electrons overlap the N 1s core level peak. Note that photoelectron spectra of the elements are compiled in handbooks.

In order to evaluate the chemical state of a specific element, deconvolution of the spectra is necessary. Measured peaks typically consist of contributions from different bonding or valence states.

II.1.3 Quantitative spectra analysis

Quantification is accessible from XPS data through the number of atoms emitting photoelectron per unit of volume. The raw intensity of the signal collected at a given depth is given by eq. II.3.

$$I = C \times \sigma \times \lambda \times \Phi_{source} \times A_\theta \times T \times D \quad \text{II-3}$$

Where:

- C is the concentration of the element (at.cm^{-3}),
- σ is the photoelectric scattering cross-section (cm^2),
- λ is the inelastic electron mean-free path (cm),
- Φ is the X-ray flux (photon.cm^2.sec^{-1}),
- A is the analysed area at angle θ (cm),
- T is the analyser transmission function,
- D is the efficiency of the detector.

The quantitative data provided in this manuscript are shown by the Avantage ThermoFisher software and the data are given in relative atomic percentage (at. %) using eq. II.4.

$$N_a = \frac{A}{\sigma \times \lambda \times T} \quad \text{II-4}$$

Where:

- N_a is the relative atomic percentage of the considered element (at. %),
- T is the time taken to collected the photo-emitted electron.

The calculations of the at. % of gallium, nitrogen, oxygen and carbon in this thesis are based on the deconvoluted spectra of Ga 3d, N 1s, O 1s, and C1s, respectively. The use of chlorine-based, sulphur-based and phosphorus-based treatments, led us to investigate the Cl 2p, S 2p, P 2p spectra, respectively, as this kind of etchants are reported to leave some adsorbates. The Ga 2p peak is used for the estimation of the oxide thickness and this will be explained in section II.1.4.

II.1.4 Spectra deconvolution

To evaluate the impact of each of the different treatments on GaN, we analysed the Ga 3d, Ga 2p, N 1s, O 1s and C 1s peaks. The measured peaks also have a background level that has to be subtracted. The most commonly used background is the Shirley type, which is based on an integral function. Each peak is then deconvoluted into several components where the number of components depends on their chemical environment at the surface. Figure 16 shows

an example of the deconvoluted peaks of an as-grown sample of GaN, with BG referring to the background for all spectra.

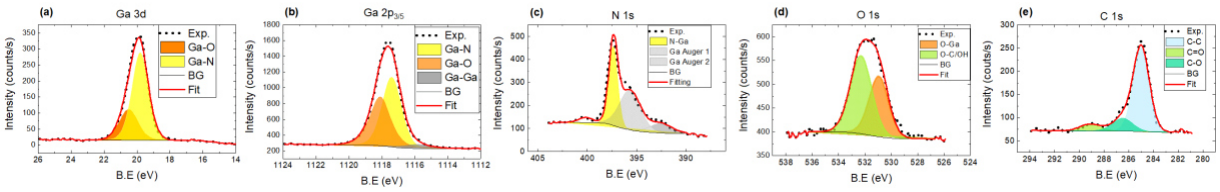

Figure 16. XPS spectra of Ga 3d, Ga $2p_{3/5}$, N 1s, O 1s, and C 1s of an as-grown GaN sample

The Ga 3d peak is composed of two major contributions separated by 0.7 eV. One contribution is related to Ga bonded to N atoms ascribed "Ga-N", and the second one corresponds to Ga bonded to a more electronegative atom, usually oxygen and is noted Ga-O on the graph Figure 16 (a).

As for the Ga 3d peak, the Ga $2p_{3/5}$ peak is also composed of several contributions of which Ga-O and Ga-N. However, a third contribution is necessary to fit the peak. This third contribution is reported as metallic Ga [67, 68], noted Ga-Ga in Figure 16 (b). Due to the inelastic mean free path of the electrons of the Ga 2p shell, the Ga 2p gives information about the extreme surface area (top 2 nm) whereas, the Ga 3d gives information on the top 10 nm. Therefore, in the example above, metallic Ga is more clearly present on the Ga 2p core level than on the Ga 3d core level. Note that in the manuscript all Ga 2p peaks refer to the Ga $2p_{3/5}$ only.

The N 1s (Figure 16 (c)) peak is more complicated to deconvolute since it overlaps with the two Auger electrons of Ga. However, setting a fixed B.E separation between each components allows us to compare the impact of different treatments on the surface.

The O 1s spectra (Figure 16 (d)) was deconvoluted with two components that are O bonded to Ga and O bonded to C and/or H. Note that in some cases, the O 1s peaks were intentionally not deconvoluted since a large number of chemical compounds include oxygen.

Finally, the C 1s spectrum is also shown in Figure 16 (e) and is deconvoluted into three components. The first is related to C-C bonds, while at higher binding energy C-O and C=O are found.

During the analyses to the insulating properties of some sample, which is the case of semi-conductors, positives charges appear resulting from the photo-ionisation. These positive charges are not completely neutralised by the electrons present in the material, nor by the

secondary electrons. As a consequence, the positive potential created decrease the kinetic energy of the photo emitted electrons. This phenomenon results in an increase of the binding energy on the spectra. Therefore, a flood gun is used in order to compensate, at least partially, this charge effect. However, the data analyses sometimes require to calibrate the peaks according to a reference peak. Usually, the peak used to recalibrate is the C 1s core-level. Therefore, all the peaks were shifted with respect to the C 1s binding energy that was set at 285 eV.

II.1.5 Oxide thickness estimation

One of the main advantages of using a parallel Angle Resolved XPS is its ability to collect photo-emitted electrons simultaneously over eight angles without tilting the sample. In this manner, the scanned area is the same whatever the angle. This gives access to accurate depth resolved information and allows to estimate the oxide thickness on GaN. The data were acquired from angles ranging from 23.75° to 76.25° with respect to the surface normal. Figure 17 shows an example of the Ga 2p peak measurement at 76.25° and 23.75°.

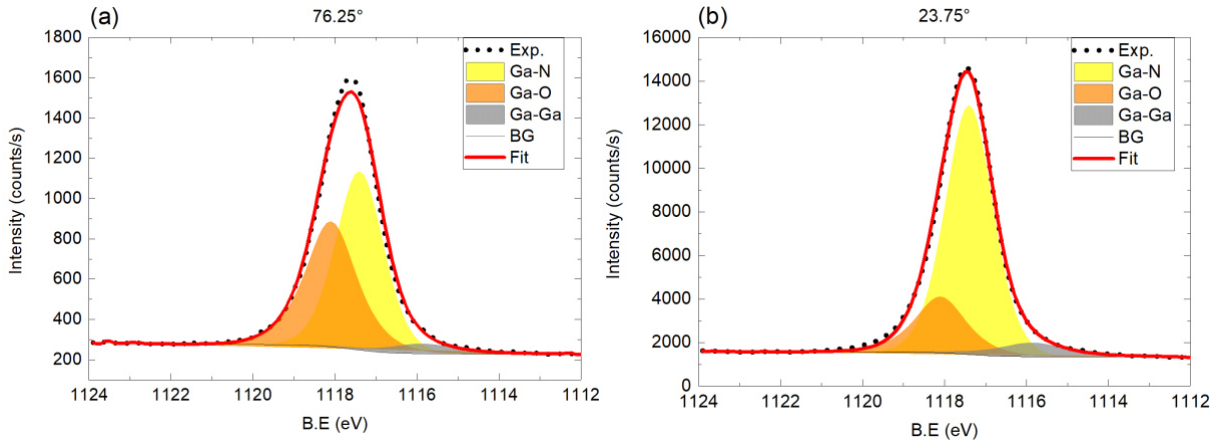

Figure 17. Example of Ga 2p spectra at (a) 76.25° and (b) 23.75°

Comparing these two peaks, we see that the data collected at the emission angle 75.25° clearly exhibits a larger Ga-O contribution compared to the data collected at 23.75°, which means that most of the Ga-O bonds are found at the extreme surface. Indeed, the formation of an oxide layer starts with the adsorption of oxygen atoms which will migrate to the bulk overtime.

An estimation of the oxide thickness can be performed using the Beer-Lambert relationship (eq. II.5), which describes the photo-electron signal intensity as a function of depth and emission angle.

$$I = I_0 e^{\frac{-d}{\lambda \cos\theta}} \quad \text{II-5}$$

Where:

- I is the intensity of the signal,
- I_0 is the intensity of the near-area surface,
- d is the electron depth,
- λ is the free mean path of the electrons,
- θ is the emission angle of the electrons.

The estimation of the oxide thickness relies on a mathematical model, the two-layer model consisting of a system composed of one layer (a) with a thickness d on top of another layer (b) [66]. The ratio I_a/I_b between the intensity of the signal of layer a and the intensity of the signal of the layer (b) is:

$$\frac{I_a}{I_b} = \frac{I_a^0 \int_0^d \exp\left(-t/\lambda \cos\theta\right) dt}{I_b^0 \int_d^\infty \left(-t/\lambda \cos\theta\right) dt} \quad \text{II-6}$$

Where the signal from layer a comes from depth 0 → d, and the signal from layer b comes from d → ∞. By replacing I^0a and I^0b by:

$$I_{a,b}^0 = \frac{n_{a,b}\rho_{a,b}S_{a,b}}{MW_{a,b}} \quad \text{II-7}$$

And:

$$N_{a,b} = \frac{I_{a,b}}{S_{a,b}} \quad \text{II-8}$$

Rearranging and integrating the equation leads to the eq II.9 :

$$\frac{d}{\lambda_a \cos\theta} = \ln\left(\frac{N_a n_b \rho_b \lambda_b MW_a}{N_b n_a \rho_a \lambda_a MW_b} + 1\right) \qquad \text{II-9}$$

When plotting the right-hand side of the eq. II.9 as a function of 1/cos θ, the slope of the line is d/λ_a giving access to the thickness. Figure 18 shows an example of the oxide thickness estimation for an as-grown sample of GaN. As stated in the previous paragraph, the estimation of the oxide thickness is based on the Ga 2p peak. The model used during the thesis was developed at the LTM laboratory and is based on the ratio of the Ga-N and Ga-O peaks area.

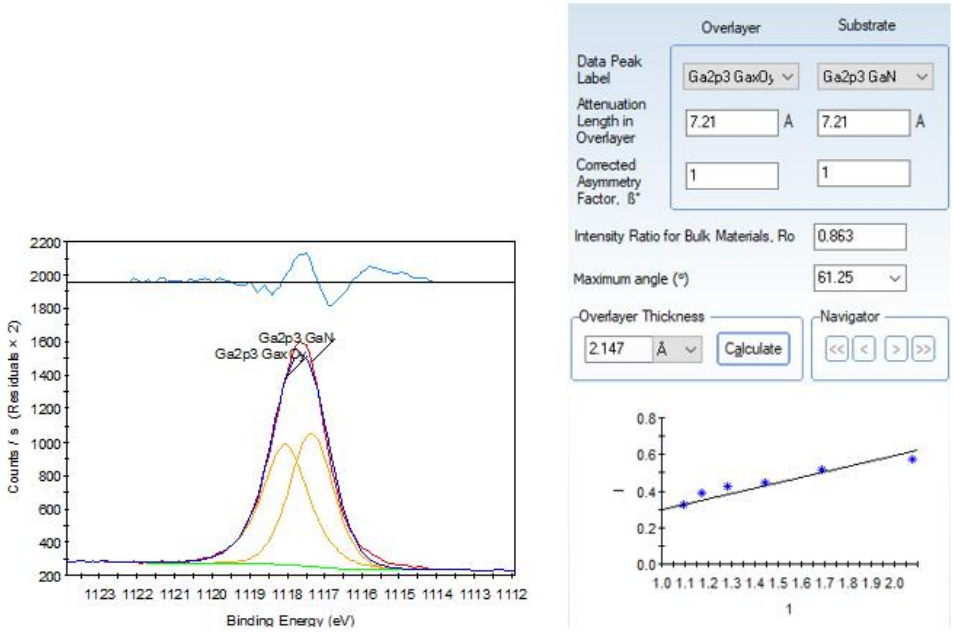

Figure 18. Example of oxide thickness estimation based on the Ga 2p peak for an as-grown sample

As XPS is a powerful technique to examine the chemical properties of the surface, and even to give quantitative analysis of the elements and surface layer thickness, it will be extensively used in this PhD project along with other techniques described below.

II.2. Investigating the surface morphology by Atomic Force Microscopy

Atomic Force Microscopy (AFM) is a key tool in nanoscale research for the determination of surface morphology. AFM is based on the interaction of atomic forces between the probe and the surface. Depending on the distance between them, different forces are in place: attractive Van der Waals forces or repulsive coulombic forces. As the tip approaches the surface, attractive Van der Waals forces attract the cantilever toward the surface. Van der Waals interactions are dominant for distances of the order of a few tens of nanometres. Approaching closer, to the length of a chemical bond i.e. a few Angstroms, the repulsive coulombic forces become dominant, deflecting the cantilever away from the surface.

The deflections of the cantilever are detected by a laser beam and recorded by a photodetector (Figure 19) and the sample is then moved in the z to correct the deflection. While scanning, the tip goes back and forth across the surface and the z-connections applied at each point are assembled to form the image.

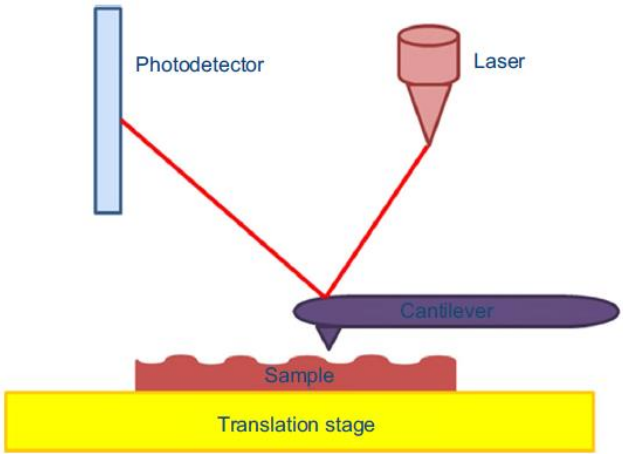

Figure 19. Principles of AFM [69]

Different working modes are available on AFM equipment, with the most common being contact mode, and tapping mode. In contact mode, repulsive forces are dominant (Figure 20). The tip touches the surface and is pushed away according to Pauli's principle, deflecting the cantilever. In tapping mode, the tip makes short-time contact with the surface. In this mode, the cantilever oscillates at a resonant frequency (50-100 kHz). As the tip interacts with the

surface the oscillation amplitude of the cantilever decreases. Once again, a z-correction is applied to get the cantilever back to back the desired frequency.

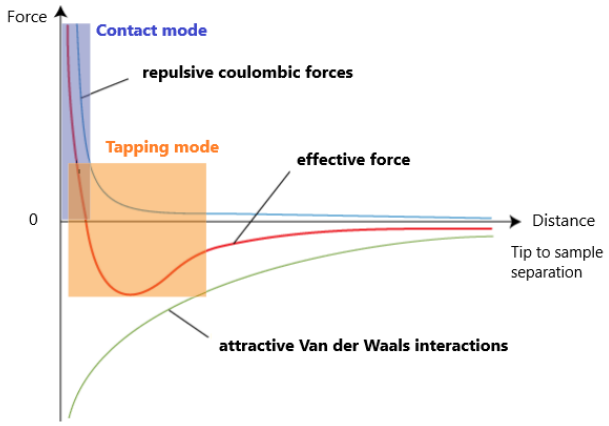

Figure 20. Relationship between forces as a function of the distance between the tip and the surface

During the PhD project, AFM was used in tapping mode to image and measure the roughness of samples before and after dry and/or wet treatments. AFM images were acquired with 512 lines, at a scan rate of 0.9 Hz. Figure 21 shows a typical AFM image of an as-grown GaN sample, where we clearly see the atomic steps formed during the epitaxial growth, which correspond to a height of 2.6 Å, half the unit height of GaN in the c-direction.

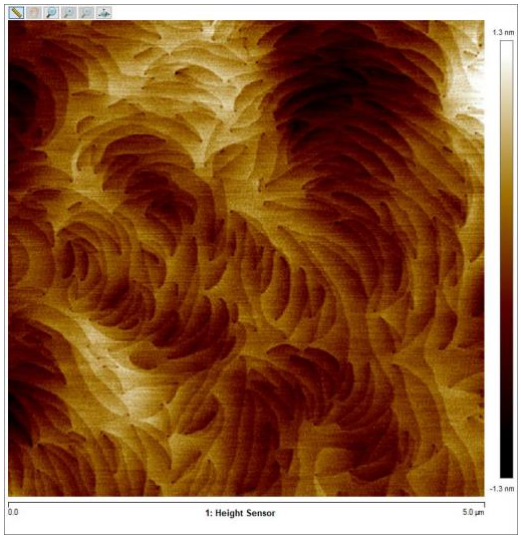

Figure 21. AFM image of as-grown GaN

II.3. X-ray reflectivity

X-ray reflectivity (XRR) is a non-destructive technique used to determine thin film structural parameters, such as thickness, density and surface or interface roughness. The principle of this technique is based on the analyses of X-ray reflection intensity curves from grazing incident X-ray beam. The reflected intensity is collected as a function of angle.

The generated X-rays are reflected on a surface in a specular direction, i.e. the incident angle is equal to the reflected angle, as shown in Figure 22.

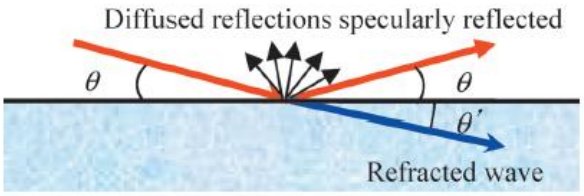

Figure 22. Reflection and refraction of X-rays on material surface [70]

The refractive index of a material is slightly less than 1. Total reflection occur at, or below a critical angle (θ_c), which means that below this angle, the X-rays are fully reflected from the film and the incident X-rays do not penetrate. This angle varies depending on the electronic density of the material. When the incident angle (θ) is bigger than the critical angle, the incident X-rays penetrate the material and are both reflected and refracted.

II.4. X-ray diffraction

X-ray diffraction (XRD) is a non-destructive technique for characterising crystalline materials. It provides information on structures, phases, and preferred crystal orientations. A beam of X-rays is scattered by the average spacing between layers of the atoms or crystallographic planes within the material. The interaction of the incident rays with the material produces a constructive interference and forms diffraction peak when the Bragg's equation is satisfied:

$$n\lambda = 2d \sin\theta \qquad \text{II-10}$$

Where:

- n is an integer,
- λ is the wavelength of the incident X-rays,
- d is the distance between two crystallographic planes.
- θ is the angle of the X-ray beam with respect to the sample

Peaks intensities are determined by the position of the atoms composing the crystal lattice. Consequently, the XRD pattern is the fingerprint of periodic atomic arrangement in a given material and the identification can be performed by comparing the obtained pattern to a database of pattern known.

XRD was an accurate technique used in order to determine the crystalline structure of the purchased GaN powder.

The XDR measurement were performed on an Empyrean, Malvern Panalytical tool.

II.5. Fourier Transform Infra-Red spectroscopy

Fourier Transform Infra-Red spectroscopy is a non-destructive technique used to determine the nature of the chemical bonds and to detect functional groups composing the sample. A FTIR instrument is usually composed of a source, interferometer, a sample compartment, a detector, an amplifier, an A/D convertor, and a computer. The light source that passes through a Michelson interferometer, which allows the signal modulation and the generation of the interferences. Then the radiation passes through the sample and reach the detector. Then the signal is amplified and converted to digital signal by the amplifier and analogue-to-digital converter, respectively.

The preparation of solid samples implies the grinding the powder and mixing it with KBr. The mixture is then squeezed into a pellet via a hydraulic press.

II.6. Electrical characterisation of MIS capacitors

The capacitance-voltage method or C-V method is commonly used for electrical characterisation of thin-film dielectrics and their interfaces by estimating the quantity if charges present within the interface. Such method probes the variation of the charge distribution in the semiconductor in response to a time-varying voltage applied to the metal contact [71].

The fabrication of the Metal Insulator Semiconductor (MIS) capacitors consists of a substrate covered by a thin film dielectric over which metal gate contact are deposited defining the device area. For my PhD project, the MIS capacitors were fabricated as follows. On a n-doped GaN substrate was deposited a 20 nm thermal alumina (Al_2O_3) as a dielectric layer, and 30 nm of Nickel (Ni) and 100 nm of gold (Au) as metal contacts (Figure 23).

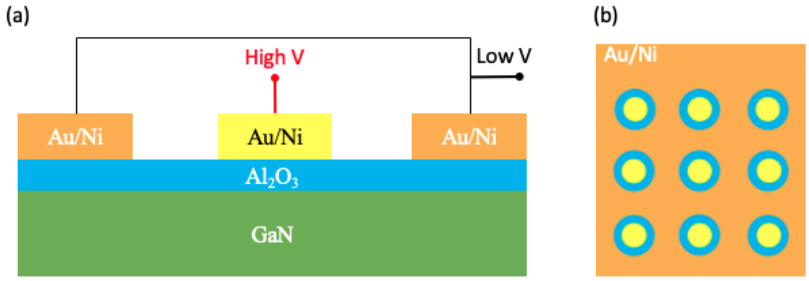

Figure 23. Schematic of the MIS structure used for the C-V measurements (a) one capacitance and (b) top view of one chip with nine capacitors with an inner circle diameter of 100 µm

The configuration included two capacitances in series, in which one formed a circular contact and another one covering the whole chip. The C-V measurements were performed with an LCR meter from Agilent, model 4284A Precision, from -4 V to 6 V at a frequency of 10 kHz.

Chapter III - Conventional wet etching on GaN sample (wafers and powders)

III.1. Systematic review on GaN wafer (0001)

III.1.1 Structure of the samples used in this study

The GaN wafers used in this work consist of GaN grown by Metal Organic Chemical Deposition (MOCVD) on 200 mm diameter, 1 mm thick silicon (111) substrates. The nucleation layer is a 300 nm thick AlN followed by a 1.5 µm of various GaN/AlGaN buffer layers. Next, we have a 1.8 µm thick GaN layer. A schematic of these layers is shown in Figure 24 .

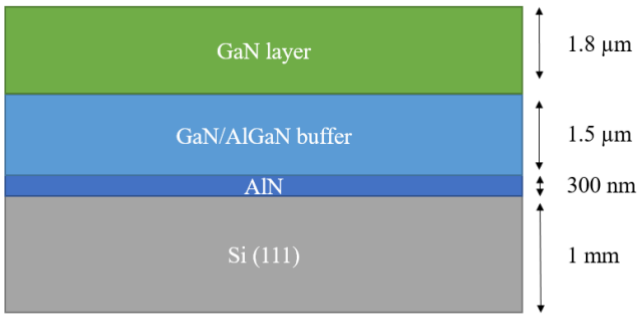

Figure 24. Schematic of the epitaxial layers used in this study for GaN on silicon

Although a typical HEMT structure would also have an AlGaN barrier and a GaN or SiN cap, in order to understand the mechanism and how the extreme surface bonds of GaN interact during wet etching processes, this study does not include the AlGaN barrier layer. Indeed, this study only focuses on the surface of GaN and the possible wet chemicals that can be proposed to get rid of the contaminants such as oxygen and carbon. Therefore, the first part of our study will focus on the chemical modifications of as-grown GaN after immersion in several etching solutions usually encountered in the literature and used in the microelectronic industry.

III.1.2 Surface preparation

For all of the treatments used in this work, unless otherwise stated, GaN wafers were cut into small pieces (1x1 cm^2) before treatment using a diamond scribe. To minimise chemical changes at the GaN surface and to only evaluate the impact of acids and bases, the samples were directly immersed into solutions without a degreasing step. Degreasing steps usually employ alcohol-based solvents, which tend to increase the total amount of carbon at the surface.

Furthermore, since our interest mainly concerns the first ten nanometres of the surface, we avoided degreasing steps to prevent adsorbed monolayers of carbons to hinder XPS analyses.

Therefore, the samples were directly immersed into solutions at room temperature unless stated otherwise. The immersion were performed into 50 mL PTFE beaker (Poly-Tetra-Fluoro-Ethylene) for 10 minutes. After wet etching, the samples were rinsed with deionised water. The tanks used for the rinsing step were equipped with an electrical conductivity meter, which indicated when the samples were completely rinsed. The samples were then dried under N_2 flow.

We examined the effect of several chemical treatments commonly encountered in the microelectronic industry: H_2SO_4 98%, HCl 37%, $(NH_4)_2S$ 26%, NH_4OH 27%, $(NH_4)_2S_2O_8$ (ammonium persulfate), H_3PO_4 85% and Caro acid 3:1 (H_2SO_4:H_2O_2). Additionally, 1M citric acid was tested. Unless specified otherwise, all treatments were performed at room temperature (RT).

Treated samples were immediately transferred into a specific vacuum carrier at 10^{-5} mbar for surface analyses by pAR-XPS. The time between wet treatment and loading into the vacuum carrier did not exceed 20 minutes.

III.1.3 Systematic review on GaN wafer (0001)

The process flow for the treatments included an immersion into the chemicals for 10 minutes followed by 5 minutes of rinsing in deionised water. The samples were then dried under N_2. The effect of the different wet etchants on GaN samples was further investigated by parallel Angle Resolved X-ray Photoelectron Spectroscopy (pAR-XPS).

The impact of each wet treatments was evaluated based on the relative atomic percentage (at.%) of different elements (oxygen, carbon, chlorine or phosphorus). Their impact on the oxide thickness is shown in Figure 25 (a). Unless stated otherwise, treatments were performed at room temperature.

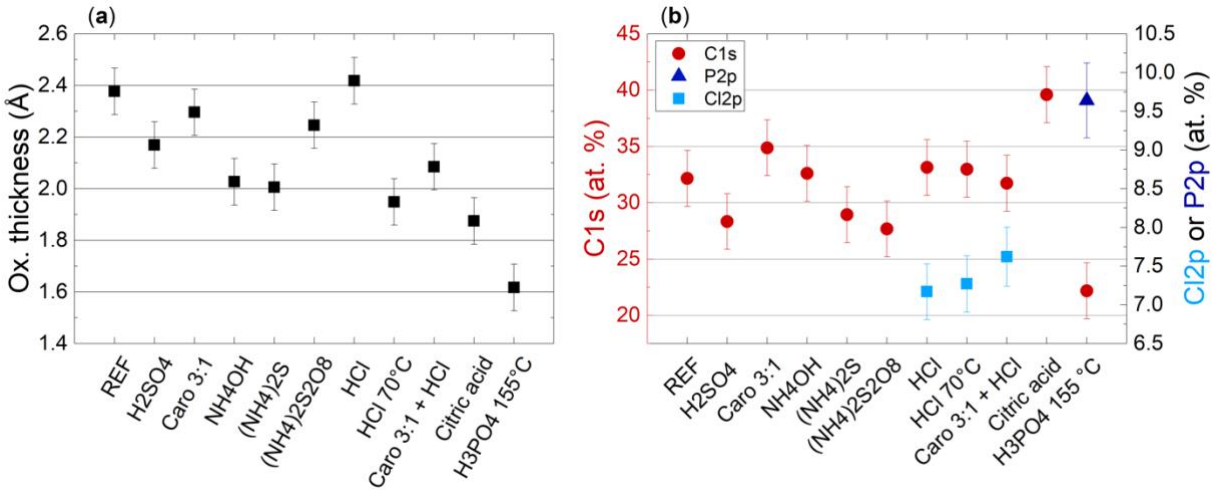

Figure 25. (a) Oxide thickness estimation on GaN by pAR-XPS after several wet treatments and (b) atomic % of the total amount of C and Cl or P adsorbates on GaN induced the by treatments.

The first effect that we can note is that oxidizing agents, such as sulphuric acid (H_2SO_4) and Caro 3:1 (H_2SO_4:H_2O_2) solution, did not increase the oxide thickness. The H_2SO_4:H_2O_2 mixture has been reported to induce hydroxyl group adsorption [48] and is commonly used to remove the carbon contamination, although we see in Figure 25 (b) that the reduction of carbon level is negligible in our experiments.

Concerning basic treatments, $(NH_4)_2S$ and NH_4OH removed some of the oxide from the surface as expected (2.03 Å and 2.01 Å vs 2.38 Å for the reference sample), as described in section I.5.2.1. On the contrary, persulfate ammonium had no significant impact on the oxide thickness. From Figure 25 (b) it can be seen that sulphur-based treatments tend to reduce the carbon level while, for other treatments, except citric acid and H_3PO_4, this level did not change. However, no peak related to the presence of sulphur was observed. One possible explanation might be that the sulphur level was below the detectability threshold, or it may be that the sulphur desorbs easily when loaded into the vacuum chamber of the XPS equipment.

Chlorine-based treatments showed a decrease of the oxide thickness, especially at 70°C and when a Caro 3:1 pre-treatment was performed prior to HCl treatment. It is noteworthy that the same amount of chloride was found (about 7 at. %) whatever the conditions, as shown in Figure 25 (b).

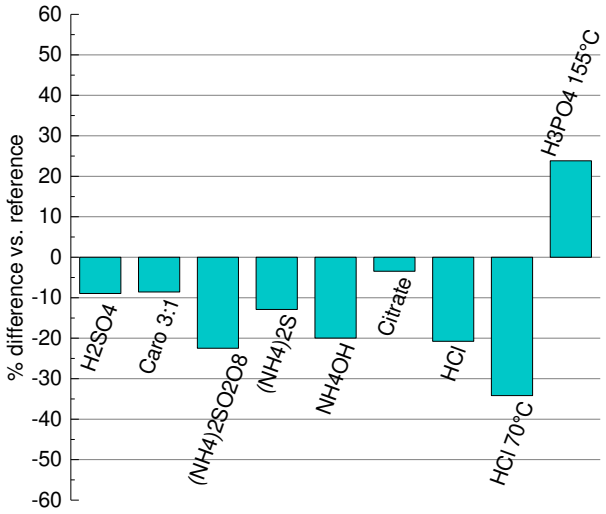

Figure 26. Percentage difference of the total at. % of oxygen based on O1s peak compared to the O1s peak of the reference

The decrease of oxide thickness is usually accompanied by a decrease in oxygen level. Figure 26 represents the evolution of the total oxygen level found using the O 1s peak. However, it is important to note that the O 1s peak may include a contribution related to the presence of carbonyl groups due to organic contamination of the atmosphere, therefore the level of oxygen may not be in agreement with the oxide thickness found. This can be seen when comparing Figure 25 (a) and Figure 26. In particular, citric acid exhibited a decrease of the oxygen level less than 10 % but the equivalent oxide thickness decreased by 26% compared to the reference. Moreover, all sulphur-based treatments exhibited a decrease of the oxygen level that might be related to carbonyl desorption as well as oxides. Indeed, we saw from Figure 25 (a) and (b) that the oxide thickness decreased as well as the carbon level with those species. Those results highlight the fact that a small amount of sulphur may have been adsorbed at the surface, preventing the re-adsorption of atmospheric oxygen or compound containing carbonyl groups.

For other chemicals treatments, the opposite was observed and the oxide thickness was reduced while the oxygen level increased. As an example, after H_3PO_4 treatment, the oxide thickness was reduced whereas the oxygen level compared to the reference sample increased. This increase was due to the presence of PO_4^{3-} residues (Figure 25 (b)). A similar result was observed with citric acid. The oxide thickness was indeed reduced but the oxygen level indicated only a small decrease of 3.5 %. This observation can be explained by the fact that a certain amount of citric acid is adsorbed. As seen in Figure 25 (b), the amount of carbon had

reached the level of 39.6 at. % versus 32.0 at. % for the reference sample. Since the oxide thickness was lowered, it can be deduced that the adsorption of citric acid at the surface prevented oxidation. This result was in agreement with previous work done on Ge substrates [72].

In summary, although it is hard to analyse the total amount of O 1s peak, analysis of the oxide thickness after these treatments shows that the clearest trend is the higher reduction of oxide thickness observed for the treatments that involved subsequent etchant adsorption after treatment. An additional aspect we can note is that the temperature seemed to have an impact on the etching properties. When comparing HCl treatment at room temperature and at 70°C, we can see from Figure 25 and Figure 26 that the level of oxygen decreased as well as the oxide thickness when increasing the temperature of the solution.

To better understand the impact of the temperature during HCl treatments, we studied the kinetic of desorption of chloride ions.

III.1.4 Chloride adsorption of HCl-based treatments

In the previous paragraph, we saw that HCl removed some oxide at the surface, and adsorbed chlorides were observed at the same time. The oxygen concentration is reported to be inversely proportional to the detected amount of chlorine [73]. Figure 27 shows the relative atomic percentage of O 1s and Cl 2p detected at the take-off angle of 76.25°, for several chlorine-based treatments.

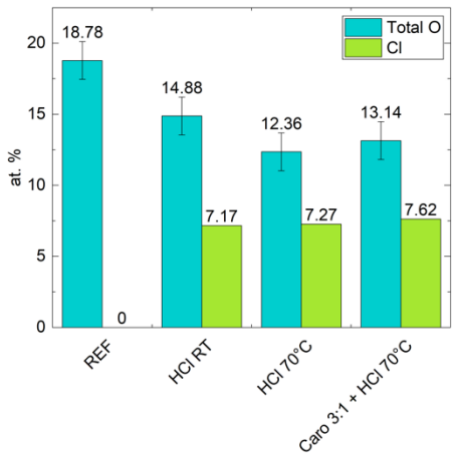

Figure 27. Relative atomic percentage of O 1s and Cl 2p detected

As observed, the amount of chloride detected at the surface was slightly higher than the amount of oxygen lost. Furthermore, the relative atomic percentage of chloride and oxygen did not significantly evolve whatever the conditions. However, an estimation of the equivalent oxide thickness (Figure 25 (a)) suggested that HCl at 70°C and pre-treatment with Caro 3:1 reduced the oxide. As previously explained, the data collected from the Ga 2p peak was related to the first 2 nm, therefore, solutions of HCl heated at 70°C and "Caro 3:1 + HCl" have affected the 6 first nm of the GaN since changes were visible at the O 1s core-level. It can be suggested that somehow the adsorption of chlorides ions prevented the surface from re-oxidation. It is important to note that no major changes were observed on the Ga 3d spectra (Figure 28) after each treatment. Indeed, the Ga-O component did not significantly change after each treatment. This can be explained by the fact that the Ga 3d spectra at this core-level was related to the first 10 nm. However, the change of the O 1s spectra (Figure 28) aspect indicated that only the surface chemistry was modified along the 6 first nm.

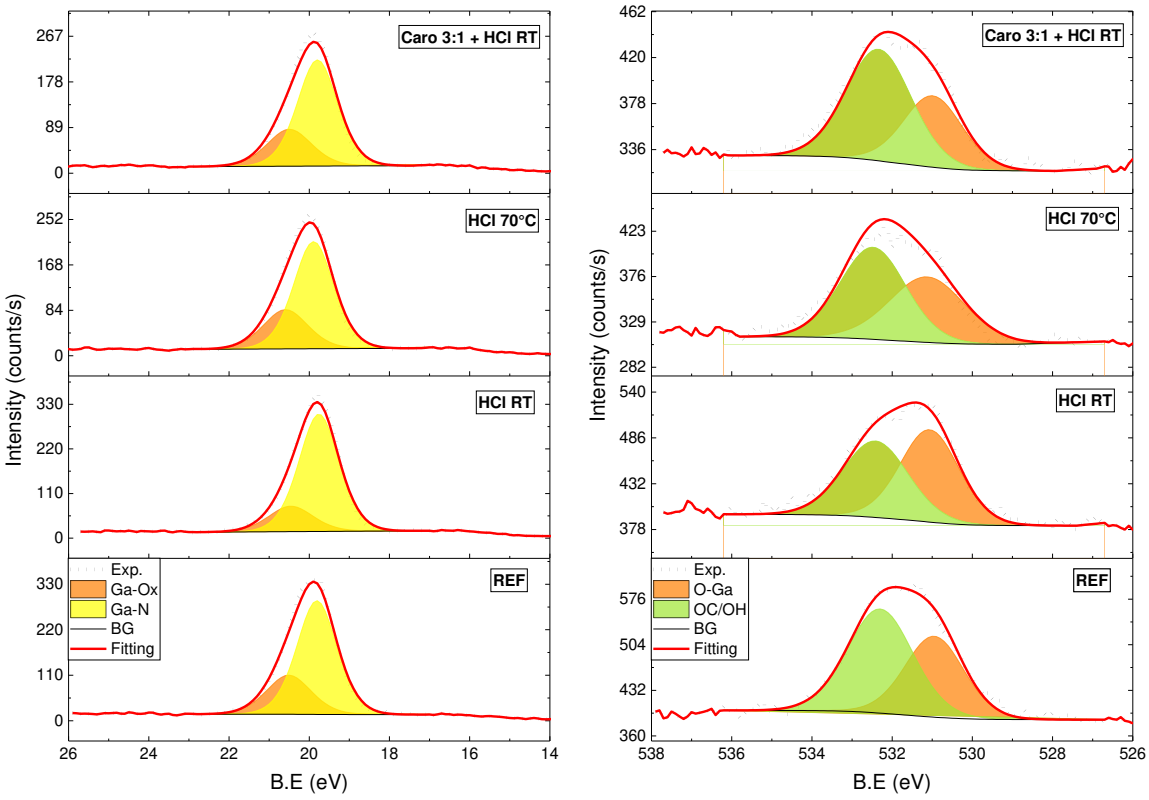

Figure 28. Ga 3d (left) and O1s (right) peaks after chlorine-based treatments

The O 1s spectra presented in Figure 28, were deconvoluted into two major components related to oxygen bonded to Ga or to carbon and/or hydroxyl groups, referred to as O-Ga and

O-C/OH respectively. It can be noticed that for all treatments, the O-Ga component was affected. The impact of the chlorine-based treatments over the O-Ga component, can be seen in Figure 29. Before dipping the sample in the etchant chemicals, the surface presented 7 at. % of oxygen bonded to gallium and 12 at. % of oxygen bonded to carbon and/or hydrogen. The O-Ga component was reduced by 4.8 after a dip in HCl at 70°C and after a dip in Caro 3:1 followed by HCl. No effect on the O-Ga component was observed when the HCl treatment was performed at room temperature. Indeed, the reduction of the total amount of oxygen is a consequence of a decrease of the O-C/OH component.

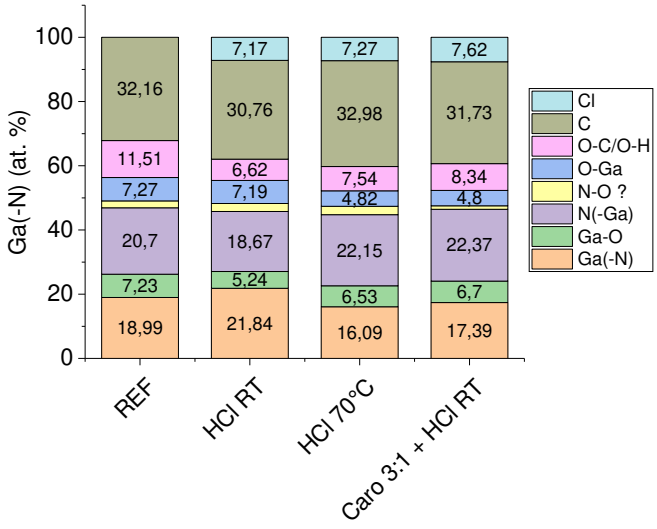

Figure 29. Relative atomic percentage after chlorine-based treatments

These results are coherent with the equivalent oxide thickness estimation, indicating that HCl at 70°C and "Caro 3:1 + HCl" removed some gallium oxide at the surface while chloride ions were adsorbed probably as $Ga^{+}Cl^{-}$ [73]. Note that the small increase in at. % of the Ga-O component from the Ga 3d could be attributed to Ga-Cl bonds. The presence of the chlorine species was suggested by the shift of the Ga 3d peaks (Figure 28 (a)) toward higher binding energy with the HCl at 70°C treatment and the "Caro + HCl" sequence. This shift indicates oxidation state changes of the Ga atoms being surrounded by electronegative species, here Cl^{-}. Therefore, the temperature might play a role on the position of the Cl^{-} among the atomic structure, preventing re-oxidation more efficiently.

III.1.5 Desorption

An additional observation noted with HCl treatments was the decrease of the amount of chloride detected at the surface over time, when the sample was exposed to air. The "Caro 3:1+HCl" sequence is shown as an example in Figure 30 (a).

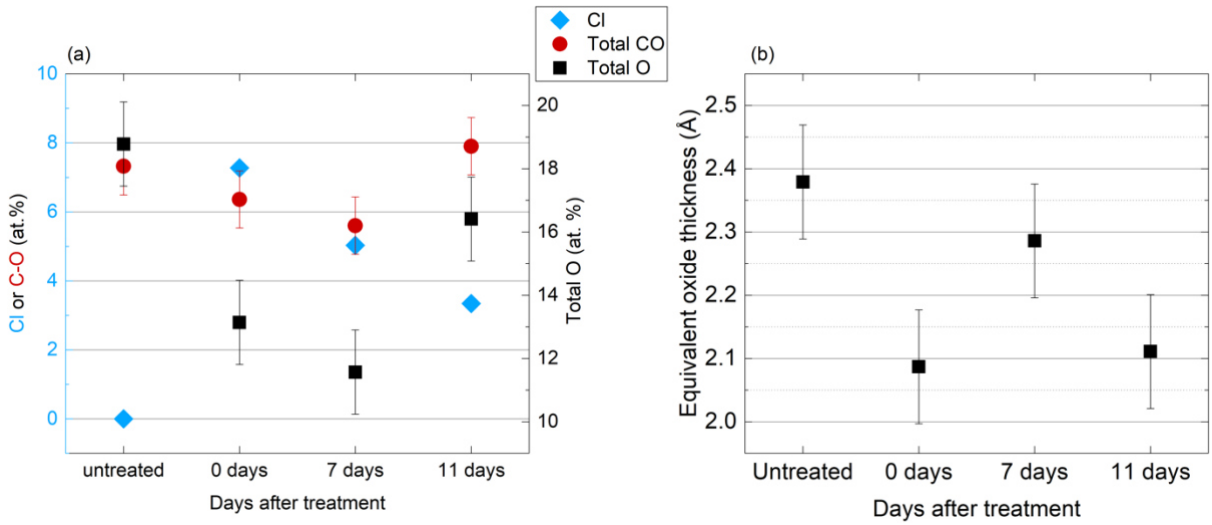

Figure 30. Evolution of (a) the total amount of oxygen and chlorine detected at the surface (b) the estimated oxide thickness 11 days after treatments

The amount of chloride detected at the surface decreased over time, when the sample was exposed to air. The amount of chloride present on the surface was almost divided by two, 11 days after treatment. At the same time, the total amount of oxygen started to increase 11 days after the treatment. Surprisingly, the equivalent oxide thickness (Figure 30 (a)) did not increase over time. This result suggests that the chloride detected at the surface 11 days after treatment still prevented oxidation. The increase of the total amount of oxygen observed 11 days after treatment could be attributed to an increase of C-O component from the C 1s peak.

III.1.6 Conclusion

The study on GaN wafer has shown that the decrease of the oxide thickness was related to the adsorption of chloride ions, phosphate, or carbonyl groups following the HCl, H_3PO_4, and citric acid treatments respectively. The adsorption of these species played a role in preventing re-oxidation. When heating the etchant, the oxide thickness was even lowered, with the lowest oxide thickness obtained with H_3PO_4 at 155°C. The example of chlorine-based treatments have shown that the amount of detected chlorine was the same whether the temperature or the pre-treatment. Eleven days after treatment, the amount of chloride was divided by two and was still detected.

Although, no sulphur was detected, $(NH_4)_2S$ treatment allowed a decrease of the oxide thickness as well. Generally, sulphur-based treatments exhibited the lowest amount of carbon, which indicated that sulphur might have adsorbed at the surface.

This systematic review on GaN wafer highlighted the inertness of GaN (0001) and the difficulty of attacking the (0002) facets. In order to understand the interactions occurring between the chemical etchants and the GaN surface, we oriented our researches on GaN powders.

III.2. Systematic review of chemical treatments on GaN powder

Having evaluated the impact of conventional wet etchants on GaN wafer surfaces oriented on the c-plane, the pAR-XPS analyses unveiled that acids and bases had little impact on the GaN surface which is not surprising as it is well known that c-plane GaN oriented (0001) is quite inert. Therefore, to understand the interactions between the chemicals species in the etchant solutions and the GaN surface, an alternative approach was attempted by analysing the effect of various chemicals on GaN powder, as a previous study performed on Ge particles for passivation [72]. The study has several interests. First, powdered materials can have important surface area to volume ratio, and so any signal showing modification of the surface is expected to be amplified. Second, GaN powders allow three-dimensional analysis like Fourier Transform Infra-Red (FTIR) and as the surface area is higher, we may observe more surface signals. Indeed, FTIR analysis on hetero-structure of GaN wafers are disturbed by the multiple layers underneath. Third, this study was performed at the C2P2 laboratory, which is equipped with high vacuum lines allowing to perform experiments under strictly controlled atmosphere, hence allowing to understand the role of oxygen from air. It should be noted that with powdered samples, all the different facet orientations are treated at the same time, which was expected to help illustrating the general effects of different chemical treatments.

In addition to the FTIR measurements performed directly at C2P2 laboratory, XPS measurements were performed at LETI on the same powdered samples in order to try to correlate the results to those already found for GaN on silicon wafers.

III.2.1 Analysis on the untreated GaN powder

For the wet etching treatments on GaN powders, we used a commercially available GaN powder purchased from abcr®. Scanning Electronic Microscopy (SEM) images of the GaN particles are shown in Figure 31.

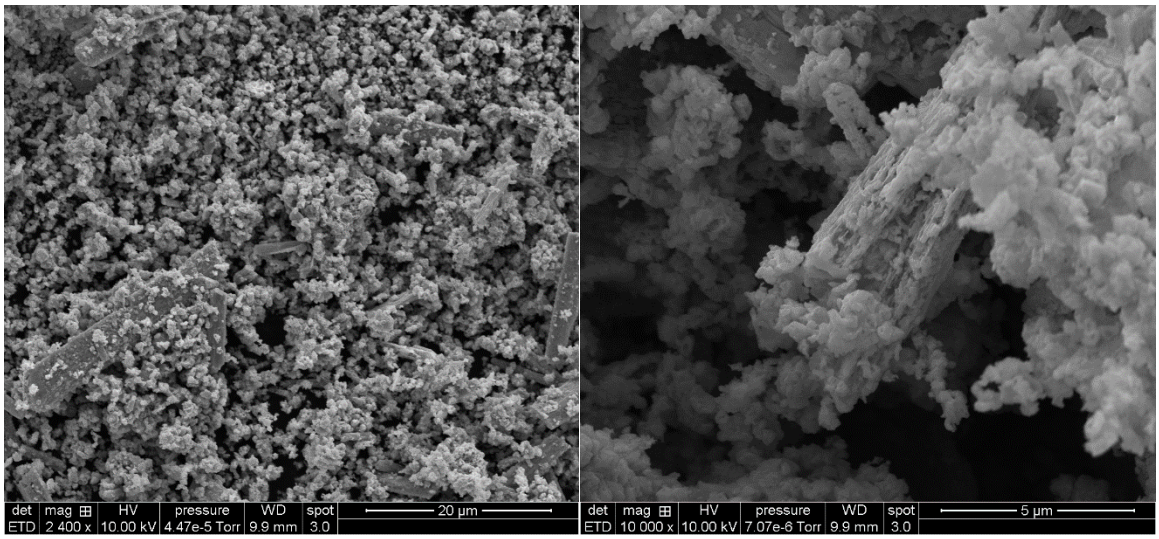

Figure 31. SEM images of commercial GaN purchased from abcr®

Comparison with the SEM micrographs (Figure 31) to the literature disclosing the synthesis of GaN powders, our purchased GaN particles are likely synthetized by a solvo-thermal method or via sol-gel techniques [73, 74].

The specific surface area of the powder was estimated using the Brunaeur-Emmet-Teller equation (BET) from N_2 adsorption-desorption experiments at 77 K. It is based on the determination of gas quantity necessary to cover the surface of the powder (either external surface of inner pore surface). The measured specific surface area was unfortunately very low and found equal to: 5.6 $m^2.g^{-1}$.

The crystalline phase of the powder was determined by X-Ray Diffraction (XRD) as shown in Figure 32. The diffraction lines indicate a hexagonal wurtzite structure with lattice parameters a=3.188 Å and c=5.184 Å (versus bulk values for relaxed GaN of 3.189 Å and 5.185 Å), which is therefore considered to be relaxed material, despite these slightly smaller values.

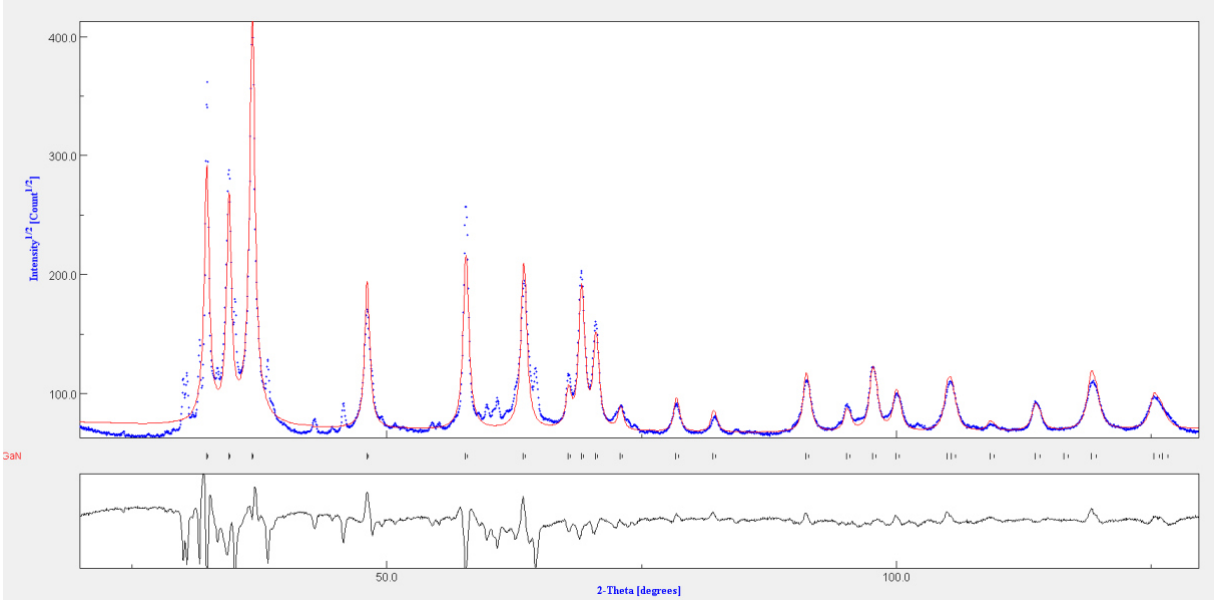

Figure 32. XRD pattern of the GaN powder used in the following experiments. The red line is the fit for hexagonal wurtzite GaN, the blue line is the data

III.2.2 Etching experimental protocol under ambient air

Initial works on GaN powders were performed under ambient air as for the previous experiments on GaN wafers (same conditions). All the treatments were carried out with the same time duration and temperature. The GaN particles were dispersed into the chemicals and stirred for ten minutes. For each treatments, 500 mg of powder were dispersed into 6 mL of etchant. The rinsing step was then performed in a Büchner funnel combined with a Büchner flask where a partial vacuum was created in order to filter the particles. Rinsing was performed with de-ionised water several times until a neutral pH was reached. The volume used for rinsing can be found in Table 4.

Etchant	Rinsing volume (mL)
NH_4OH	180
$(NH_4)_2S$	180
H_2SO_4	210
HCl 70°C	120
Citric acid	90
H_2O_2	60
1-octanethiol	-

Table 4. Rinsing volume used for each treatment performed on GaN powders

The drying step was carried out at room temperature in a Schlenk flask connected to Schlenk lines. In order to completely remove the water adsorbed on the particles, this treatment under vacuum (10^{-2} mbar) was performed overnight.

After drying, the powders were loaded into a glovebox containing a hydraulic press to make the pellets using dry KBr as dilutant for further FTIR measurements. With the aim of limiting the exposure to ambient air of the treated powders, the prepared KBr pellets were put into a customised Schlenk flask. This customised Schlenk flask allowed to isolate the pellet for ambient air before and during the FTIR analysis.

After each treatments, the remaining powders were kept in sealed Schlenk under Ar in order to further study the surface chemistry *via* XPS. The XPS used for GaN powder was located outside the cleanroom, contrary to the pAR-XPS used for the GaN wafers. Nevertheless, the analyses were performed with the same conditions as for the GaN wafers (same source Al, same level of vacuum…).

III.2.3 Experimental protocol under inert atmosphere

In an attempt to understand the role of oxygen during wet etching, the treatments were performed on GaN powder under inert atmosphere. The gas used in our researches were Argon (Ar). Argon has the advantage of being heavier than O_2 thus avoiding rapid O_2 diffusion into the samples.

Before treating the GaN particles, all chemical solutions were degassed *via* Schlenk lines as shown schematically in Figure 33.

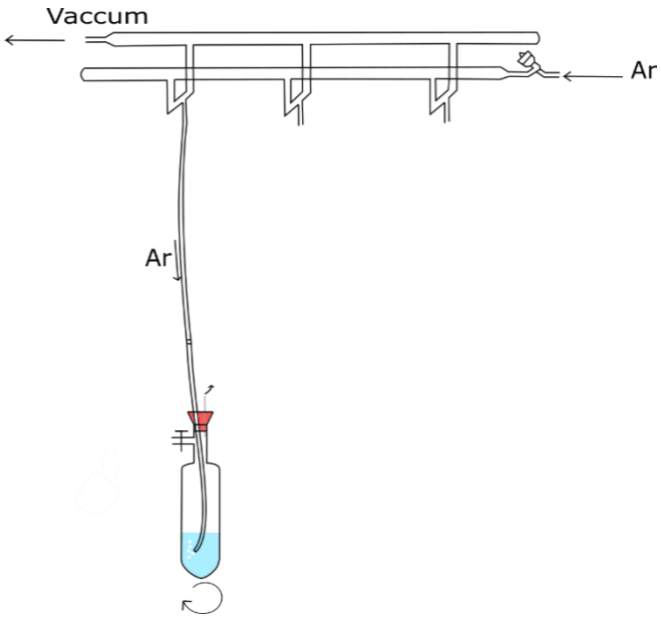

Figure 33. Schlenk line set-up for degassing solutions

Purging was also performed via bubbling Ar into the chemicals. Ar is introduced through a clean long pipe attached to the gas source. The pipe is connected to a needle that enters the Schlenk flask containing the solutions to be degassed through a rubber septum. Another needle is placed in the septum to act as a pressure vent.

Another technique used is called Freeze-Pump-Thaw. Due to the relatively ease of use, this technique was mostly used for sulphur-based solutions and solvents. It consisted of freezing the liquid, evacuating the gas collected in the headspace and allowing the liquid to thaw. The freezing step was achieved by immersing the flask in a cold bath (liquid N_2). Once the solutions were completely frozen, the flask valve was opened to expose the frozen solutions to vacuum during two minutes. Next, the flask was put into static vacuum and removed from the cold bath to allow the frozen solutions to thaw. The freeze-pump-thaw cycles were repeated at least two more times. After the final thawing, the flasks were sealed under Ar.

Once all the solutions were degassed, the treatment of GaN powders under inert atmosphere could be performed. The powder and a stir bar were first placed in a Schlenk flask and put under vacuum, then exposed to Ar gas. The vacuum/Ar cycles were repeated three times to ensure that no oxygen was present in the flask. A pumping step was further performed to ensure that that the flask was under Ar partial pressure. Then the treatments steps could proceed.

The first step consisted of transferring the degassed solution contained in flask A through a thin cannula to flask B, containing the GaN powder (Figure 34, step 1). The valve of flask A is opened and connected to the Ar gas source. Because the pressure difference is $P_A > P_B$ the liquid migrates from flask A to flask B. The suspension in flask B was stirred for several minutes under Ar (Figure 34, step 2). Flask B was then connected to the Ar gas source. Once the treatment was complete, the suspension was transferred to a Schlenk frit under Ar (Figure 34, step 3). The powder contained in the Schlenk frit was then rinsed by introducing a syringe containing degassed de-ionised water. Before the introduction of the syringe into the oxygen-free flask, the syringe was purged by inserting the needle through the septum of the water flask until reaching the headspace. Then the inert gas is drawn up and expelled out of the flask. This step was repeated three times and performed while the water flask was under Ar pressure to avoid any contamination with oxygen.

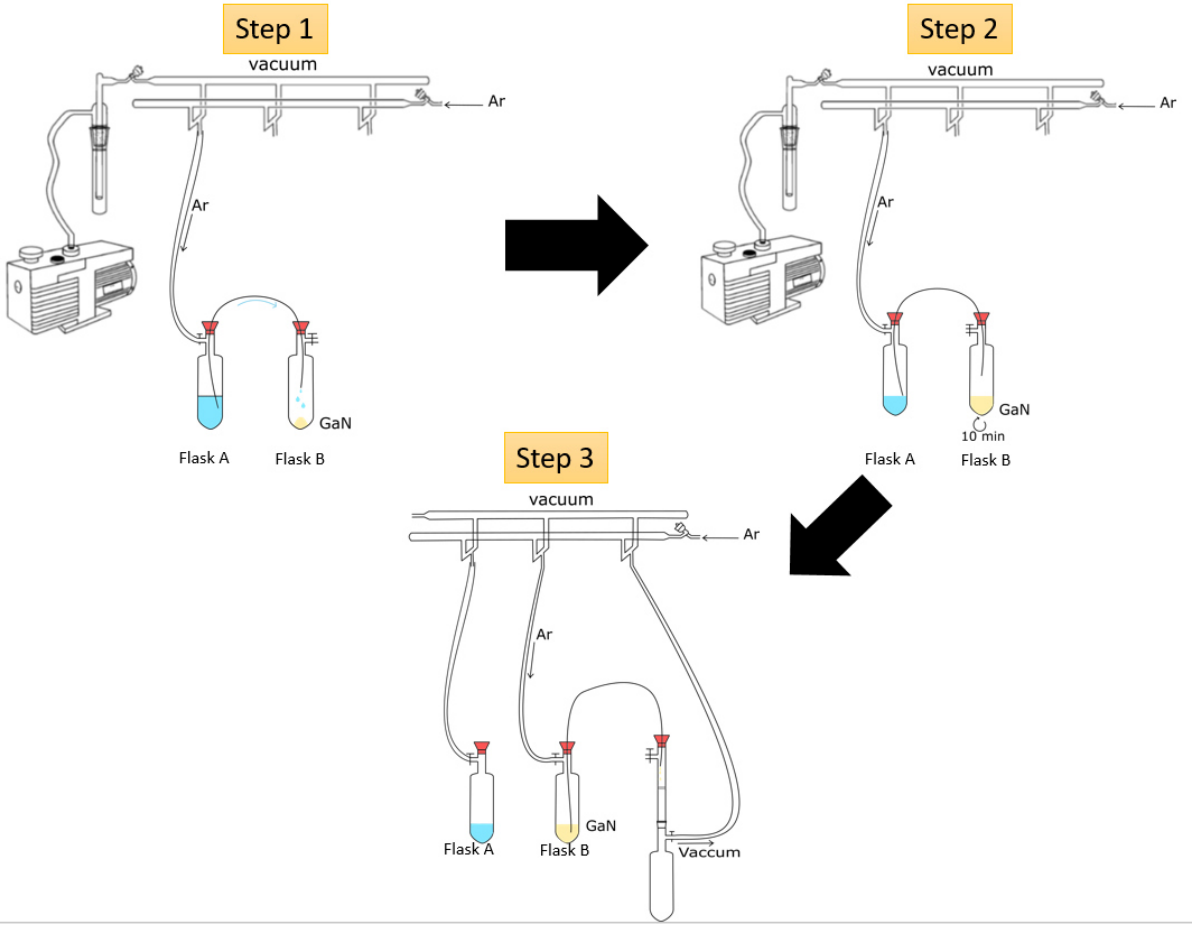

Figure 34. Schlenk line set-up for treating GaN powder under inert conditions

The drying step and loading for analyses were the same as presented in section III.2.2.

III.2.4 Impact of acids and bases on GaN powder under ambient air

The selected chemicals for this study were NH_4OH, $(NH_4)_2S$, H_2O_2, HCl, Citric acid (CA), and H_2SO_4. The choice was based on the initial work performed on GaN wafer (III.1.1). Chemicals which allowed us to obtain a decrease of the equivalent oxide thickness were selected, as well as oxidizing agents such as H_2SO_4 and H_2O_2. The FTIR spectra of the untreated GaN powder and the GaN powders treated with HCl, H_2SO_4, and citric acid are presented in Figure 35.

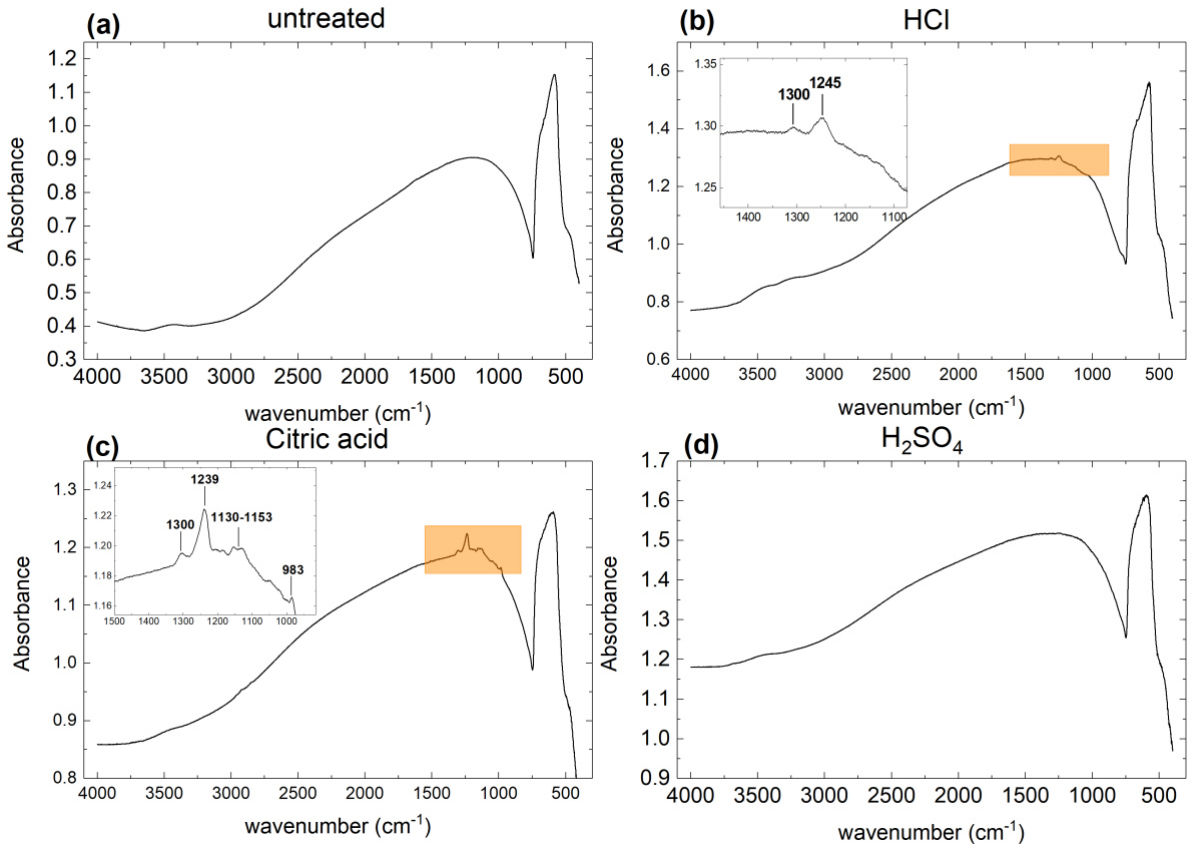

Figure 35. FTIR spectra of the (a) untreated, and (b) HCl, (c) citric acid and (d) H_2SO_4 treated GaN powders

The untreated GaN powder exhibited one major peak at 590 cm^{-1} and a shoulder around 650 cm^{-1} assigned to Ga-N vibration [75, 76] and Ga-O vibrations [75–77], respectively. A large bump from 1000 to 2500 cm^{-1} was also observed and had no particular assignment. Around 3450 cm^{-1} a small peak can be observed and was assigned to adsorbed water [76, 78].

As shown in Figure 35, the treatments had a small impact on the powder. A few peaks were detectable but their intensity was very low. In addition, the presence of Ga-Cl bonds after HCl treatment could not be verified since the related band is found below 400 cm^{-1}. However, after citric acid and HCl treatments (Figure 35 (b) and (c)), the FTIR spectra revealed peaks around 1239-1245 cm^{-1} and at 1300 cm^{-1}. Those two peaks are not reported in the literature for GaN particles. However, the peak found at 1245 cm^{-1} could be assigned to vibrational Si-O-Si [79, 80] coming from the beaker. The FTIR spectrum of the powder treated with H_2SO_4 (Figure 35 (d)) did not exhibit new peaks.

The analysis of the FTIR spectrum of the powder treated with H_2O_2 (Figure 36 (b)) also exhibited small bands at 1244 and 1300 cm^{-1}. Another small band appeared at 1016-1020 cm^{-1} after H_2O_2 and NH_4OH treatments (Figure 36 (b) and (c)). The assignment of this band is reported in the literature to be Ga-OH bending modes [77, 81]. Bands at this positions were observed in the spectrum of synthetized GaO(OH). Additionally, the NH_4OH (Figure 36 (c)) treatment allowed the appearance of a small peak at 3265 cm^{-1} that was reported to be N-H vibrations in adsorbed ammonia $–NH_2$ surface groups [79].

It can be noticed that, like H_2SO_4 treatment, the GaN powder treated with $(NH_4)_2S$ (Figure 36 (d)) showed no band in the spectrum. However, it can be noticed that the band assigned to O-H stretching vibration (around 3450 cm^{-1}) disappeared. This result reinforces the assumption that a tiny amount of sulphur is adsorbed on GaN.

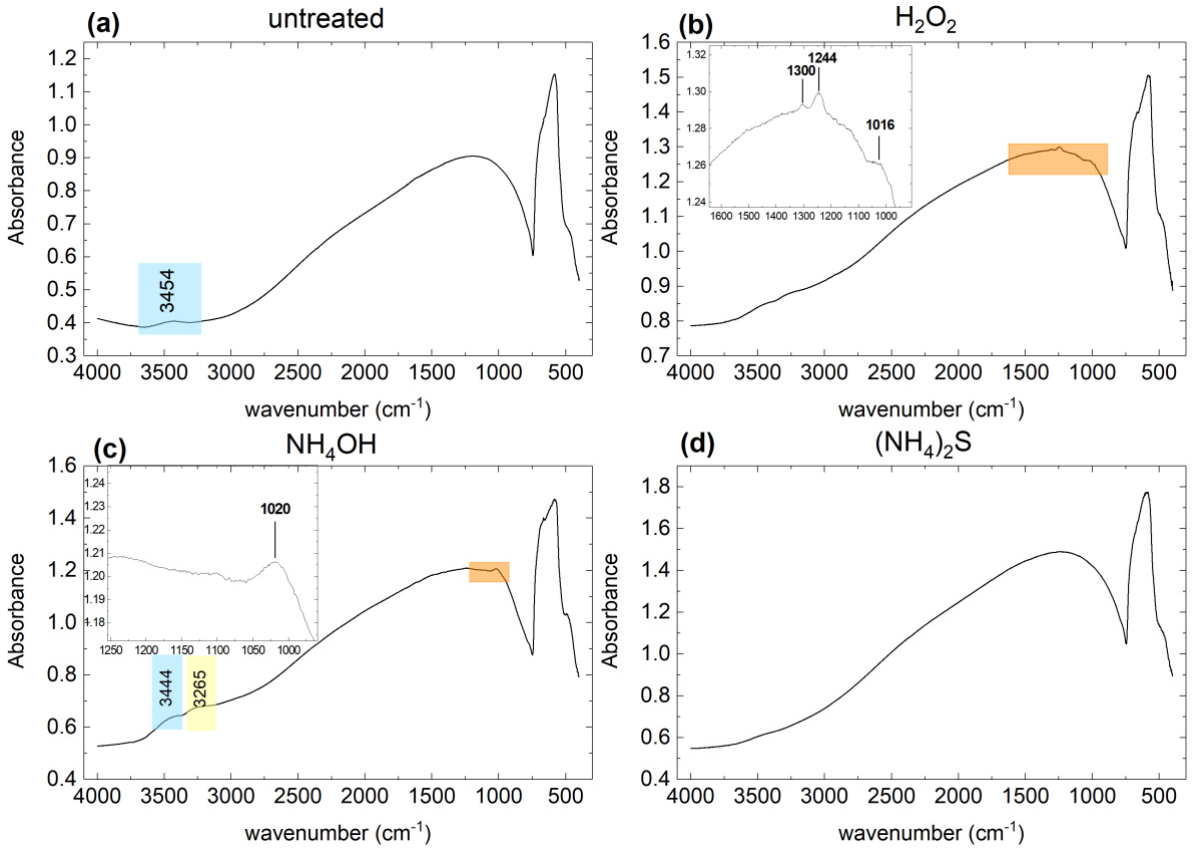

Figure 36. FTIR spectra of the untreated, H_2O_2, NH_4OH and $(NH_4)_2S$ treated GaN powder under ambient atmosphere

While the FTIR measurements showed small modifications, the XPS analyses showed much bigger variations, in particular for the Ga 2 p spectra. The Figure 37 shows the percentage contributions of the Ga 2p peak before and after each treatment. All the spectra exhibited an increase of the Ga-O component. Except for H_2O_2, the powders treated with acids, i.e. HCl, citric acid, and H_2SO_4, clearly led to the highest amount of Ga-O component, with a contribution larger than 50%.

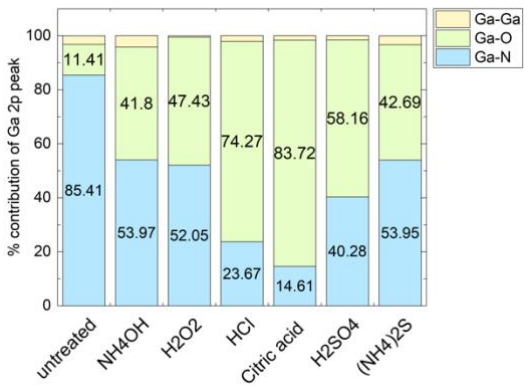

Figure 37. Percentage contribution of the Ga 2p components for treatment under ambient atmosphere

Another notable point is that all Ga 2p peak positions shifted toward higher binding energy (Figure 38), which is in accordance with the fact that Ga atoms were bonded to a more electronegative atom or group of atoms like Cl^-, OH^-, or SO_4^{2-} for example. The peak position shifted by 0.58 eV, 0.75 eV and 0.37 eV for HCl, citric acid, and H_2SO_4 respectively.

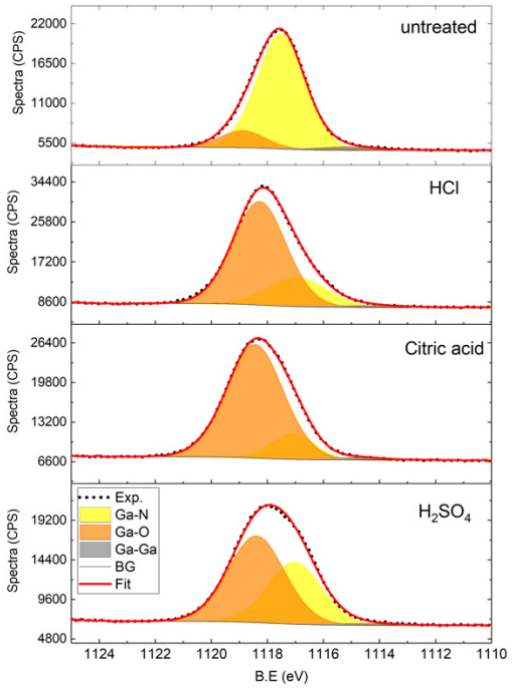

Figure 38. Ga 2p spectra before and after HCl, citric acid, and H_2SO_4 treatment on GaN powder under ambient atmosphere

The Ga 2p signal arising from the GaN powders treated with other etchants, H_2O_2, NH_4OH and $(NH_4)_2S$ are showed in Figure 39. As a reminder, these species presented a higher Ga-N contribution in Ga 2p than HCl, citric acid and H_2SO_4, but still lower than that of the untreated powder. After H_2O_2 treatment, the Ga 2p peak position shifted to lower binding energy (0.34 eV lower). However, after NH_4OH and $(NH_4)_2S$ treatments, the peak position shifted to higher binding energy 0.99 eV for both. The basic solutions exhibited the highest shifts toward higher binding energies.

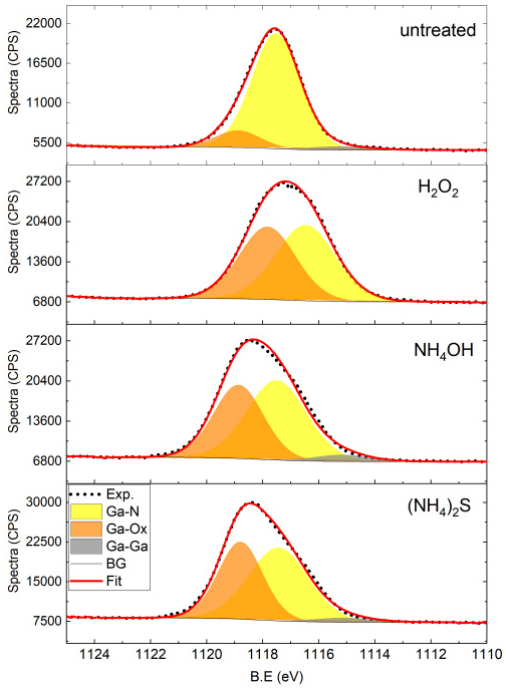

Figure 39. Ga 2p before and after H_2O_2, NH_4OH and $(NH_4)_2S$ treatment on GaN powder under ambient atmosphere

The Ga 3d spectra are shown in Figure 40 (a) and the deconvolution parameters were slightly different from the deconvolution used when the spectra were acquired in the pAR-XPS equipment. Due to a lower resolution, the Ga $3d_{5/2}$ and the Ga $3d_{3/2}$ doublet was used and was assigned to the Ga-N bond. The doublets were 0.45 eV apart for all spectra. Furthermore, the N 2s core-level positioned at 17 eV had to be added to deconvolute the spectra. Based on previous works done at LETI, the Ga-O component was 1.2 eV apart from the Ga $3d_{5/2}$ peak. The increase of the Ga-O component can be seen on the Ga 3d peaks as well (Figure 40 (a)). The comparison of the Ga-O component of the Ga 2p peak and the Ga 3d peak of the untreated powder exhibited a smaller amount of Ga-O contributions in the Ga 2p spectrum. Since the Ga 2p signal usually gives information on the 2 first nm, this means that more oxygen were found in the bulk than at the surface. However, after HCl, citric acid and H_2SO_4 treatments the amount of Ga-O contribution was clearly higher for the Ga 2p peak, which means that electronegative atoms or groups of atoms as discussed previously were mainly located at the surface of the particles. It can be noticed that the Cl 2p peak was barely distinguishable, therefore, there was a strong possibility that the HCl treatment acted as an oxidizing agent on the GaN powders. Unfortunately, no consistent quantification was possible since the N 1s spectra could not be deconvoluted due to a large contribution of the overlapping Gallium Auger electrons.

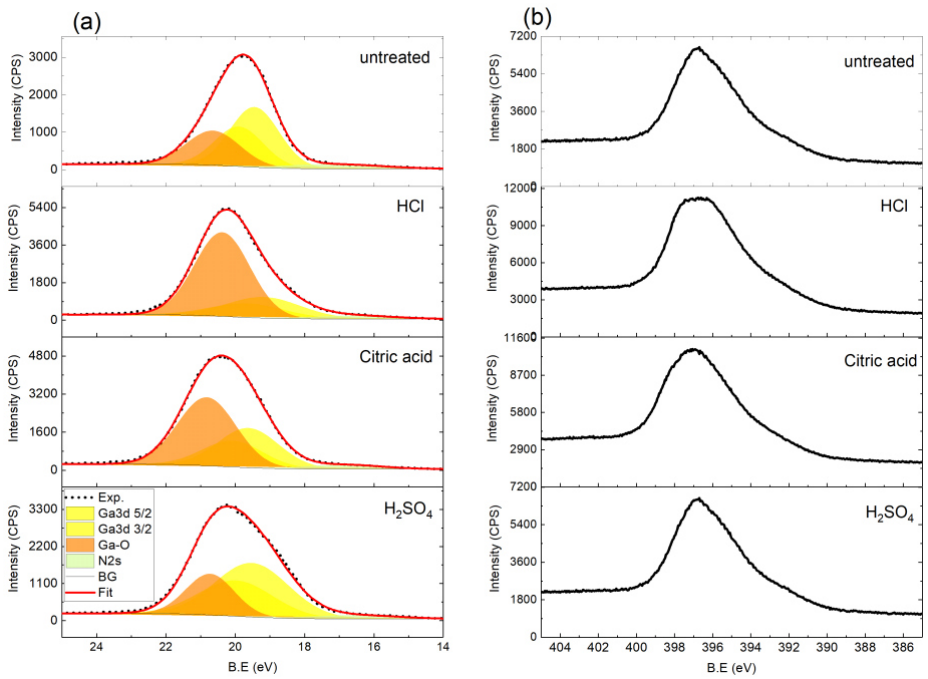

Figure 40. (a) Ga 3d and (b) N 1s spectra before and after HCl, citric acid and H_2SO_4 treatment on GaN powders under ambient atmosphere

However, after HCl and citric acid treatments, the N 1s spectra showed a broadening (Figure 40(b)). This broadening suggested that the nitrogen atoms might be bonded to oxygen or hydrogen, forming NO_x or NH_2/NH_3 groups. For the HCl treatment, the presence of N-H bonds could be confirmed with the FTIR spectra where a small peak positioned at 3250 cm^{-1} and assigned to N-H vibrations were detected (Figure 35 (b)).Concerning the H_2SO_4 solution, both XPS and FTIR spectra showed that no specific atoms or groups were present at the surface. Moreover, the aspect of the N 1s spectra after H_2SO_4 treatment was similar to that of the untreated powder, therefore the nitrogen bonds were not affected by the acid treatment. However, the Ga 2p suggested that an electronegative group could have adsorbed at the surface of the particles, however no peak related to the presence of SO_4^{2-} nor clear S 2p peak were detected. As suggested before for XPS analyses of the GaN wafers, the amount of sulphur could be below the detection limit.

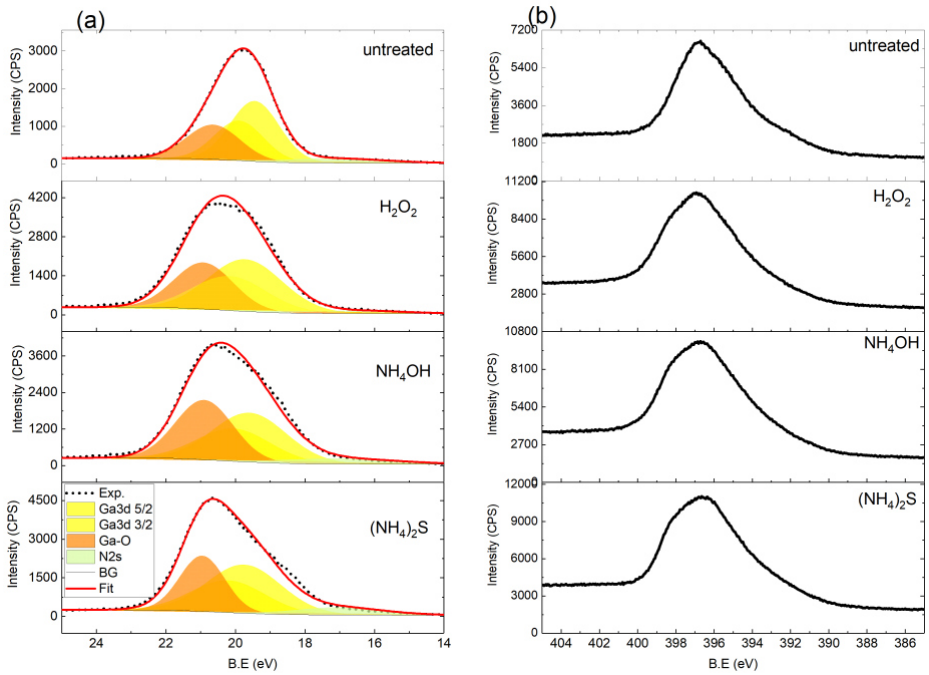

Figure 41. (a) Ga 3d spectra and (b) N 1s spectra before and after H_2O_2, NH_4OH and $(NH_4)_2S$ treatments on GaN powder under ambient atmosphere

The analyses of the Ga 3d spectra of the GaN powders treated with H_2O_2, NH_4OH and $(NH_4)_2S$ are shown in Figure 41 (a). As observed for previous treatments, the Ga-O contributions were higher for the Ga 2 peaks compared to the Ga 3d peak which means that the effects of the treatment were mainly located at the surface of the particles. The aspect of all the Ga 3d peaks changed after treatments. These changes were also visible on the N 1s peaks (Figure 41 (b)). Indeed, as observed for the other treatments presented in the previous paragraph, the N 1s signal was broadened which suggested the formation of NO_x and N-H in the case of H_2O_2 and NH_4OH treatments, in agreement with the band observed in the FTIR spectrum. The $(NH_4)_2S$ treatment clearly indicated the appearance of new bonding states, suggesting thus that something was adsorbed at the surface, although, like the H_2SO_4 treatment, no S 2p peaks clearly were detected. Nevertheless, the shift observed on the Ga 3d peak revealed the presence of electronegative species present at the surface, and the presence of S^{2-} could not be out ruled.

Figure 42 exhibits the evolution of the O 1s peak before and after the treatments. It revealed that the lowest intensity was obtained after the $(NH_4)_2S$ treatment, which was in agreement with the assumption that a little amount of sulphur, in the form of S^{2-}, may be adsorbed at the surface of the GaN particles. In the same way, the intensity of the O 1s peak was slightly lower after the H_2SO_4 treatment compared to that of the untreated particles. The difference with the $(NH_4)_2S$ example could be explained by the adsorption of SO_4^{2-}.

On the contrary, all the other treatments led to an increase of the intensity. The highest increase was obtained after H_2O_2 treatment, and came with a shift toward lower binding energies. Therefore, the increase of intensity of the O 1s peak might be correlated with the adsorption of oxygen. In the case of citric acid, this increase can be related to the adsorption of carbonyl groups.

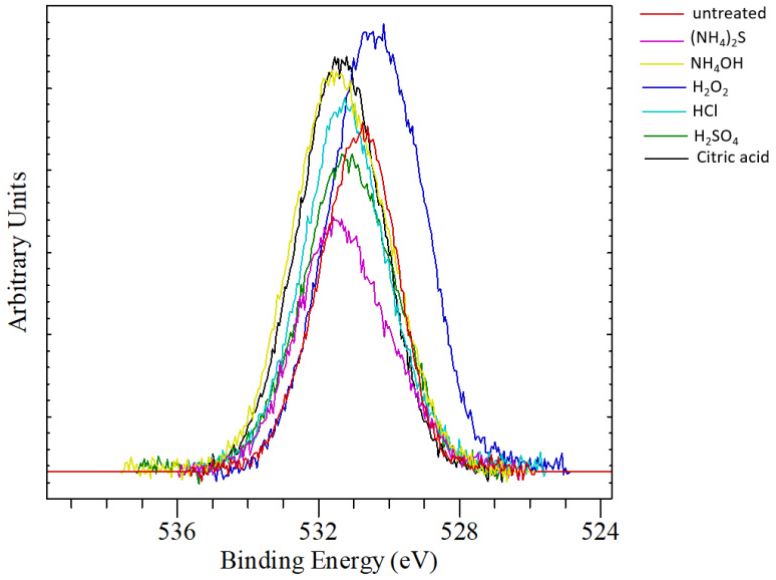

Figure 42. Evolution of the intensity of the O 1s peak after treating the GaN powders with acids and bases

Unlike the GaN wafers, the GaN powders reacted differently with the chemicals. Indeed, all treatments indicated a decrease of the percentage of Ga-N bonding contribution in favour of an important increase of the Ga-O bonding contribution. Although no major impact was recorded *via* FTIR analyses, combining the investigations *via* XPS led to the following conclusions. The increase of the Ga-O contributions was attributed, in the case of NH_4OH and H_2O_2 treatments, to the formation of N-H, N-O_x, and Ga-OH bonds. For the HCl treatment, this was assigned to the adsorption of chloride ions, as observed on the GaN wafer. No specific groups were assigned for the increase of the Ga-O contribution after citric acid treatment. However, the increase of the O 1s peak suggested the possible presence of carbonyl groups. Concerning the sulphur-based treatments, H_2SO_4 and $(NH_4)_2S$, the FTIR and XPS analyses led to the conclusion that a small amount of sulphur was present, since the spectra exhibited the lowest O 1s intensity, and no band related to water was present in the FTIR spectra. The sulphur detected might be in the form of SO_4^{2-} and S^{2-}, after H_2SO_4 and $(NH_4)_2S$ treatments, respectively.

For all the treatment performed under ambient atmosphere, the comparison between the Ga 3d and the Ga 2p peaks revealed that the modification of the chemical states was more located at the surface of the particles.

III.2.5 Impacts of acids and bases on GaN powder under Ar

The role of oxygen during the immersion of the particles in the different solutions was also investigated, by performing the treatments under Argon as previously described. As for the experiments under ambient atmosphere, GaN powder treated by sulphur-based chemicals did not exhibit any absorption band under both inert and ambient atmosphere. However, the spectra of GaN treated by citric acid, H_2O_2, HCl and NH_4OH treatments under Ar revealed small absorption peaks previously assigned to Si-O-Si vibrations around 1240 cm^{-1} as shown in Figure 43. The peak at 1240 cm^{-1} was not present in the case of NH_4OH under ambient air. Since commercial NH_4OH solutions are mainly composed of dissolved NH_3 gas in water, after degassed solution would have lost all the NH_3 during the cycling and so only contained a large amount of OH groups that can easily attack the beaker. Therefore, no band related to N-H vibration, around 3265 cm^{-1}, was found when GaN was treated under inert conditions. However, after NH_4OH a new band appeared around 981 cm^{-1} that could be assigned to Ga-O bonds. No band related to N-H vibration was found after HCl treatment either. Concerning citric acid, the band recorded around the 1133 – 1153 cm^{-1} region was no longer visible when the treatment was performed under Ar. The peak around 1016 – 1020 cm^{-1} was no longer present when powders were treated with NH_4OH and H_2O_2.

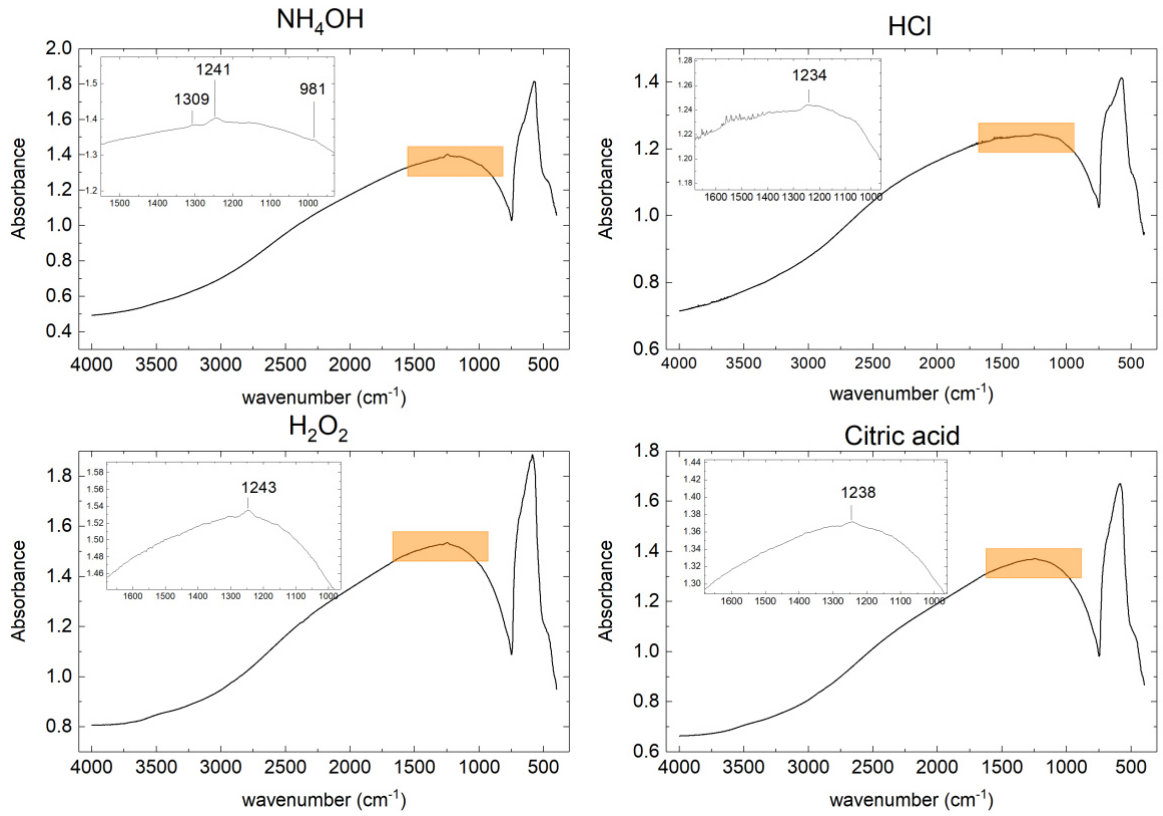

Figure 43. FTIR spectra of citric acid, H_2O_2, HCl and NH_4OH treated GaN powder under inert atmosphere

Figure 44 shows the XPS Ga 2p spectra of the untreated GaN powder and after treatment with NH_4OH, H_2O_2, HCl and citric acid. The analysis of the Ga 2p spectra showed a shift toward higher binding energies of 0.75 eV and 1.0 eV after NH_4OH and HCl treatments respectively. This shift could be attributed to the increase of the Ga-O component. The percentage contribution of the Ga-O component was 42 % and 81 % for NH_4OH and HCl respectively. Compared to the experiment performed under ambient atmosphere, the percentage of the Ga-O component did not change in the case of the NH_4OH. This could therefore be attributed to the possible binding of Ga with oxygen, since no band related to Ga-OH were detected in the FTIR spectra. In the case of HCl, the Ga-O component had raised up to 81 %, while it was 74 % under ambient conditions.

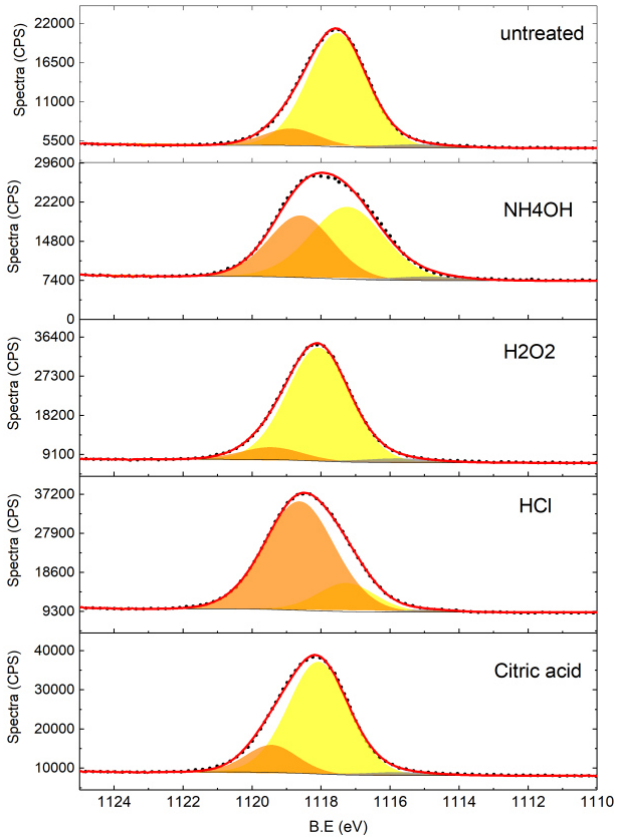

Figure 44. Ga 2p spectra of untreated, NH_4OH, H_2O_2, HCl and citric acid treated GaN powder under Ar

This increase could be related to the presence of chloride detected at the surface of the powder (Figure 45). Due to the intensity of the Cl 2p peak of the GaN treated under inert atmosphere, it could be deduced that a larger amount of chloride groups was absorbed.

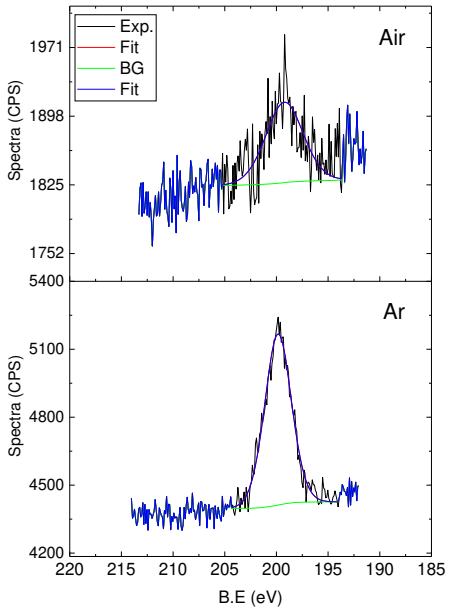

Figure 45. Cl 2p spectra of GaN powder treated by HCl under ambient atmosphere (Air), Argon atmosphere (Ar)

Concerning H_2O_2, and citric acid, the percentage of the contribution of Ga-O was lowered when the treatment were done under inert conditions compared to ambient air (Figure 38, Figure 39 and Figure 44) . After H_2O_2 treatment, the Ga-O contribution was 8.5 % vs 36 % under ambient air and the Ga-O contribution was 16 % under Ar versus 88 % under air for citric acid. Surprisingly, the amount of Ga-O decreased after H_2O_2 treatment under inert atmosphere compared to that of the untreated sample which was 12 %.

The analyses of the Ga 3d spectra are shown in Figure 46 (a). Once again, the Ga-O contribution were more important on the Ga 2p peaks, except after the citric acid treatment. The difference indicated that the bulk was affected by the treatment.

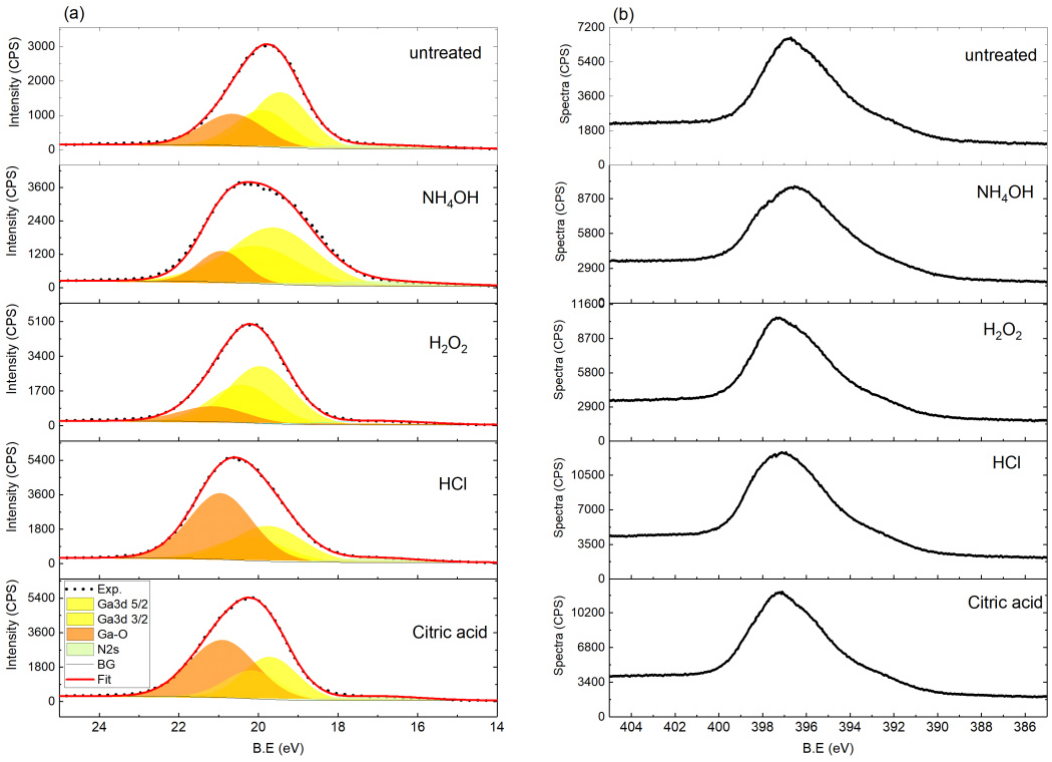

Figure 46. (a) Ga 3d spectra and (b) N 1s spectra before and after NH_4OH, H_2O_2, HCl, citric acid treatments on GaN powder under inert atmosphere

The N 1s spectra (Figure 46 (b)) of the powder treated with NH_4OH and HCl reinforce the assumption that electronegative atoms were present at the GaN surface. Indeed, a shoulder could be observed at higher binding energies. No shoulder could be observed after H_2O_2 and citric acid treatments.

In conclusion, without the presence of oxygen in the atmosphere or dissolved in the solutions, H_2O_2 and citric acid had no particular impact on the GaN particles. The changes observed after HCl, and NH_4OH were attributed to the presence of chloride and OH^- groups

adsorbed at the surface of the particles. The results showed that in order to adsorb more chloride ions at the surface, oxygen has to be eliminated, since chlorides and oxygen are in competition. The XPS analyses did not allow bringing to light the assignment of the 1245 cm^{-1} peak.

In order to better understand the adsorption of atoms at the surface of GaN and to the possible passivation by sulphur atoms the next paragraph deals with the adsorption of an alkanethiol reagent.

III.2.1 Investigation of sulphur adsorption on GaN

The difficulty to observe a peak related to the presence of sulphur on GaN *via* pAR-XPS, gave an additional interest in the experiments performed on GaN powders, which possess a higher surface area and enable the use of other characterisation techniques. Note also that various crystalline planes are exposed, increasing the chance to detect sulphur. Since only a very few publications show the XPS peak S 2p, we decided to replace $(NH_4)_2S$ by 1-octanethiol. In this manner, the presence of 1-octanthiol could be indirectly suggested by the presence of carbon, and by a higher amount of carbon at the GaN surface via FTIR and XPS analysis respectively. In a study, Bermudez investigated the adsorption of vapour phase 1-octanethiol on GaN (0001) wafer and revealed a saturation coverage of 0.28 monolayers [83]. However, he could not determine the nature of the bond between gallium and sulphur.

Due to the low specific surface of the GaN powder used, we increased the time of treatment. The duration time was initially set on 10 minutes in order to be in line with the experiments performed on GaN wafer.

First, the experiments were conducted under ambient atmosphere. Since the impact of the chemicals on the GaN powder was very little for 10 minutes of treatments, the treatment duration was also set to 2 hours.

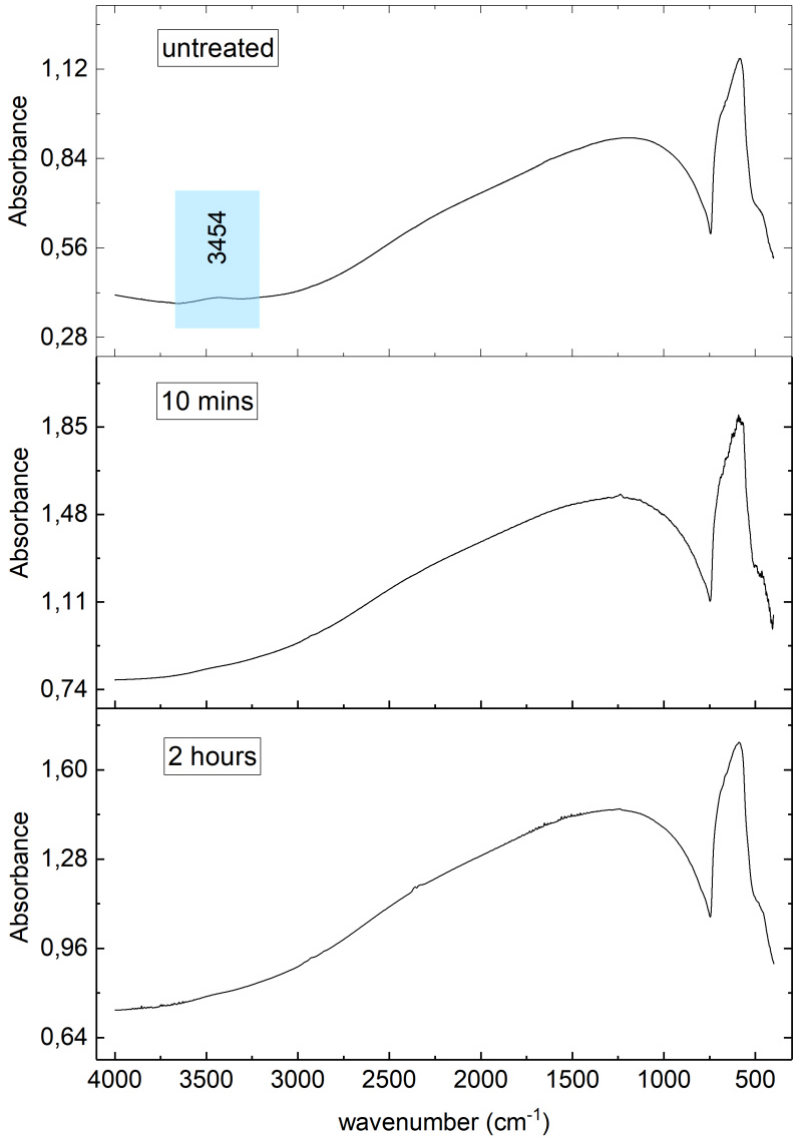

Figure 47. FTIR spectra of untreated GaN powder and GaN powder treated by 1-octanethiol for 10 minutes and 2 hours under ambient atmosphere

As for the other sulphur-based treatments, for H_2SO_4 and $(NH_4)_2S$ (Figure 35 and Figure 36, respectively) no band related to water was detected after treatment for both 10 minutes and 2 hours treatment (Figure 47). However, no evidence of carbon was detected.

Based on the observations made by FTIR and pAR-XPS analyses on both GaN powder and GaN wafer treated by sulphur-based treatments, there is a strong possibility that a very small amount of sulphur was at least adsorbed. Indeed, no band related to water was detected

after treatment, and the review study on a GaN wafer revealed a lower carbon level for all sulphur-based solutions (section III.1.1). Therefore, to comprehend how sulphur could bond to GaN and detect its presence, GaN powder was treated for 4 hours under inert conditions and analysed by FTIR and XPS, still under inert atmosphere. The FTIR spectrum of the 1-octanethiol treated powder is shown in Figure 48.

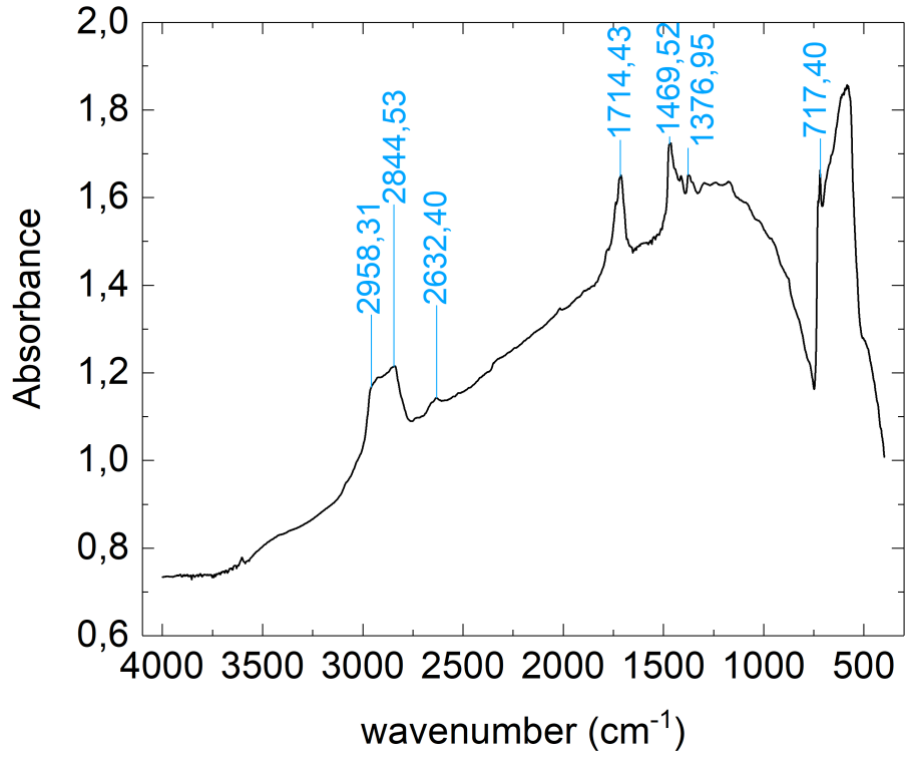

Figure 48. FTIR spectrum of GaN powder treated by 1-octanethiol under inert conditions for 4 hours

Here there was a significant change in the FTIR spectrum. Two peaks were detected at 2925 and 2844.53 cm^{-1} and were assigned to symmetric and antisymmetric stretching of -CH_2 and –CH_3 groups of 1-octanethiol [84] [85]. The presence of a weak peak positioned at 2632.40 cm^{-1} attributed to S-H stretching indicated the presence of free unreacted thiol. Therefore, there is a small probability that sulphur was chemisorbed to gallium *via* a covalent bond. However, it is more likely that 1-octanethiol was physisorbed on GaN. The region between 1430 and 1380 cm^{-1} corresponds to symmetric vibration of –CH_3 groups and scissor bonding vibration of –CH_2 groups [85]. The peak positioned at 717.40 cm^{-1} could be assigned as C-S vibration.

Although the FTIR analyses showed evidence of 1-octanethiol on GaN particles, the survey spectrum from XPS analysis did not reveal peaks related to sulphur at the surface as shown in Figure 49.

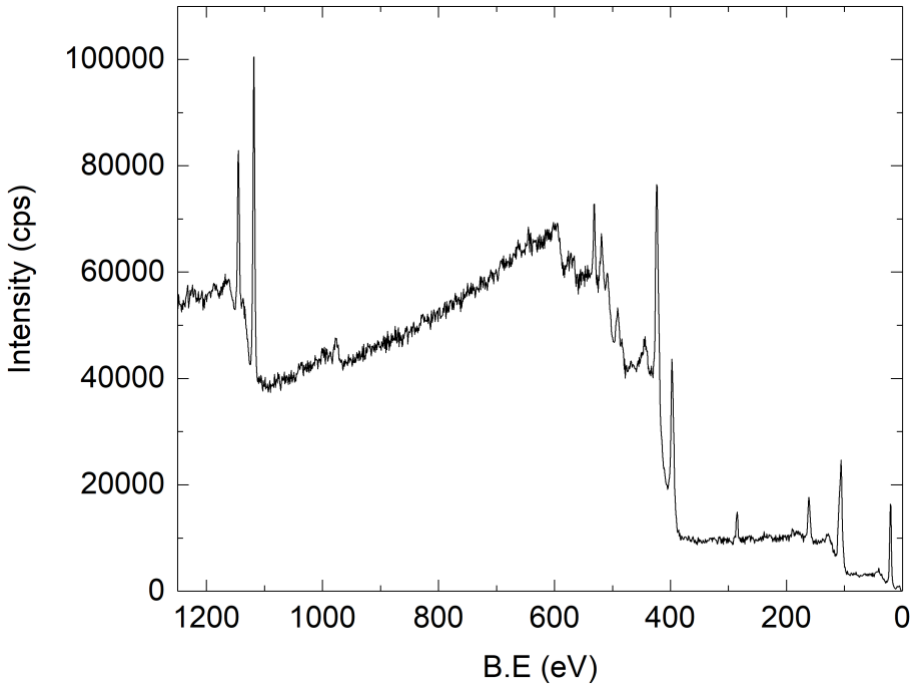

Figure 49. XPS survey spectrum of GaN power treated by 1-octanethiol under Ar for 4 hours

However, the S 2p, which overlaps the Ga 3s peak, was not clearly detected (Figure 50 (a)), and it was not found in the spectrum of the GaN powder treated by H_2SO_4 for 10 minutes under Ar either (Figure 50 (b)). Nevertheless, the S 2p region of the latter revealed a peak assigned to SO_4^{2-} adsorption. Thus, there was some amount of sulphur at the surface, even if no well defined S 2p was revealed.

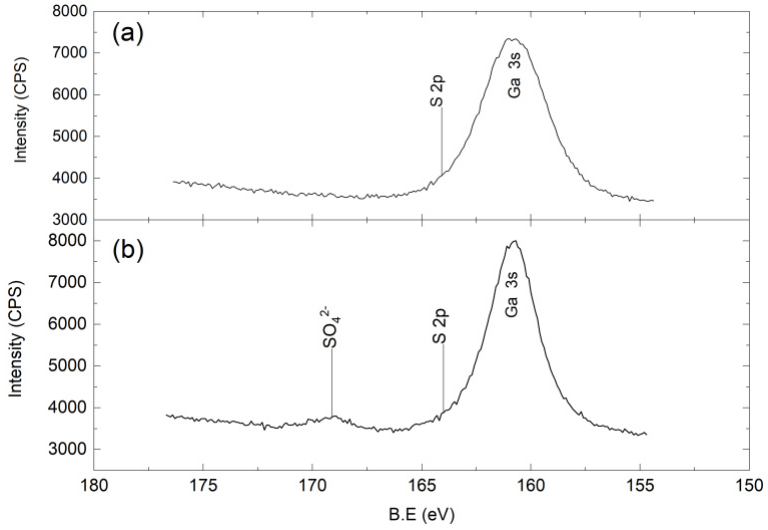

Figure 50. XPS spectra of GaN treated with (a) octanethiol for 4 hours and (b) H_2SO_4 for 10 minutes under Ar

The investigation on the sulphur adsorption revealed that sulphur-based species could adsorbed on the surface of GaN. However, the presence of the oxygen in the solution tends to hinder their adsorption and the presence of oxygen in the atmosphere facilitates their desorption after treatment.

III.3. Conclusions

An initial work was performed on a GaN on silicon wafer in which a systematic study of chemicals commonly used in the microelectronic industry was conducted. The evaluation of the impact of each chemical on GaN surface chemistry was performed by pAR-XPS which revealed a few changes. Indeed, oxidizing agents such as H_2SO_4 and Caro acid did not induce an increase of oxygen content. However, HCl, H_3PO_4, citric acid and $(NH_4)_2S$ acted as etchants at the surface of GaN. As those chemicals decreased the estimated equivalent oxide thickness. The lower oxide thickness compared to that observed on untreated GaN is related with the fact that those chemicals leave adsorbates on the GaN surface, preventing oxidation. Except for $(NH_4)_2S$, those adsorbates were all detected by pAR-XPS. The particularity of sulphur-based treatments lies in the fact that they all exhibited a lower amount of carbon.

Based on the little impact of these chemicals on GaN wafer, a systematic review was also performed on GaN powders to better understand the interactions between the etching reagents and the GaN surfaces using complementary FTIR analyses. The experiments were conducted under ambient air atmosphere and under Argon. The investigations on GaN powders under ambient atmosphere exhibited a different result if compared to the same treatments performed on GaN wafers. This could be explained by the fact that several orientations are exposed on GaN particles, whereas for the GaN wafers, only a few planes are accessible. No etching effects were recorded with FTIR and XPS. On the contrary, the deconvoluted Ga 2p spectra showed an increase of the Ga-O component after all treatments. Indeed, due to the accessibility of all the orientations, the reactivity of the GaN is thus increased. While the solutions induced a reduction of the Ga-O contribution, an increase was observed with the powders. Therefore, it can be suggested that due to the variation of the planes available on powders, the reactions led to a larger amount of OH^-, Cl^-, SO_4^{2-} , S^{2-} at the surface of the particles. The adsorption of sulphur could be deduced from a decrease of the O 1s peak intensity after H_2SO_4 and $(NH_4)_2S$ treatments.

For experiments run under inert atmosphere, only HCl and NH_4OH treatments revealed an important increase of the Ga-O contribution. This increase was attributed to the adsorption of Cl^- and OH^- groups respectively.

We also studied the reaction occurring when treating GaN with 1-octanethiol in order to decipher the nature of the interactions between GaN and sulphur containing compounds with the putative formation of Ga-S bonds. The experiments under ambient atmosphere did not lead to significant changes on the FTIR spectra except from the fact that no adsorbed water was detected. However, the FTIR spectra of GaN powder treated with 1-octanethiol under Ar revealed the presence of carbon on the surface of the particles. However, a small peak attributed to S-H vibration suggested that thiol molecules were likely physisorbed on the GaN surface. Moreover, XPS measurements did not reveal a well defined S 2p peak. The presence of a peak assigned to SO_4^{2-} for GaN powders treated by H_2SO_4 and the absence of a well-defined S 2p peak due to the overlapping Ga 3s peak, allowed us to conclude that a small amount of sulphur was physisorbed on the surface.

The different results obtained between the GaN wafer samples and the GaN particles came from the polycrystalline nature of the powders. Although the specific surface of the powders allowed to get closer to the surface of the wafers, the FTIR measurements was not an appropriate technique due to poor signals.

Another point to highlight is the possible SiO_2 contamination coming from the use of beaker made of borosilicate glass. The use of polytetrafluoroethylene (PTFE) beaker might be more appropriate for the experiment under ambient atmosphere, and a subsequent FTIR measurement might confirm or not this assumption.

Chapter IV - Destabilising the surface of GaN by dry techniques

The initial systematic review, with chemicals commonly used in the microelectronic and the encouraging results of the H_3PO_4 suggested that the temperature had a role to obtain significant changes on the surface chemistry. Consequently, we oriented our researches on methods that could bring a significant amount of energy in order to break the Ga-N bonds of the surface. On one hand, the destabilised surface of GaN yielded by dry treatments would be less inert when exposed to wet etching treatments. On the other hand, this method could induce the formation of oxides that could be easily removed by wet treatments. This way, we could perform some sort of digital etching by oxidising the surface with dry techniques and remove the oxide with wet treatments.

The dry techniques investigated during my PhD were LASER annealing and Rapid Thermal Processing (RTP) with the impact of both types of annealing on the surface chemistry and on the morphology investigated. We investigated as-grown GaN samples, and dry-etched GaN samples. For the LASER annealing study, the dry etching was an ICP-RIE plasma and for the RTP annealed samples the etching processes included an ICP-RIE, followed by an Atomic Layer Etching (ALE) and a stripping sequence. More details will be given in the following paragraphs.

IV.1. Nanosecond LASER annealing

IV.1.1 Equipment and annealing conditions

The LASER anneals were performed on an industrial LT-3100 tool from SCREEN. The XeCl LASER source was developed by SCREEN-LASSE. The wavelength was at 308 nm with a FWHM of 160 ns pulse duration. A schematic of the tool is present in Figure 51.

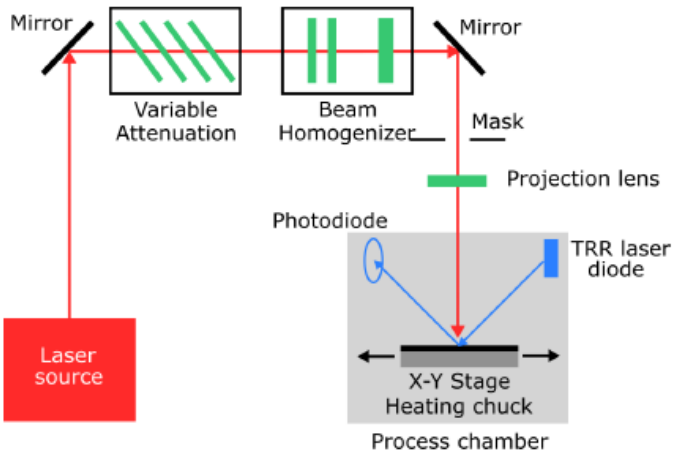

Figure 51. Schematic representation of a typical optical line for a nanosecond laser annealing [86]

The projected beam onto the surface was shaped by a mask. The mask used in our experiments was 15x15 mm^2. During the anneals, single or multiple laser shots can be performed at the same location. Furthermore, unless stated otherwise the anneals were performed under controlled N_2 atmosphere and at room temperature.

Right after the anneals, the GaN wafer was directly loaded to the vacuum system of the pAR-XPS.

IV.1.2 GaN samples

The GaN substrate used for this study was a single wafer for which half has been dry-etched and the other half was as-grown. Indeed, to get closer to the transistor process fabrication, we investigated the impact of LASER annealing on a dry-etched surface. Figure 52 shows the cartography of the wafer before the annealing experiment. Each number corresponded to specific conditions and energy that will be discussed in the following paragraph.

Figure 52. Shots pattern used in the experiments

Furthermore, the LASER anneals were performed on an industrial equipment that can only treat full-sheet wafers therefore this method allowed to load and analyse several LASER annealing conditions at the pAR-XPS at once.

The dry-etching process of half-part of the wafer included a Cl_2/BCl_3-based chemistry ICP-RIE plasma, at high bias voltage of 237 V. The etching depth was about 300 nm. Figure 53 shows the stacking of the layers of the GaN substrates.

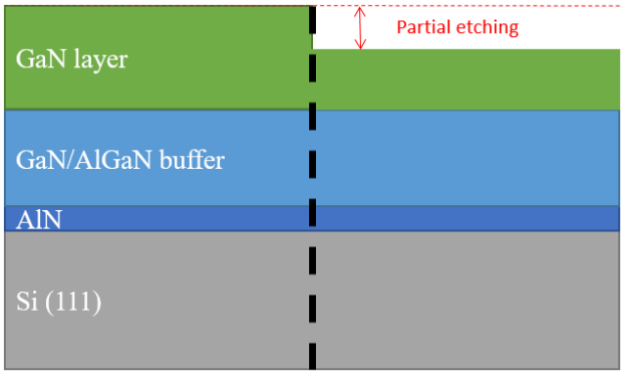

Figure 53. Layer stack of the GaN wafer used for the LASER annealing investigations

IV.1.3 Energy selection

The first step of this study consisted in determining the energy required in order to destabilise the Ga-N bonds of the surface without degrading the surface morphology, for example, by creating N-vacancies. We investigated the required energy necessary for the material to start melting and this energy was called "melt point" in the manuscript. To do so, we performed cumulative shots on a specific area on the wafer. The energy of the shots was gradually increased from 0.3 J.cm^{-2} with a step of 0.1 J.cm^{-2}. The melt point was found to be around 1.30 J.cm^{-2} and 1.40 J.cm^{-2} for the as-grown GaN and the dry-etched GaN, respectively.

Next single shots were performed on different areas of the wafer. We started with shots slightly higher than the melt point at 1.50 J.cm^{-2} then decreased the energy with a step of 0.05 J.cm^{-2}. The SEM images in Figure 54 show the evolution of the morphology with a reduction of the shots energy from 1.50 to 1.00 J.cm^{-2}. The full range SEM images can be found in the Appendix section (A- 1 and A- 2).

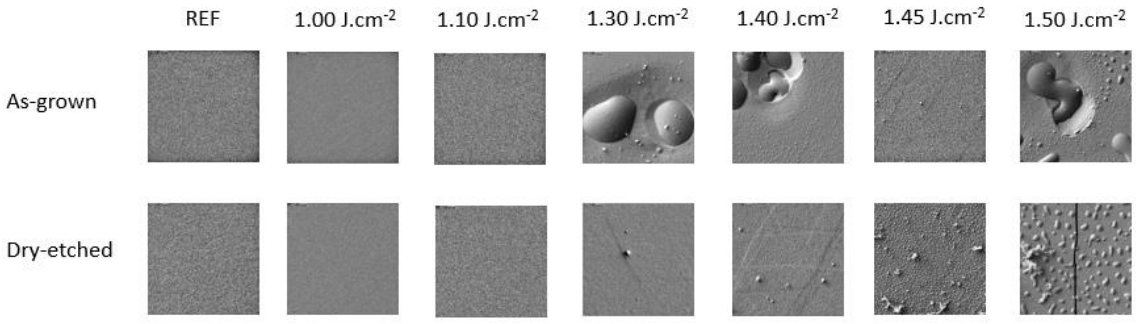

Figure 54. SEM images (2x2 µm) after laser shots from 1.50 to 1.00 J.cm^{-2} on as-grown GaN (top line) and dry-etched GaN (bottom line). REF stands for GaN surface prior to laser annealing

When the energy of the shot was set at 1.50 J.cm^{-2}, 0.20 J.cm^{-2} higher than the melt point determined previously for the as-grown GaN, some droplets were observed. The nature of the

droplets could have been determined by EDX, but there is a strong probability that the droplets were composed in majority of gallium, since nitrogen tends to desorb more easily. Laser shots at 1.40 and 1.30 J.cm^{-2} led to the emergence of triangular structures, which might be due to large thermally induced strain. Large droplets were seen till decreasing the energy to 1.30 J.cm^{-2}, which was the original melt point energy found for the multi-shot test. A few particles are also visible and these were probably coming from neighbouring shots. Around 1.10 and 1.00 J.cm^{-2}, the atomic steps were visible, which indicated a non-degraded surface.

For the dry-etched surface (Figure 54, bottom line), droplets were also seen at 1.50 J.cm^{-2}, but smaller than those found on the as-grown GaN. Another difference was the emergence of cracks and particles on the dry-etched GaN after laser annealing. A few droplets could be found on the surface at 1.45 and 1.40 J.cm^{-2} which was consistent with the value of the melt point found previously. After shots of 1.40 and 1.30 J.cm^{-2}, triangular structures were also visible on the dry-etched surface as for the as-grown sample. At 1.10 and 1.00 J.cm^{-2}, no more particles were detected and the surface showed a similar morphology too that prior to laser annealing.

The screening of energy shots on these two kinds of GaN surfaces, i.e. as-grown and dry-etched, illustrated that each surface reacted differently toward laser annealing. Indeed, as-grown GaN had a melt point at a lower energy than the dry-etched GaN surface. However, at 1.00 J.cm^{-2}, both surfaces exhibited a morphology similar to that of the surface prior to laser annealing.

IV.1.4 Influence of the energy on the surface chemistry

Having determined the melt point and evaluated the morphological impact of the energy of the laser shots, we chose the energies for detailed surface investigations. Since our purpose was only to destabilise the Ga-N bonds of the surface, we selected the highest and the lowest energy where little degradation was detected on the SEM images i.e. 1.30 J.cm^{-2} and 1.00 J.cm^{-2} for both surfaces. Figure 55 shows the evolution of the Ga 3d spectra before and after laser annealing at 1.0 and 1.3 J.cm^{-2} for both surfaces.

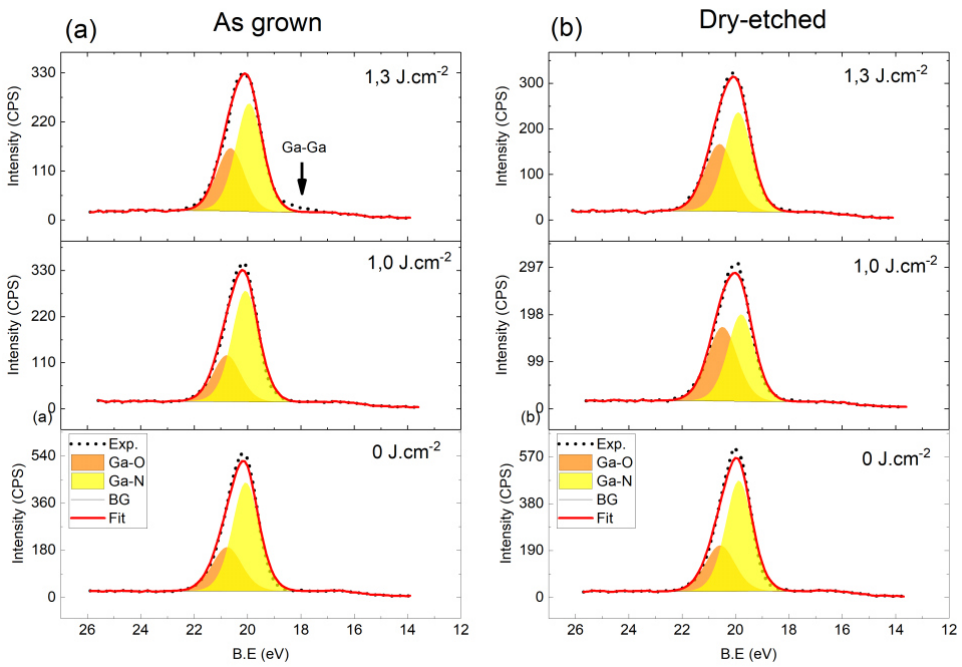

Figure 55. Ga 3d spectra (a) as-grown GaN and (b) dry-etched GaN before and after laser annealing at 1.0 eV and 1.3 J.cm^{-2}

For both surfaces, no significant shift of the peaks was recorded. However, the Ga-O component significantly increased after a shot at 1.3 J.cm^{-2} for the as-grown GaN. Moreover, a third contribution has been added at the lower binding energy related to metallic Ga-Ga bonds. This was in agreement with the SEM images where droplets were observed at this energy (Figure 54, top line). Therefore, the droplets could be attributed to metallic gallium formed at the surface after laser annealing. In the case of the dry-etched GaN, the Ga-O component started to increase at 1.0 J.cm^{-2}, and no presence of Ga-Ga bonds could be detected. This is also coherent with the SEM images (Figure 54, bottom line). The increase of the Ga-O component also came with the increase of a component on the N 1s spectra noted “Ga Auger” (Figure 56).

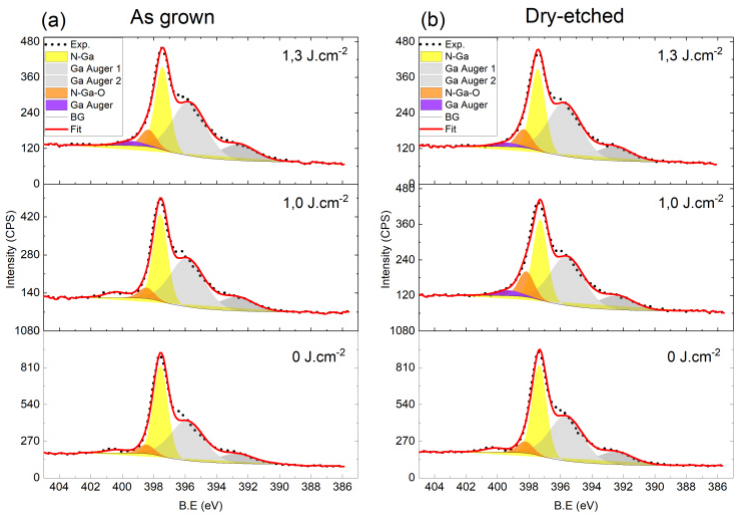

Figure 56. N 1s spectra (a) as-grown GaN and (b) dry-etched GaN before and after laser annealing at 1.0 and 1.3 J.cm^{-2}

As observed with the Ga-O component of the Ga 3d peaks, the increase of the "Ga Auger" component started at 1.3 J.cm^{-2} and at 1.0 J.cm^{-2} for the as-grown and dry-etched GaN respectively. This component was attributed to Ga Auger related to oxidation. The increase of the "N-Ga-O" contributions was assigned to N for which the closest N neighbours have been replace by O . Therefore, we can assume that a mixed oxynitride of gallium might have been formed. This is consistent with the SEM images since no oxide clusters were observed.

The quantitative analyses showed the increase of the Ga/N ratio for both surfaces, with the highest value obtained for the as-grown GaN (Figure 57 (a)). This result was in agreement with the SEM images showing Ga droplets, thus, a nitrogen desorption was probably occurring upon laser annealing. This increase was less pronounced on the dry-etched surface.

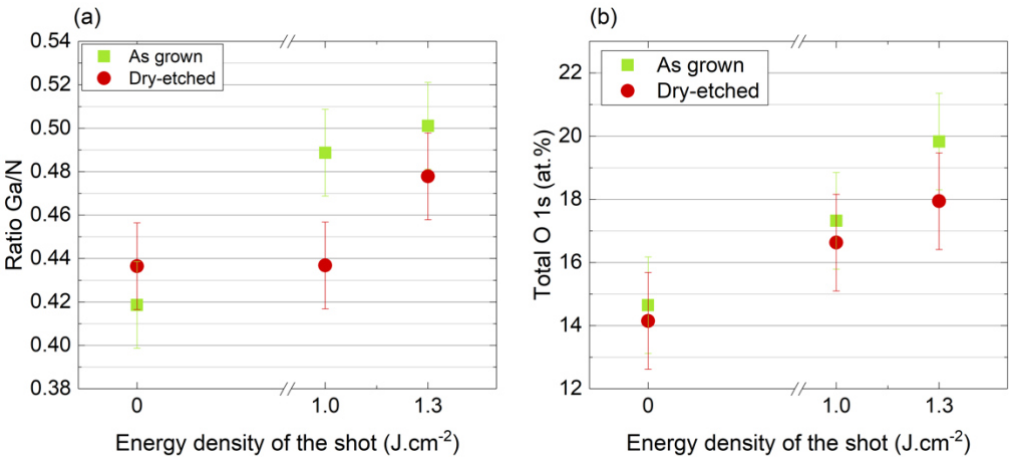

Figure 57. Evolution of the (a) Ga/N ratio (b) total O 1s at.% as a function of

The desorption of nitrogen came with an increase of oxygen amount detected at the surface (Figure 57 (b)). Thus, annealing induced the replacement of nitrogen atoms by oxygen atoms.

Combining the observations of the SEM images with the Ga 3d and N 1s XPS spectra, and the quantification, led to the conclusion that, the dry-etched surface tended to oxidise more easily (i.e. with the lowest energy (1.0 J.cm^{-2})) than the as-grown surface. Nevertheless, the as-grown GaN surface contained a larger amount of oxygen after a laser annealing of 1.3 J.cm^{-2} which came with the desorption of some nitrogen atoms, leading to the formation of Ga-Ga bonds related to Ga droplets. For both surfaces, a mix of oxynitride of gallium might be formed after laser annealing at 1.0 J.cm^{-2} for the dry-etched GaN, and at 1.3 J.cm^{-2} for the as-grown GaN.

IV.1.5 Influence of the number of shots

As an alternative method for using laser annealing to destabilise the surface without degrading its morphology, we conducted multi-shots of 1.0 J.cm^{-2}. Between 100 and 3000 shots were performed on different areas of the wafer. The impact of the number of shots on the surface morphology was investigated on both surfaces (Figure 58).

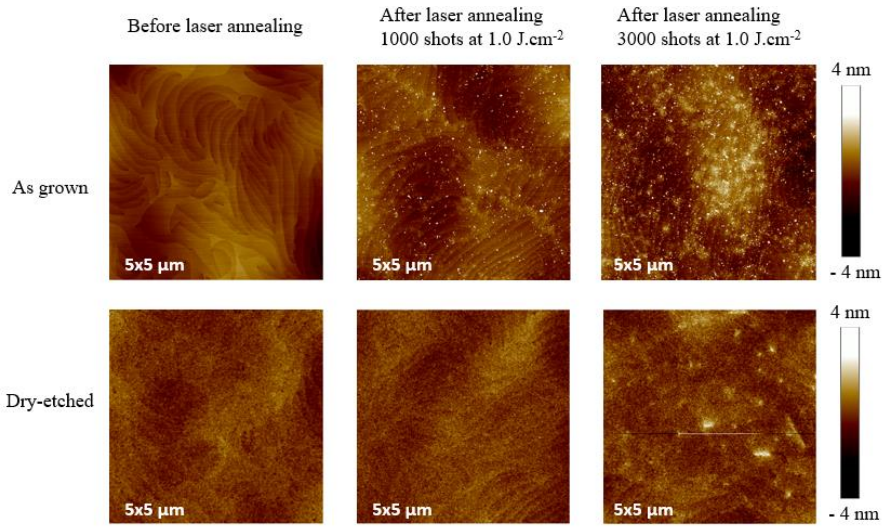

Figure 58. AFM images of the as-grown (top line) and dry-etched (bottom line) GaN surface before and after laser annealing with 1000 and 3000 shots of 1.0 J.cm^{-2}

For 1000 shots, the as-grown sample exhibited small white dots on its surface. The white dots seemed to lead to the formation of extended white areas after 3000 shots that could correspond to the beginning of an oxidation. On the contrary, the dry-etched GaN no modification after 1000 shots of 1.0 J. cm^{-2} and the less extended white areas started to appear

after 3000 shots. Therefore, for both surfaces, the roughness of the surface after laser annealing increased. The root mean square (RMS) roughness measured are summarised in Table 5. The as-grown surface exhibited a significant increase of the RMS, from 0.39 to 0.61 nm, after 1000 shots, and reached 0.87 nm after 3000 shots. Conversely, the dry etched GaN did not exhibit an increased RMS after 1000 shots, but did increase after 3000 shots to 0.54 nm.

Nb of shots at 1.0 J.cm^{-2}	As grown	Dry-etched
0	0.39 nm	0.35 nm
1000	0.61 nm	0.39 nm
3000	0.87 nm	0.54 nm

Table 5. RMS roughness measured by AFM of the as-grown and dry-etched GaN surface before and after laser annealing with 1000 and 3000 shots of 1.0 J.cm^{-2}

The surface chemistry was analysed by pAR-XPS. Figure 59 shows the evolution of the Ga 3d spectra after multi-shots.

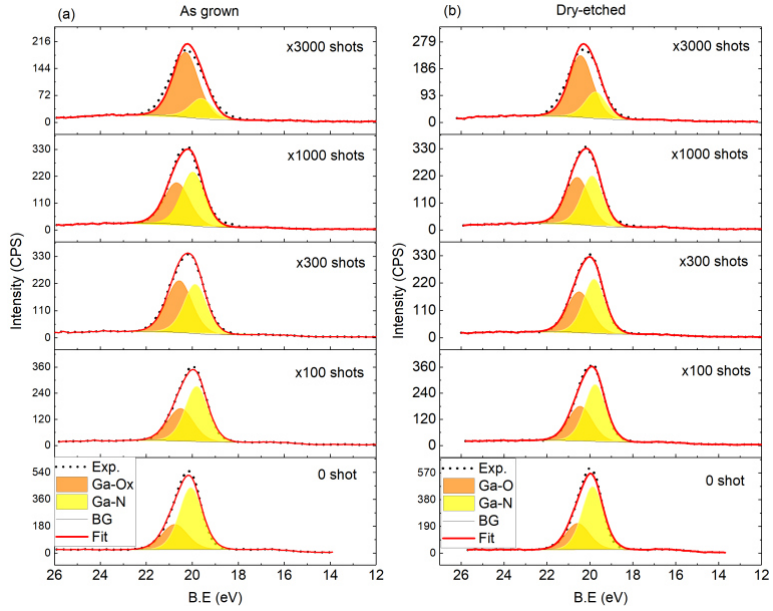

Figure 59. Ga 3d spectra of (a) a grown GaN and (b) dry-etched GaN after 0, 100, 300, 1000 and 3000 shots of 1.0 J.cm-2

For both surfaces, a progressive increase of the Ga-O component was observed. Annealing with 3000 shots at 1.0 J.cm^{-2} induced a big increase of the Ga-O component by 47% and 40% for the as-grown and dry-etched GaN, respectively. Between 100 and 1000 shots, the assumption of the creation of oxynitride gallium seemed coherent as the evolution of the N 1s spectra indicated that the "N-Ga-O" components progressively increased in the same way as the Ga-O component of the Ga 3d peaks (Figure 60).

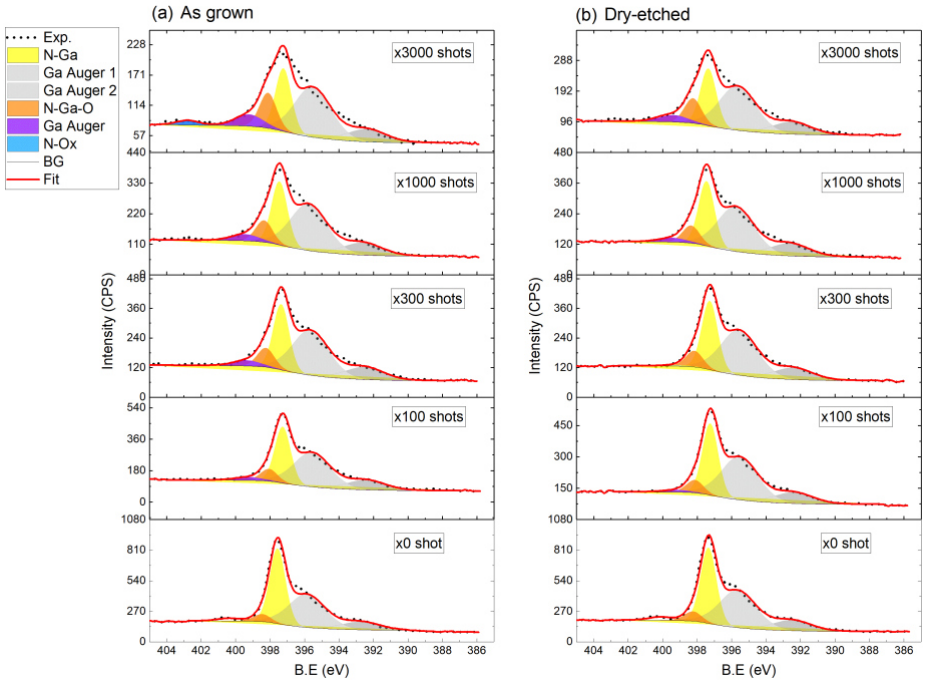

Figure 60. Evolution of N 1s spectra of (a) as-grown GaN and (b) dry-etched GaN before and after multi shots at 1.0 J.cm^{-2}

However, after 3000 shots, the N 1s spectra became more difficult to deconvolute, especially for the as-grown surface, since more nitrogen might have desorbed at this stage. Furthermore, another peak, ascribed "N-Ox" appeared only in the case of the as-grown GaN after 3000 shots. This new peak was assigned to NO_x [87] and was also detected at 23.78°, which implied the creation of an oxynitride gallium phase at a deeper level. It was however unclear why the as-grown surface exhibited NO_x and the dry-etched surface did not.

The O/N ratio, calculated from the total at.% of O 1s and the N-Ga component from N 1s (Figure 61 (a)) progressively increased with the number of shots. These results indicated that nitrogen tends to desorb in favour of oxygen adsorption from 100 to 3000 shots. It is noteworthy to highlight that starting from 300 shots, the as-grown GaN exhibited a slightly higher O/N ratio than the dry-etched GaN. As observed on the N 1s spectra (Figure 60(a)), the as-grown surface tended to produce more oxynitride than the dry-etched one.

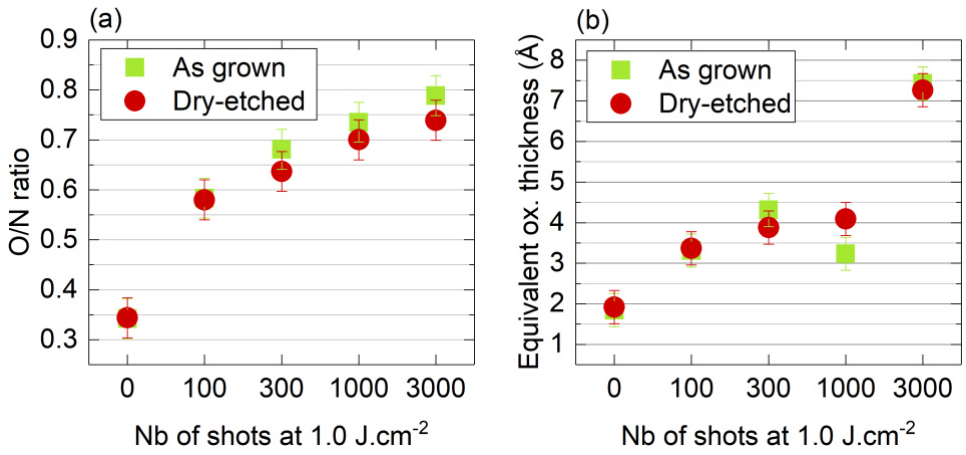

Figure 61. Evolution of (a) the O/N ratio and (b) the equivalent oxide thickness as a function of the number of shots at 1.0 J.cm^{-2} on as-grown and dry-etched GaN

The estimation of the equivalent oxide thickness follows the same evolution (Figure 61 (b)), and after 3000 shots, both surfaces showed an oxide layer of around 7Å. It is worth noting that the increase of the RMS for the as-grown sample might have an impact on the estimation of the equivalent oxide thickness and that the slightly lower oxide thickness estimate (for 1000 shots and more) for the as-grown GaN might be misleading.

Overall, this study showed that once again that as-grown GaN surface behaved differently from the dry-etched GaN surface. As grown GaN appeared to adsorb more oxygen, resulting from a higher RMS related to oxide clusters. Starting from 1000 shots at 1.0 J.cm^{-2}, it was possible to destabilise the Ga-N bonds of the surface without creating any major surface degradation.

IV.1.6 Influence of the atmosphere during annealing

In order to further increase the oxide thickness layer without damaging the surface, the standard N_2 flow was removed during annealing to create a more oxidising atmosphere. Our previous results indicated that after 3000 shots at 1.0 J.cm^{-2} the surface exhibited oxide-like areas and to reduce the thermal budget, we investigated the behaviour of as-grown and dry-etched GaN after laser annealing for a range of 100 to 1000 shots only, still at 1.0 J.cm^{-2}.

As shown in the AFM images (Figure 62), increased roughness interpreted as oxidation, was clearly visible for both surfaces.

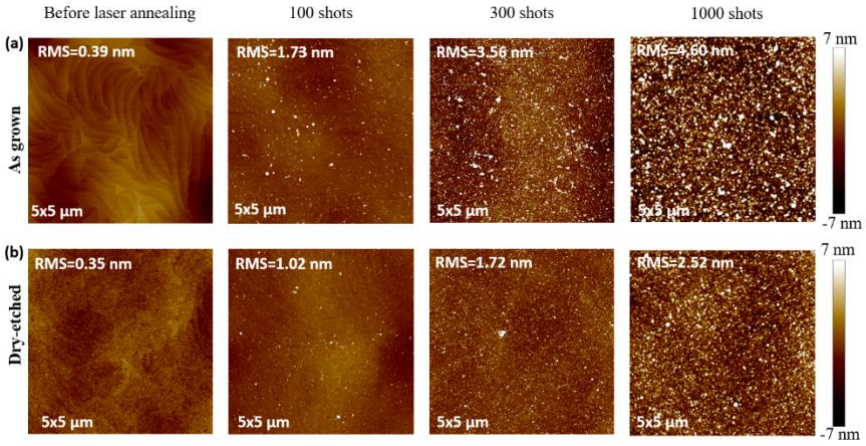

Figure 62. AFM images of the (a) as-grown GaN and (b) dry-etched GaN before and after LASER annealing, with several shots without N_2 flow

Due to the height of the clusters, the RMS roughness is not necessarily a relevant measurement, although there is a clear increase in the roughness with the increasing number of shots. It can also be seen from Figure 62 that the as-grown GaN exhibited larger oxide grain size than the dry-etched GaN, again suggesting that the oxidation of the as-grown GaN is easier than for the dry-etched surfaces. Figure 63 gives an example of the differences existing between the two surfaces after annealing with 300 shots.

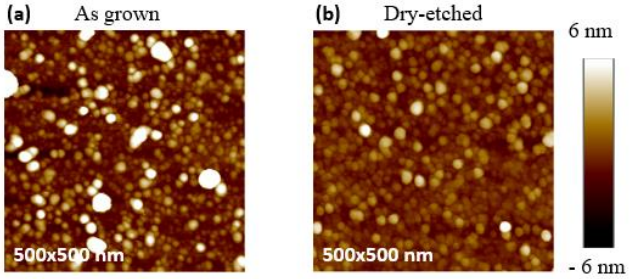

Figure 63. AFM images of (a) as-grown and (b) dry-etched GaN after 300 shots under ambient atmosphere

Indeed, for the as-grown GaN, disparity in size grain can be seen. The larger grains were around 45 nm across while the smaller ones were around 25 nm. In contrast, the dry-etched surface exhibited uniform grain size around 30 nm.

The impact of the number of shots while annealing under ambient atmosphere was investigated by pAR-XPS. The Ga 3d spectra are presented in Figure 64.

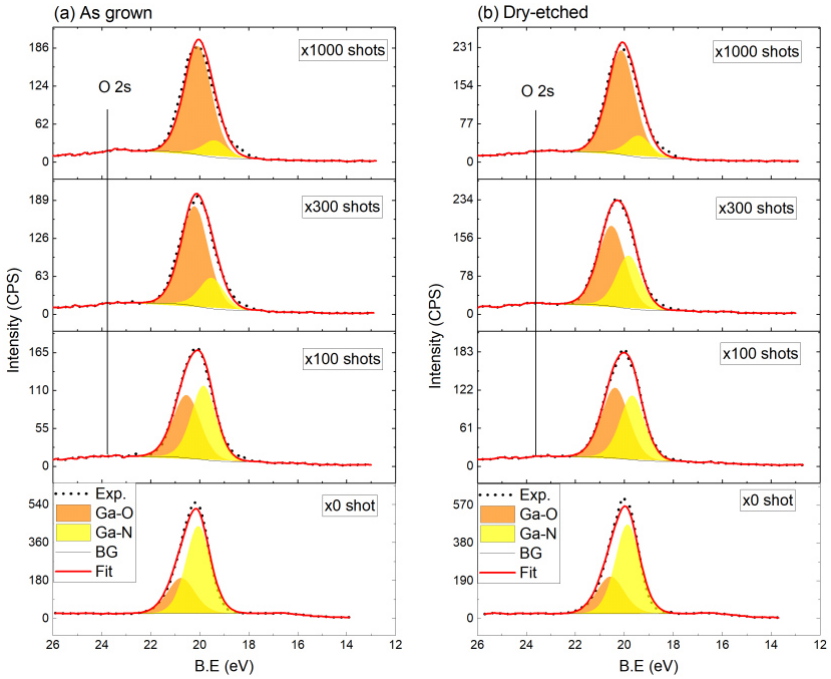

Figure 64. Evolution of the Ga 3d spectra of (a) as-grown GaN and (b) dry-etched GaN before and after multi shots at 1.0 J.cm^{-2} under ambient atmosphere

Starting from 300 shots, the presence of O 2s peaks, which were not detected in the previous study, revealed a higher amount of oxygen present on the surface. Figure 65 shows the evolution of the Ga-O contribution from the Ga 3d peaks as a function of the number of shots.

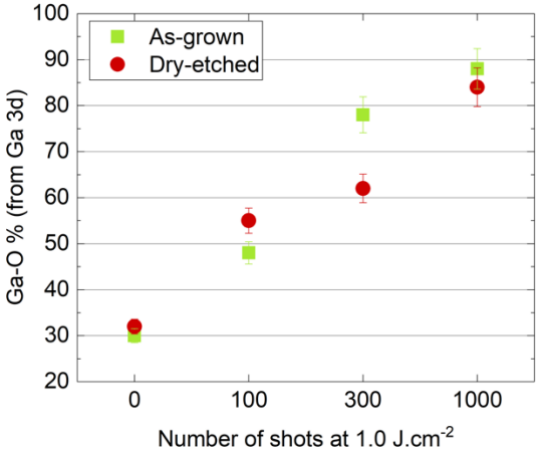

Figure 65. Evolution of the Ga-O contribution from the Ga 3d peak before and after several shots at 1.0 J.cm^{-2}

After 100 shots, the Ga 3d spectrum of the dry-etched sample exhibited a contribution of 55% of the Ga-O component, while for the as-grown GaN it was around 48%. However, after 300 shots, for the Ga 3d peak of the as-grown sample, the contribution of the Ga-O component on the Ga 3d peak of the as-grown sample became greater than that of the dry-

etched GaN, perhaps due to more exposed-time before measurement. The Ga-O component was 78 % for the as-grown sample, but only 62% for the dry-etched GaN. However, after 1000 shots, both surfaces exhibited the same amount of Ga-O contributions, 88% and 84%, for the as-grown and dry-etched GaN respectively. The increase of the Ga-O contributions, suggesting a higher amount of oxide also came with an increase of N-Ga-O and the Ga Auger components from the N 1s core-level (Figure 66). While a higher amount of oxide and the presence of a NO_x component was observed for the as-grown GaN after 300 shots this was not the case for the dry-etched GaN. After 1000 shots, it became difficult to deconvolute the N 1s peak due to the overlapping Ga Auger signals. Furthermore, the "N-O_x" contributions disappeared, that might explain the desorption of a considerable amount of nitrogen atoms. For the dry-etched GaN, the deconvolution of the N 1s peak was still possible, however the increasing "Ga Auger" might mislead the quantification.

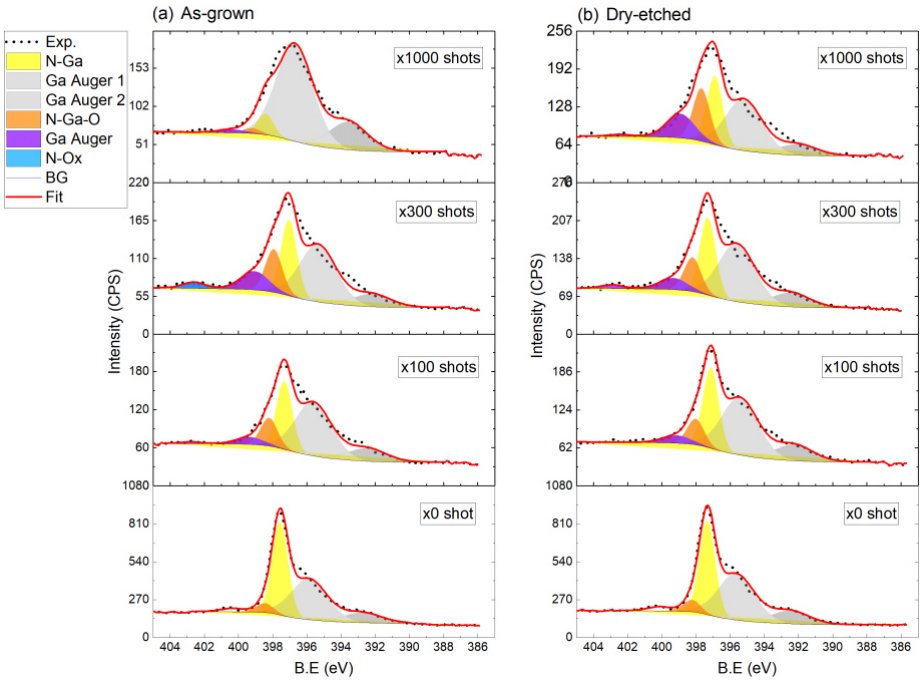

Figure 66. Evolution of the N 1s spectra of (a) as-grown GaN and (b) dry-etched GaN before and after multi shots at 1.0 J.cm^{-2} under ambient atmosphere

Once again, the O/N ratio was also found to be slightly higher for the as-grown GaN (Figure 67(a)), which might be also due to an underestimation of the N-Ga component. With 300 shots and more, the O/N ratio was around 0.8-0.9 for both surfaces. This result suggests that the majority of N 1s remaining was "N-O" contributions or Ga Auger signals, therefore most of the nitrogen might have desorbed.

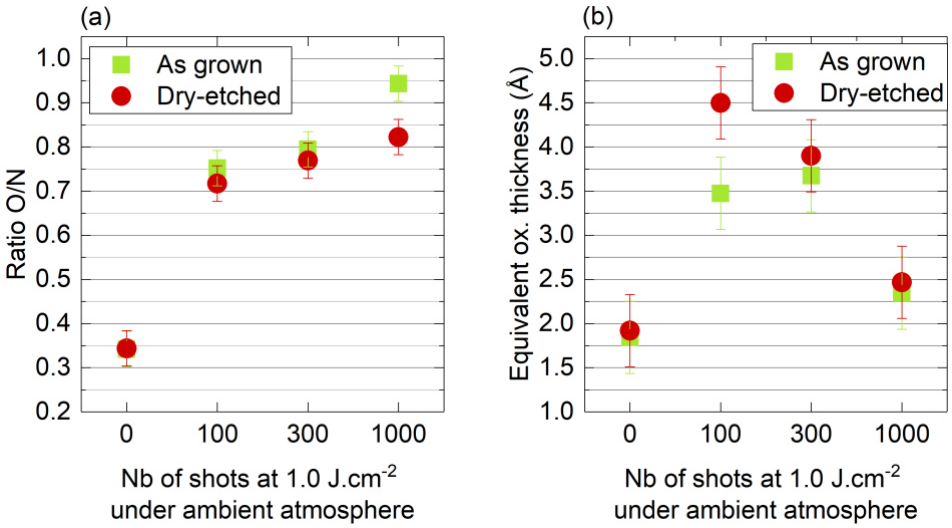

Figure 67. Evolution of (a) the O/N ratio and (b) the equivalent oxide thickness as a function of the number of shots at 1.0 J.cm^{-2} under ambient atmosphere on as-grown and dry-etched GaN

Note that the estimation of the equivalent oxide thickness (Figure 67 (b)) is difficult to interpret after 300 and 1000 shots because above 300 shots, the model did not fit well, and so gave inconsistent results. As observed in the case of the annealing under N_2 flow with 3000 shots at 1.0 J.cm^{-2}, this phenomenon was related to an increased roughness.

The comparison between annealing with and without N_2 flow showed, as expected a higher amount of oxygen detected at the surface when N_2 flow was removed. The Figure 68 shows the total amount of oxygen for as-grown GaN (a) and dry-etched GaN (b) samples.

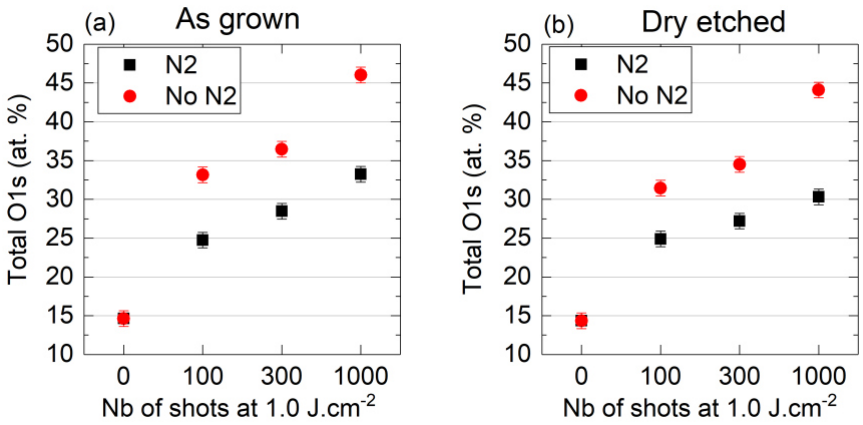

Figure 68. Evolution of the total amount of O 1s for (a) as-grown GaN and (b) dry-etched GaN with and without N_2 flow as a function of number of shots at 1.0 J.cm^{-2}

Firstly, we can see that, the total O 1s percentage increased gradually with the number of shots for both surfaces. The difference between annealing under N_2 and without N_2 was approximately 5.5 to 6.6 at.% from 100 to 300 shots for both GaN samples. However, after

1000, the total O 1s detected after annealing without N_2 flow was 13 at. % higher than annealing with N_2 for the as-grown GaN. On the contrary, the difference of total O 1s between annealing with N_2 and without N_2 was around 4 at.%. This disparity could come from the deconvoluted N 1s peaks where the error might have increased due to the overlapping Ga Auger signals. Although the relative quantification of the species detected from the pAR-XPS might not give the exact amount of oxygen, the AFM images from Figure 62 and Figure 63, show that as-grown GaN tended to exhibit more grains than dry-etched GaN, which we associate with the oxide formation. Therefore, the as-grown GaN is again shown to adsorb more oxygen atoms than the dry-etched GaN.

In order to better understand the oxidation process of both GaN surfaces, we analysed in-depth pAR-XPS on the entire studied GaN layer, i.e. 10 nm (Figure 69), and compared the results with those obtained with GaN samples annealed under N_2 flow.

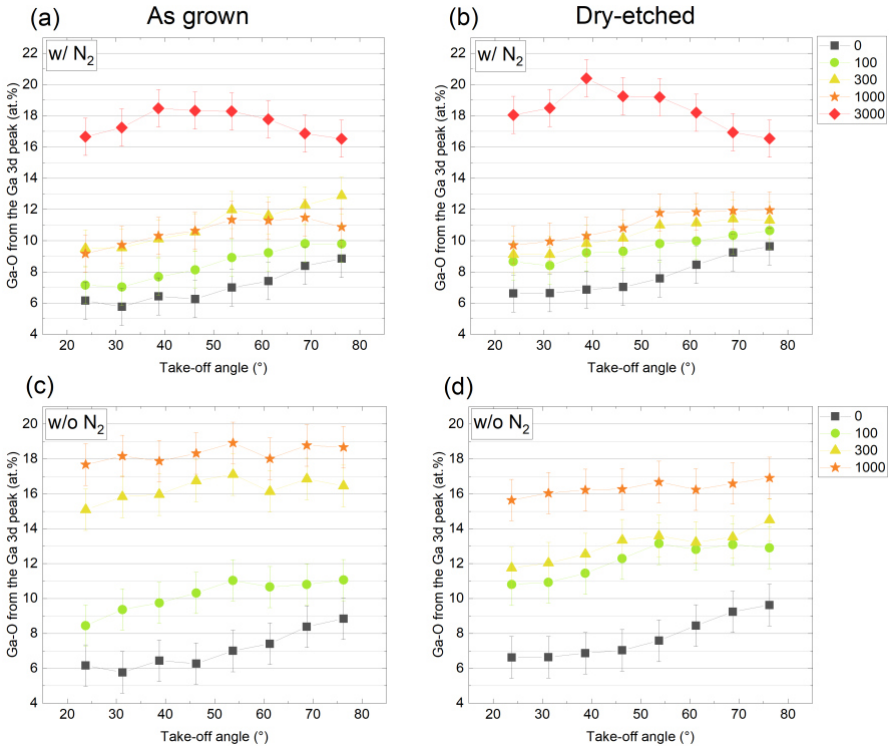

Figure 69. In-depth analyses of the Ga-O contribution from the Ga 3d peaks before and after annealing with multi shots at 1.0 J.cm^{-2} of (a) as-grown GaN under N_2 flow, (b) dry-etched GaN under N_2 flow, (c) as-grown GaN without N_2 flow and (d) dry-etched GaN without N_2 flow

Under N_2 flow, the as-grown and dry-etched GaN samples exhibited an increasing amount of Ga-O while approaching the surface, between 100 and 1000 shots. However, for the as-grown GaN sample, after 3000 shots, the difference between the bulk angle (23.75°) and the surface angle (76.25°) was around 0.13%. The more even distribution of Ga-O along the depth

was attributed to the grain oxides observed on the AFM images (Figure 58). After 3000 shots, the distribution of the Ga-O of the dry-etched GaN sample became unclear. In spite of this, the dry-etched surface revealed a more important Ga-O contribution compared to that of the as-grown surface regardless the take-off angle, mainly due to the prior plasma treatments. The trend was reversed when annealing without the N_2 flow. Indeed, the as-grown GaN sample globally exhibited a more important Ga-O contribution than the dry-etched GaN sample. The distribution of Ga-O became homogenous along the depth starting from 300 and 1000 shots for the as-grown and dry-etched GaN samples, respectively. Once again, this was related to the presence of oxide grains visible on the AFM images (Figure 62).

However, the higher level of Ga-O for the as-grown GaN sample indicated that oxygen atoms might have migrated more easily to form an even Ga-O distribution in depth than for the dry-etched GaN.

IV.1.7 Conclusions

The determination of the minimum energy density for annealing GaN surfaces showed us that the energy giving a detrimental effect on the surface morphology varied according to the surface, for example the formation of cracks for the dry-etched GaN. Moreover, the melt point was observed at 1.30 $J.cm^{-2}$ for the as-grown GaN, which energy is slightly lower than that needed the dry-etched GaN, which was at 1.45 $J.cm^{-2}$. Single laser shots showed considerable impact on the oxidation level measured at 1.30 $J.cm^{-2}$ for both surfaces.

In order to avoid too much damage on the surface morphology, the energy density was chosen at 1.0 $J.cm^{-2}$ to perform multi shots. Under N_2 flow, after 3000 shots both surfaces exhibited white areas on AFM images, which were assigned to oxidation. Furthermore, more white areas were observed on the as-grown GaN, since the difference the as-grown and the dry-etched surfaced is the accessibility of the dislocation, where the oxidation starts, and is in agreement with Yamada *et al* work [87]. The RMS roughness was however lower than 1 nm regardless the surface and the number of shots. The XPS results also revealed a progressive increase of the oxygen level with the increasing number of shots. The total O 1s level increase came with the rise of the Ga-O component from the Ga 3d core-level and N-Ga-O component from the N 1s core-level, which indicated the formation of mixed oxides at the surface. The estimation of the equivalent oxide thickness increased with the number of shots as well and reached around 7 Å after 3000 shots.

Removing the N_2 flow while annealing enhanced the adsorption of oxygen. Indeed, the Ga-O contribution of the Ga 3d peak became predominant for both surfaces. Moreover, the O 2s peak started to appear. Above 300 shots the equivalent oxide thickness could not be determined due to the high roughness of the surface. AFM images showed larger oxide grain size for the as-grown GaN, again suggesting easier and faster oxidation of the as-grown surface versus the dry-etched surface.

An in depth study showed that the Ga-O at.% was evenly distributed along the probed layer after 3000 shots under N_2 flow, and the Ga-O amount detected was higher for the dry-etched GaN sample that for the as-grown. In contrast, removing the N_2 flow during annealing showed a higher amount of Ga-O for the as-grown GaN sample than for the dry-etched GaN samples. The even distribution of Ga-O was related to the presence of oxide grains visible on the AFM images.

This study showed that the as-grown GaN surface tended to adsorb oxygen atoms more easily which migrate in depth, when the annealing was performed under oxidative atmosphere.

IV.2. Rapid thermal processing

One of the most reported technique to oxidise GaN surface is by Rapid Thermal Processing (RTP), which is a process used in semiconductor industry which heat the wafers at high temperatures (200-1300 °C [88]) for a few minutes. Initially, studies dealing with the oxidation of GaN using RTP were conducted with the aim of creating a good quality gallium oxide for MIS (Metal Insulator Semiconductor) or MOS (Metal Oxide Semiconductor) systems. Indeed, to reduce gate leakage dielectrics are usually deposited such as SiO_2, Si_3N_4, or Al_2O_3. Due to high trap charge density at the insulator/GaN interface, researchers used thermal oxidation to grow and oxide layer as a gate dielectric [88–90]. These studies mainly focused on thick thermal oxides (around 100 nm) [92] and it was reported that temperatures below 750°C did not induce oxide growth for GaN [86, 92].

IV.2.1 Equipment and annealing conditions

The Rapid Thermal Processing (RTP) is an equipment for rapid thermal annealing. The RTP equipment used in this study was a Jipelec Jetfirst and it is designed for rapid process with a short ramp time to reach high temperature and cool down within 10 minutes.

All the samples were annealed for temperature at 850°C, 900°C and 950°C under dry O_2 sccm for 5 minutes.

IV.2.2 GaN samples

Since the equipment allowed the loading of small samples, the GaN were cut into small pieces of 2x2 cm^2.

As-grown and dry-etched GaN surfaces were investigated. The dry etching process was the standard used for the power division at LETI. This dry etching process included a Cl_2/BCl_3-based ICP-RIE plasma at high bias voltage of 237 V. Next, an Ar-based ALE step was performed, followed by an identical stripping sequence to that used for to remove the photoresist resin and the dry etching residues. The total etching depth wad about 350 nm. The stripping sequence included an O_2 plasma and followed by a wet cleaning in DuPont™ PlasmaSolv® EKC 265™, a photoresist remover. Note that no photoresist coating was used in this study.

The layers stack of the GaN samples used is shown in Figure 70.

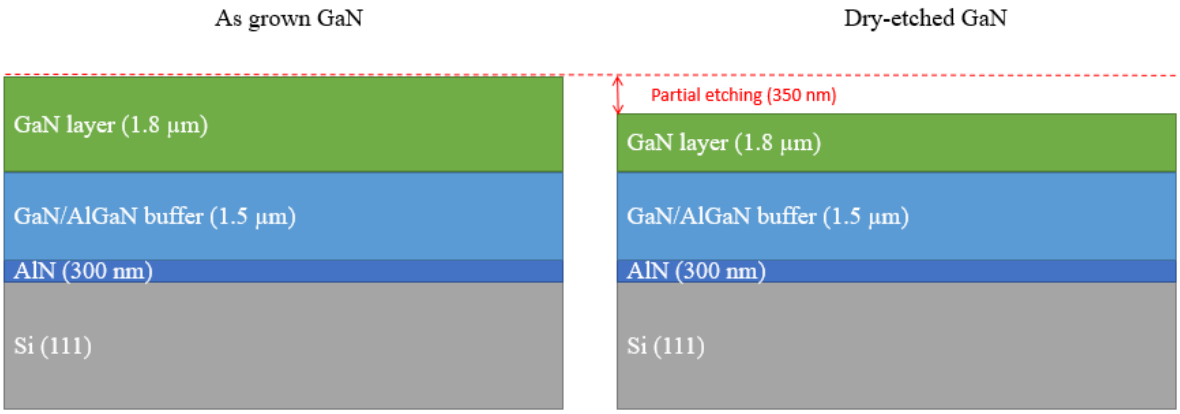

Figure 70. GaN layer stack used for the RTP study

IV.2.3 Temperature selection

As stated earlier, our goal was to break the Ga-N bonds of the surface without creating a thick oxide. Therefore, we studied the impact of short thermal oxidation time. Unlike other studies where a thermal oxidation were performed for 30 minutes to several hours, we annealed our samples for 5 minutes under dry O_2 (2000 sccm flow rate).

To see the impact of the thermal oxidation on our wafer we first investigated RTP on as-grown GaN at 850, 900 and 950°C. We investigated the morphology of the RTP annealed surfaces. Figure 71 shows the impact of each temperature on the surface morphology. As expected, the RMS roughness increased with the temperature. Between 850°C and 900°C (Figure 71 (a) and (b)), the RMS roughness slightly raised to about 1 nm. However, after annealing at 950°C, the RMS roughness strongly increased and reached 24.2 nm (Figure 71 (c)).

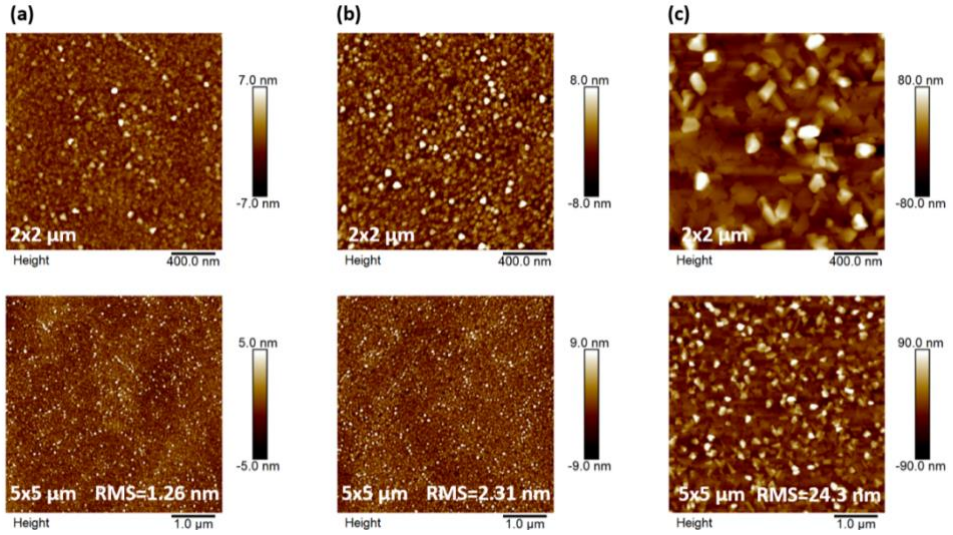

Figure 71. AFM images of as-grown GaN after RTP annealing at (a) 850°C, (b) 900°C, (c) 950°C. Note the much larger z-scale for the samples annealed at 950°C

Oxide clusters were observed after annealing at 850°C and 900°C (Figure 71 (a) and (b)) and the threading dislocations as well as the atomic step were not visible anymore. These observations are in agreement with the progressive increase of the oxygen amount (Figure 75 (a)). After annealing at 950°C, the oxide clusters gave way to bigger oxide grains (Figure 71 (c)), similar to that observed in Yamada *et al.* work [87].

RTP at 900°C (with the same conditions as previous), was carried out again on as-grown wafer and TEM and EDX were conducted (Figure 72).

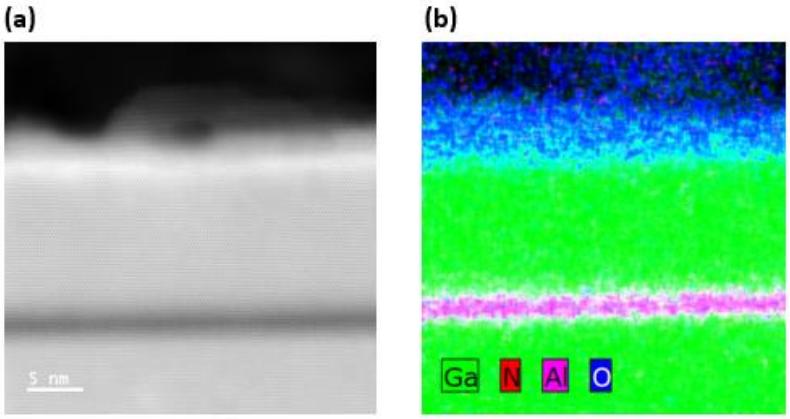

Figure 72. (a) TEM and (b) EDX images of as-grown GaN after RTP at 900°C. Note that the wafer stack layer included a GaN/AlN capping + AFM

The TEM and the EDX images supports the presence of an oxide layer at the surface. Furthermore, the comparison of the TEM image with [94] showed that the oxide formed was a β-Ga_2O_3 Figure 73.

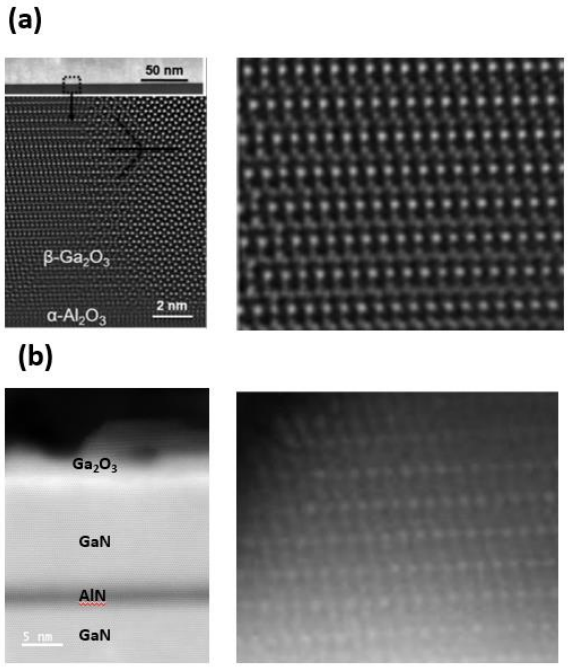

Figure 73. (a) TEM images from [94] and (b) TEM from our as-grown GaN sample after RTP at 900°C showing the phase the Ga_2O_3 formed at the surface

From the diffraction pattern, the oxide over-layer exhibited columnar shape of β-Ga_2O_3 along the grown direction of the underneath GaN layer (Figure 74).

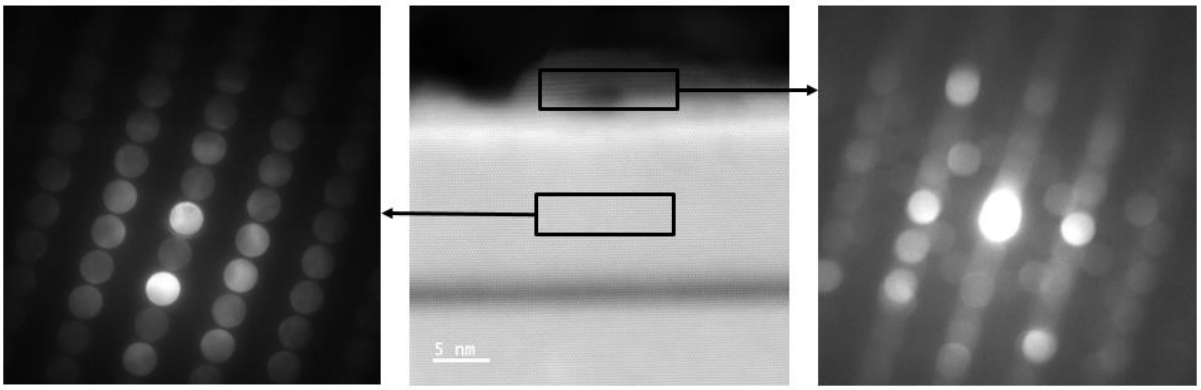

Figure 74. TEM diffraction pattern of the as-grown GaN sample after RTP at 900°C

The impact of thermal oxidation on as-grown GaN at 850, 900 and 950 °C was also investigated by pAR-XPS measurements. The analyses showed a progressive increase of the total amount of O 1s with increasing the annealing temperature (Figure 75).

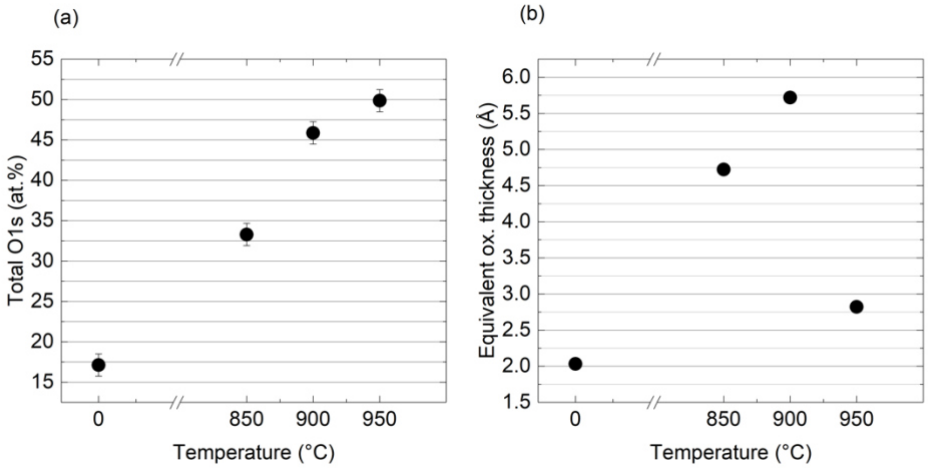

Figure 75. Evolution of (a) the total relative atomic % of O 1s core-level (b) the equivalent oxide thickness as a function of the temperature

The total amount of O 1s at.% reached around 50 at.% at 950°C. While the total amount of O 1s could be a good indicator of initial oxide growth, it can be less relevant when the oxidation is important. Indeed, as it gives a relative value of each species taken into account, the calculated amount of the N-Ga contribution from the deconvoluted N 1s peak could be incorrect as the Ga LMM Auger signal overlaps the N 1s level signal. The Ga Auger LMM signals might also have shifted due to gallium oxidation. Furthermore, nitride oxides are volatile and tend to desorb more easily than gallium, making the N 1s signal less detectable compared to the Ga LMM Auger signals. However, the Ga LMM Auger peaks affected less the deconvolution of the deeper take-off angles (from 23.25 to 68.75°). The equivalent oxide

thickness (Figure 75 (b)) exhibited a progressive increase from 850°C to 900°C. The initial equivalent oxide thickness was at 2.03 Å, and reached 4.4 Å and 5.7 Å after annealing at 850°C and 900°C, respectively. However, at 950°C, the estimated equivalent oxide thickness did not fit the model properly, as seen previously on the AFM images (Figure 71 (c)), a non-uniform growth of the oxide grains resulting with a high RMS roughness could explain the inaccurate value found.

To better understand the evolution of the oxide growth among the GaN layer, we plotted the evolution of the relative at.% of the Ga-O contribution from the Ga 3d peak through 8 angles from 23.75° to 76.25° for each studied temperatures.

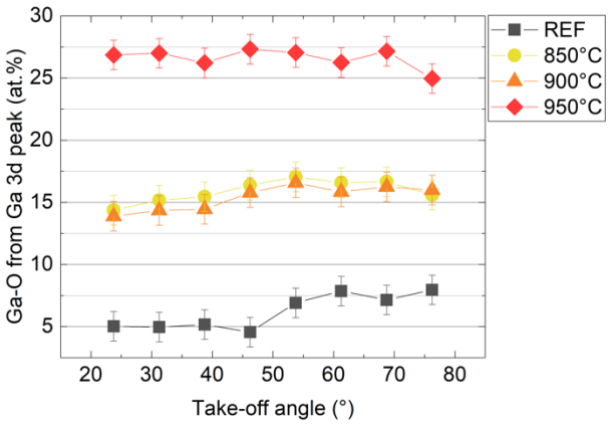

Figure 76. Evolution of the relative at.% of the Ga-O contribution (Ga 3d) of GaN before and after RTP annealing at 850, 900 and 950°C as a function of the take-off angle

Before annealing, the GaN surface exhibited a progressive increase of the Ga-O contribution along the GaN layer, with a slightly higher amount found at the very top surface, i.e. at 76.25°. Indeed, the Ga-O contribution represented relative at.% of 5 around 10 nm deep, i.e. at a take-off angle of 23.75°, to almost 8% around the first 2 nm, i.e. 76.25°. After annealing at 850°C and 900°C, the same evolution of Ga-O contribution was observed. The impact of the annealing was visible at 23.75°, with a Ga-O contribution around 14% for 850°C and 900°C which hardly evolved, with an at.% around 15.6 and 16%, for annealing at 850°C and 900°C, respectively. After annealing at 950°C, the Ga-O contribution did not significantly change along the take-off angles. The Ga-O contribution ranged from 26 to 27% from the seven first angles, i.e., from 23.75° to 68.75°. At the eighth angle (76.25°), the Ga-O contribution was slightly lower due to overlapping with gallium Auger signals that could alter this value.

The RTP anneals performed on as-grown GaN led to the formation of oxide grains that most likely evolved to be β-Ga_2O_3. The similarity with Yamada *et al.* work [87] led to think that oxide grains started at dislocation sites.

IV.2.4 Comparison of the impact of RTP on as-grown and dry-etched GaN at 850°C

In the previous paragraph, we saw that performing RTP at 850°C enabled a surface modification with the adsorption of oxygen leading to the cleavage of the surface Ga-N bonds without causing an excessively high RMS roughness. Therefore, the next study deals with the impact of RTP at 850°C on as-grown GaN and dry-etched GaN surfaces.

The AFM measurements of the samples before and after the anneals are shown in Figure 77.

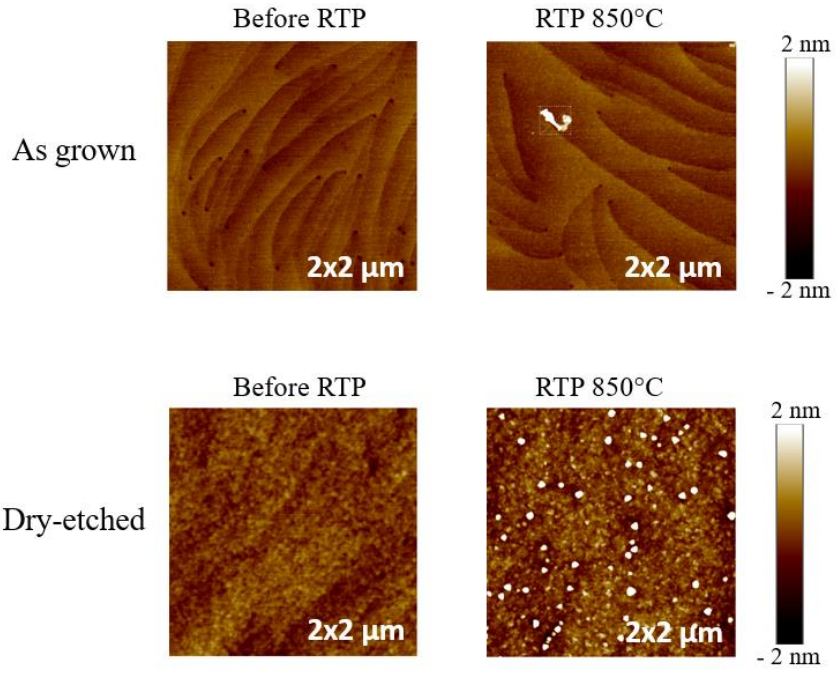

Figure 77. AFM images before and after RTP anneals at 850°C on as-grown and dry-etched GaN

Unlike the previous AFM measurements (Figure 71 (a)), the as-grown sample did not exhibit oxide grains after RTP at 850°C. This might be related to the fact that in the initial work (section IV.2.3) conducted for the selection of the annealing temperature the wafer had been stored for a longer period of time compared to those used in this study. However, the dry-etched GaN exhibited small white dots similar to that previously observed on the as-grown GaN

at 850 and 900°C (Figure 71 (a) and (b)). This observation suggested that the growth of the oxide grains might be eased on damaged surfaces.

To understand the differences observed on the surface morphology between the as-grown and dry-etched GaN we performed pAR-XPS measurements. The pAR-XPS showed a higher amount of oxygen detected on the dry-etched surface compared to that of the as-grown one (Figure 78). However, after annealing, both surfaces exhibited almost the same amount of oxygen, (ca. 33-34 at.%) which suggesting that at this temperature, the surface modification is either auto-limiting or the reaction rate slows with time.

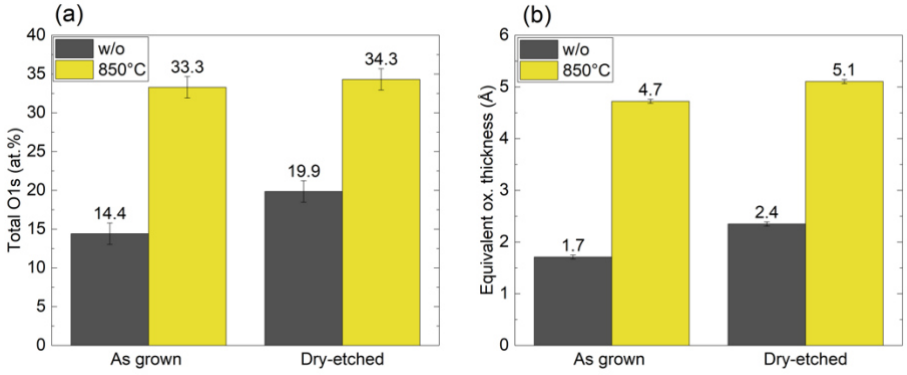

Figure 78. Impact of RTP before and after annealing at 850°C on (a) the total relative at.% of O 1s and (b) the equivalent oxide thickness

The estimation of the equivalent oxide thickness (Figure 78 (b)) showed a slightly thicker layer on the dry-etched GaN surface prior to RTP annealing compared to that observed for the as-grown GaN surface. From the evolution of the total amount of oxygen, we can conclude that similar oxide thicknesses are yielded on both samples upon annealing, with values of 4.7 Å and 5.1 Å for the as-grown and the dry-etched GaN samples respectively.

The in-depth pAR-XPS (Figure 79) analyses exhibited a similar behaviour between both surfaces as well. Indeed, as seen previously on the as-grown GaN (Figure 79 (a)), the Ga-O contribution from the Ga 3d peak gradually increased towards the surface (going from 4.4 to 7.7 at.%) while after RTP annealing the variation of the Ga-O component with take-off angle was less marked (going from 14.4 to 15.6 at.%).

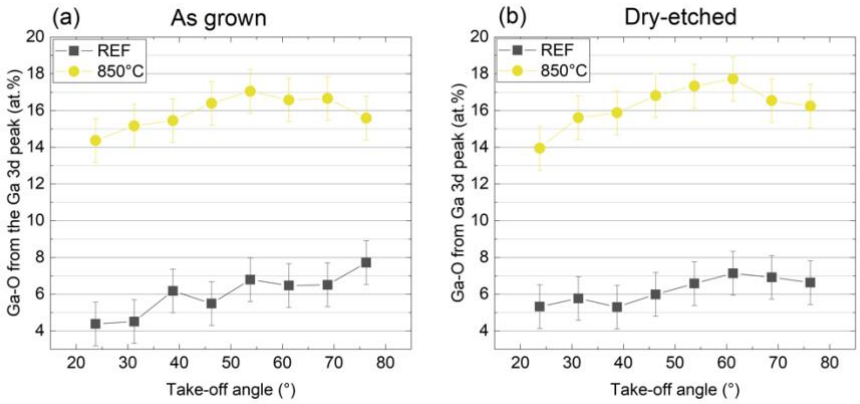

Figure 79. Evolution of the Ga-O at.% from the Ga 3d peak before and after RTP annealing at 850°C for (a) as-grown GaN and (b) dry-etched GaN

For the dry-etched GaN prior to annealing, the Ga-O contribution was initially more uniformly distributed over the entire probed depth, with a small difference between the bulk angle and the top surface of 1.31 % (Figure 79 (b)) and after annealing at 850°C, the variation of the Ga-O at.% seemed to increase but the values were within the error bars.

IV.2.5 Conclusions

This initial RTP study on as-grown GaN showed a progressive increase of the total O 1s at.% level with increasing temperature. The equivalent oxide thickness for the samples annealed at 850°C and 900°C were 4.7 Å and 5.7 Å respectively, versus 2.0 Å prior to RTP. Once again, the equivalent oxide thickness could not be determined for the sample annealed at 950°C due to a high roughness.

In depth pAR-XPS study showed as expected an increasing Ga-O at.% when approaching the surface. Along the surveyed layer, the Ga-O at.% distribution was gradually increasing toward the surface after annealing at 850°C and 900°C. The distribution was uniform after annealing at 950°C, likely due to higher roughness. Annealing at high temperature induced rougher surface, with RMS roughness around 1.2 nm and 2.3 nm for samples annealed at 850°C and 900°C respectively, it reached 24 nm when annealed at 950°C. Grains were visible regardless of the temperature, and these were interpreted as gallium oxide. Their size increased with the increasing temperature.

The comparison of an as-grown GaN and a dry-etched GaN revealed a larger amount of oxygen adsorbed on the as-grown GaN. Both surfaces ended up to exhibit approximately the same equivalent oxide thickness. In depth analyses highlighted small differences between the two surfaces.

IV.3. Comparison between the dry techniques

These studies highlighted that in presence of oxygen during annealing, as-grown GaN tended to adsorb more oxygen at the surface. Indeed, for both techniques used, when oxygen was present during the anneals, as-grown GaN exhibited more oxygen.

The in-depth analyses of the Ga-O component extracted from the Ga 3d spectra brought into light the possible migration throughout the surveyed layer. For laser annealing the migration was eased with the increasing number of shots and a uniform distribution of Ga-O bonds was reached at 1000 shots for an energy density of 1.0 $J.cm^{-2}$, if not at 300 shots. Indeed, the example of the sample, which received 300 shots, was exposed to air several days before measurement and could explain the uniform distribution of Ga-O bonds throughout the depth. By contrast, the dry-etched GaN showed a less even distribution of Ga-O bonds and less Ga-O bonds were detected at the surface angle, i.e. 76.25°, than for the as-grown GaN. This persistent Ga-O gradient for the dry-etched was assigned to a higher number of N vacancies initially present compared to an as-grown surface. However, regardless the surface, the presence of oxygen during annealing enabled an easier migration of oxygen atoms toward the bulk. Indeed, after laser annealing under N_2 flow the Ga-O bonds percentage were predominant at the surface, except when 3000 shots were performed. Unfortunately, a too high number of shots had detrimental effects on the surface morphology. For the same amount of Ga-O bonds found at the bulk, RTP annealing at 850°C allowed to keep a clean surface morphology. However, the dry-etched GaN was more prompt to exhibit a rougher surface due to initial oxide growth at dislocation sites. Concerning the surface chemistry of RTP annealed samples, a linear increase of the Ga-O bonds toward the surface was observed among the six first angles. Unlike laser annealing, the dry-etched surface exhibited a slightly higher amount of Ga-O. This behaviour could be explained by the fact that due to vacancies and dangling bonds the dry-etched surface combined with a high temperature, the nitrogen atoms desorbed more easily. Indeed, more NO_x species was found adsorbed at the surface of the dry-etched GaN. The NO_x species were not detected after laser annealing except when the sample was exposed to air several days, which was the case of the as-grown sample shots 300 times at 1.0 $J.cm^{-2}$. This observation demonstrated that while oxygen atoms migrate to the surface, the nitrogen atoms bond with oxygen forming more volatile oxides than that of the gallium oxides. The observation of NO_x at the surface was consistent with the following reaction:

$$GaN + O_2 \rightarrow GaO_x + NO_x$$

Furthermore, nitrogen removal seemed to be eased with the help of the structural defects induced by the previous plasma on the GaN surface. Indeed, the formation of small oxide cluster was observed in AFM images on the dry-etched GaN only. The vacancies, dangling bonds, and maybe the more exposed threading dislocations induced by the plasma enhanced the formation of oxide grains. A mechanism of thermal oxide growth was proposed by Yamada *et al.* [87] where they found that the formation of oxide grains was initiated at the surface defects at 850°C.

IV.4. Wet etching on RTP annealed GaN surfaces

IV.4.1 A technique toward digital etching

In order to get an atomically clean surface, a method discussed in section I.5.4 is to form an oxide film, then etch the oxide by wet etching.

Based on the systematic review, we observed that hot HCl (70°C) was a good option for etching the native oxide present at the surface of the GaN wafers. The adsorption of chlorine was assumed to hinder the re-oxidation after treatment. In addition, $(NH_4)_2S$ exhibited a reduction of the oxide thickness, and probably hinder the re-oxidation of GaN as well. Therefore, we performed, in the same conditions as presented in chapter III.1.1, HCl at 70°C and $(NH_4)_2S$ at RT wet etching, on the 850°C RTP annealed-samples. Once again, as-grown and dry-etched GaN samples were investigated. In order to appreciate the etchant effect of HCl and $(NH_4)_2S$ on the surface morphology and the possibility of oxide removal, we performed AFM measurements.

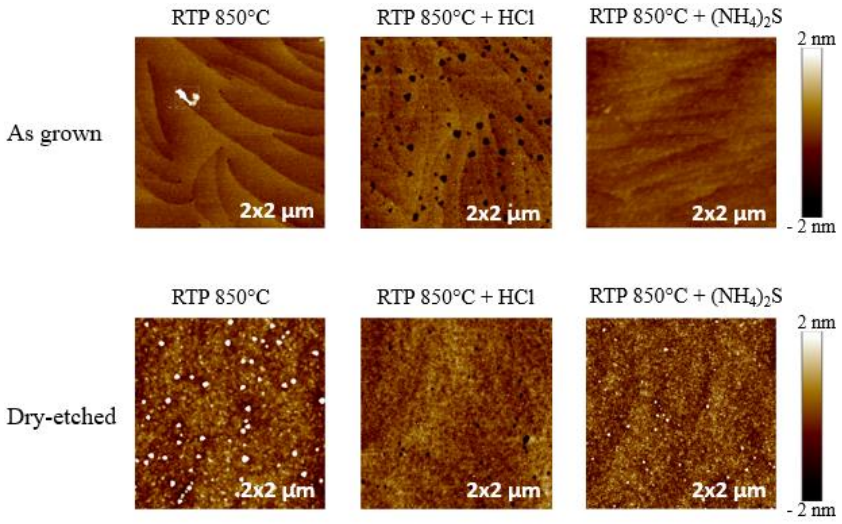

Figure 80. AFM images before and after HCl and $(NH_4)_2S$ wet etching on annealed as-grown and dry-etched GaN samples

After HCl treatment, both surfaces exhibited holes related to threading dislocations. Larger pits were present on the as-grown surface, with a size going from 0.043 µm to 0.114 µm, with a total of 80 dislocations, which was higher than the pit density after RTP annealing. Therefore, we can suggest that during the time between the annealing and the wet etching, oxide clusters started to grow at dislocations and defect points, and were etched with HCl, leaving etch pits on the surface. On the contrary, the dry-etched surface exhibited 37 pits, with a homogenous size distribution around 0.056 µm. Surprisingly, the number of pits did not match the number of the white dots encountered before the HCl treatment. Due to poor image quality, the density of pits may have been underestimated.

As for the $(NH_4)_2S$ treatment, no etch pits were visible on as-grown samples. For the dry-etched GaN sample, oxide grains were visible with a density of $2.4x10^7$ per cm^{-2}, similar to that of before the wet etching treatment ($2.1x10^7$ per cm^{-2}). However, the mean diameter of the oxide grains was 27.8 nm, versus 40.8 nm after RTP without wet etching treatment. Therefore, the $(NH_4)_2S$ wet treatment had a limited etchant efficiency on the thermal oxide grains.

The evolution of the total amount of oxygen and the equivalent oxide thickness are shown in Figure 81.

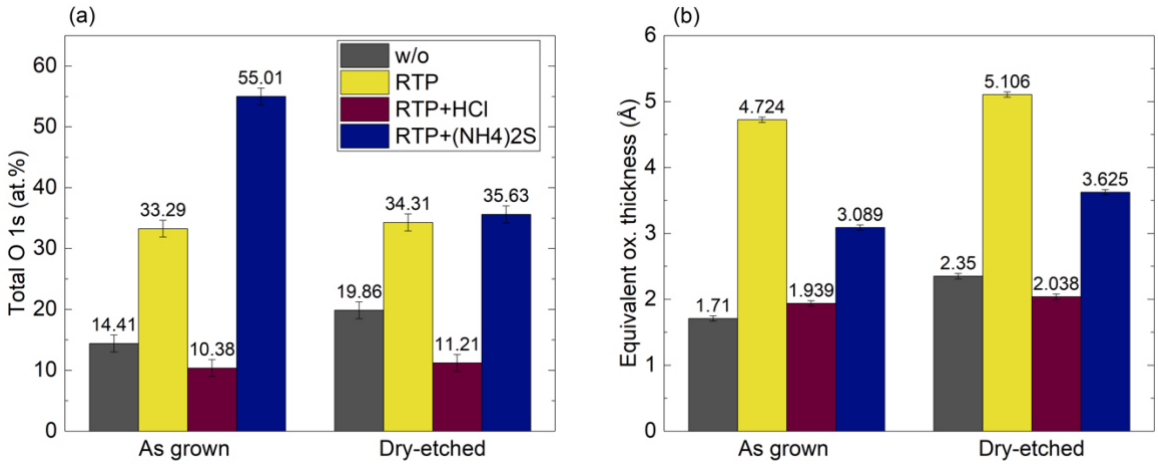

Figure 81. Impact of the RTP annealing followed by HCl or $(NH_4)_2S$ wet etching on (a) the relative total O 1s at.% and (b) the equivalent oxide thickness

The total amount of oxygen (Figure 81 (a)) detected on the oxidised samples, i.e. RTP annealed samples, decreased after immersion in HCl. This decrease was observed on both surfaces, in agreement with the AFM measurements. Moreover, the initial amount of oxygen of the untreated samples exhibited a higher at.%. Therefore, the combination of annealing and wet etching in HCl enabled a lower amount of oxygen than an untreated post-epitaxy GaN. It

can be noted that the amount of oxygen on the dry-etched sample was similar to that of the as-grown, which indicated that we might have recovered the surface from the prior damage induced by the dry-etching processes. However, the use of $(NH_4)_2S$ as an etchant on intentionally oxidized GaN was less effective to remove the oxides compared to HCl treatment. Indeed, for the dry-etched GaN the total amount of oxygen was similar to that of the annealed sample. However, for the as-grown GaN the level increased of about 20%. This important rise was mainly caused by a contamination of SiO_2 as shown in Figure 82.

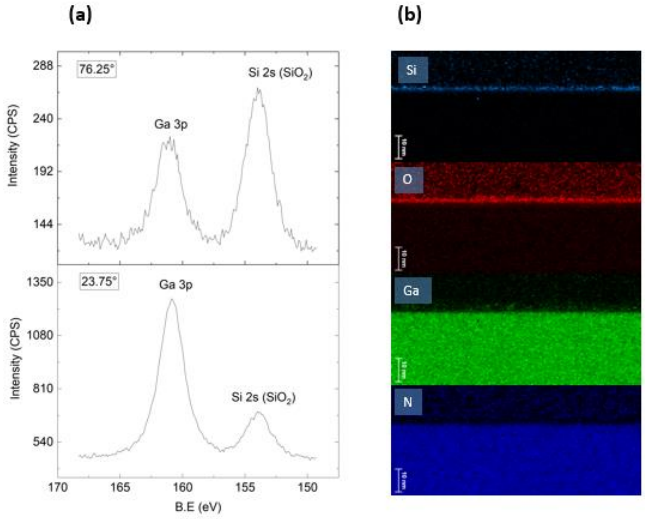

Figure 82. (a) pAR-XPS Si 2s peak and (b) EDX images related to SiO_2 contamination on the as-grown GaN samples

The intensity of the Si 2s peak (Figure 82 (a)) related to SiO_2 was higher at the extreme surface angle (76.25°) than at the bulk angle (23.75°), which indicated that the contamination was located at the surface, which is in agreement with the EDX images (Figure 82 (b)) which exhibited a thin layer of few nanometres at the surface as well. This contamination might have occurred during the annealing.

The impact of the HCl wet etching on the equivalent oxide thickness (Figure 81 (b)) exhibited a decrease on the RTP annealed sample for both surface. However, it must be noted that for the dry-etched sample, the model did not fit and the estimation was therefore wrong. Concerning the effect of $(NH_4)_2S$ treatment, we can notice a decrease of the oxide thickness for both surfaces, which indicates two things. First, that the total amount of oxygen detected after $(NH_4)_2S$ (Figure 81 (a)) was indeed not related to the oxidation of GaN but was related to the presence of SiO_2 at the surface. Second, the estimation of the equivalent oxide thickness did exhibit etchant properties, which was not revealed by the total amount of oxygen. This

difference came from the fact that the Ga 2p core-level is more surface sensitive than the O 1s core-level.

To conclude, HCl was an efficient etchant that hindered further oxidation whereas $(NH_4)_2S$ was less effective. The removal of the oxide layer after HCl treatment indicated that the oxide growth starts at dislocations in agreement with [87]. The pits were more visible on the as-grown surface. Indeed, the pits had been enlarged, which was not the case on the dry-etched surface. This difference between the two surfaces could be explained by the direct accessibility of the dislocations where oxygen atoms are adsorbed, on as-grown GaN samples. Moreover, this study highlighted the capacity of GaN to continue to oxidise after RTP.

IV.4.2 A technique to enhance chemical passivation

The combination of HCl followed by $(NH_4)_2S$ treatment was investigated with the aim to etch then passivate the surface. The annealed samples treated by HCl were immersed in $(NH_4)_2S$. AFM measurements were conducted to investigate the surface morphology (Figure 83).

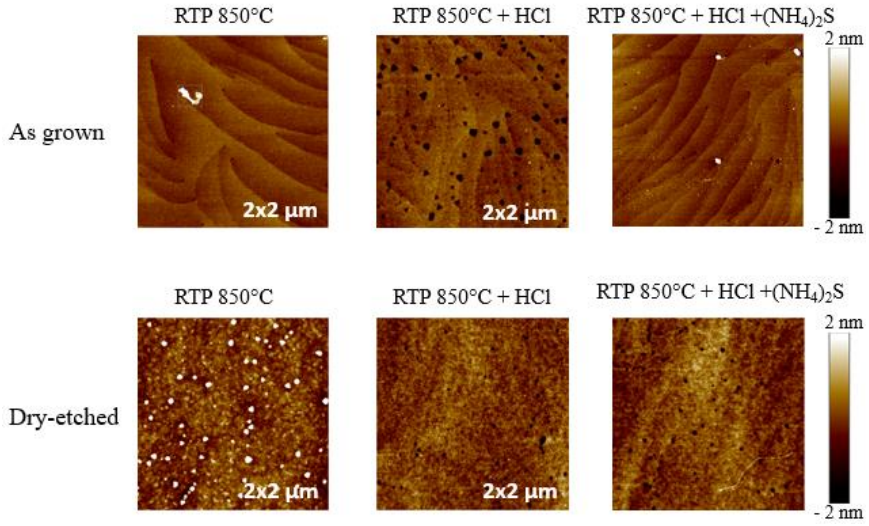

Figure 83. AFM images before and after HCl and HCl+$(NH_4)_2S$ wet etching on annealed as-grown and dry-etched GaN

The as-grown sample exhibited some white dots on the surface, probably oxide grains. Therefore, we assume that oxidation occurred after the HCl treatment. However, the dislocations were less visible than after the HCl wet treatment. Conversely, for the dry-etched GaN samples, no oxidation grains appeared after the HCl treatment or the little grains that might have grown had been etched by the $(NH_4)_2S$ treatment.

pAR-XPS analyses focused on the amount of oxygen and the oxide thickness were estimated (Figure 84).

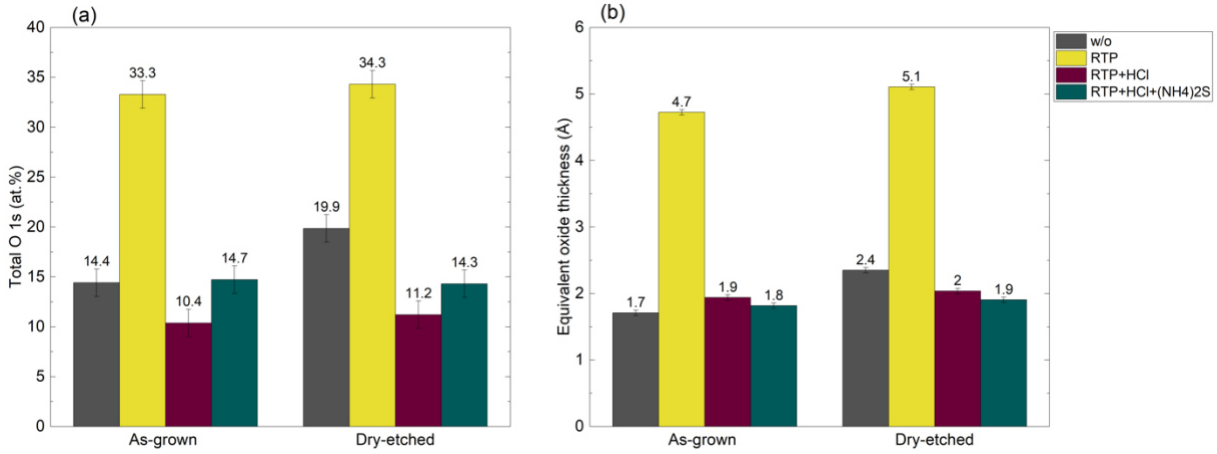

Figure 84. Impact of the RTP annealing followed by HCl and $(NH_4)_2S$ wet etching on (a) the relative total O 1s at.% and (b) the equivalent oxide thickness

The total O 1s at.% (Figure 84 (a)) exhibited a slightly higher amount compared to the samples only treated by HCl. This trend was observed for both surfaces and ended up with the same amount of about 14 at.%. The increase observed for the as-grown was in agreement with the AFM image (Figure 83, top line), where oxide grains were observed. In the case of the dry-etched GaN this increase did not lead to oxide growth but could be observed in the future. The re-oxidation process might therefore be delayed in the case of dry-etched surface. This delayed effect could come from the amorphous material to be etch in the first place, but also to the less accessible dislocations, where the oxidation seems to start.

The equivalent oxide thickness were calculated and did not show evidence of more oxidation. Indeed, the oxide thickness remained around 2 Å. However, note that the model did not fit well for both surfaces. Note that the presence of sulphur was not detected on both surfaces.

IV.4.3 Conclusions

To conclude, the use of RTP as an oxidation step for digital etching might not be suitable especially on heteroepitaxial GaN-on-Si. Indeed, the oxidation process starts preferentially at dislocations. This entry point lead then to an oxide layer. The removal of the oxide layer led to larger pits, which supports the assumption that the white dots on AFM images were oxide grains and not particles. Nevertheless, RTP on dry-etched surface showed a delayed oxidation. This was explained by the fact that the accessibility of the dislocations was restrained by the previous plasma, hindering the adsorption of oxygen at those sites.

Chapter V - Destabilising the surface of GaN by wet etching

V.1. Hot sulphuric acid: hydrogen peroxide mixture

The previous pAR-XPS systematic study on GaN wafers (section III.1.1) highlighted the fact that the temperature had an important role in etching the quasi-inter surface of c-plane, with Ga polarity GaN. In particular, we saw that H_3PO_4, which has the highest boiling point of the chemical treatments used, had the biggest impact on the estimated equivalent oxide thickness. High temperature could also be reached with H_2SO_4 and H_2SO_4:H_2O_2 mixtures. In the following paragraphs, we investigated the impact of H_2SO_4:H_2O_2 mixture and H_3PO_4 when used during a more extended period of time at high temperatures to initiate a considerable modification of the surface chemistry, with the expectation of Ga-N bonds cleavage.

V.1.1 Equipment and conditions of the wet treatments

We conducted the treatment on a semi-industrial automatic cleaning equipment from SubMicron Systems Corp. The wafer was immersed into a tank where the concentration of etchant solution was set to 110 mL of H_2O_2 (30 vol. %) in 40 L H_2SO_4. At each immersion of the wafers, a spike of H_2O_2 was automatically injected. The temperature of the tank was regulated at 110°C. In order to modify the surface chemistry, the wafer was immersed for 2.5 minutes into the tank then rinsed in warm deionised water for 30 seconds. The immersion in the H_2SO_4:H_2O_2 mixture followed by the rinsing step was repeated 40 times.

V.1.2 GaN substrate

In order to check the possibility of a relevant etching rate, we used GaN wafers caped with GaN/AlN additional layers, so that it would be possible to measure any reduction in the thickness of the GaN layer using X-ray reflectivity. The thickness of the GaN and AlN layers were 16 nm and 2.5 nm respectively (Figure 85) and were measured before and after H_2SO_4:H_2O_2 repeated treatments.

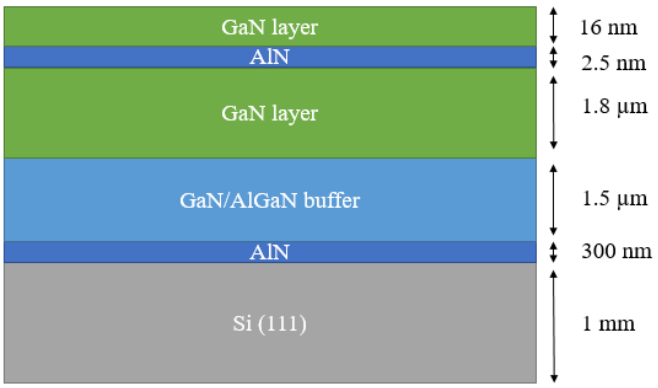

Figure 85. GaN layers stack used for the wet H_2SO_4:H_2O_2 mixture study

V.1.3 Influence on the surface chemistry

We investigated the impact of the hot H_2SO_4:H_2O_2 mixture on the surface chemistry of the GaN surface via pAR-XPS. Figure 86 shows this impact on the Ga 3d and N 1s peaks.

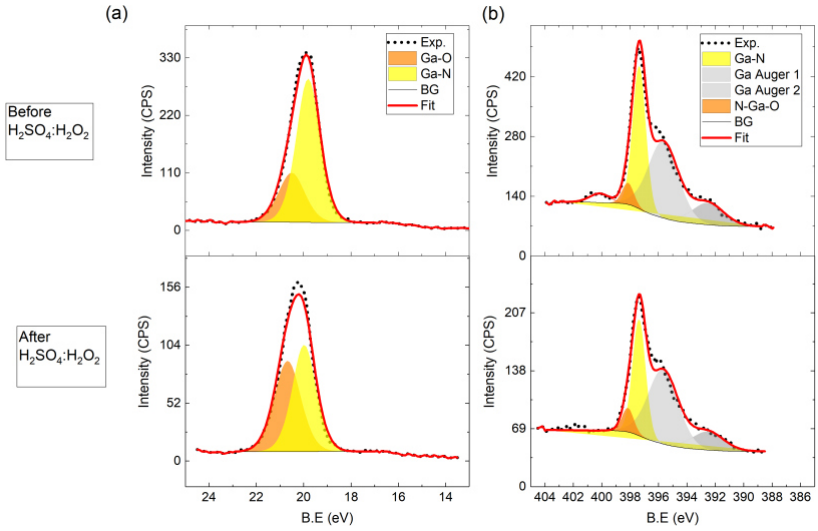

Figure 86. Evolution of (a) the Ga 3d spectra and (b) the N 1s spectra after 40 cycles of H_2SO_4:H_2O_2 mixture/ deionised water

It can be noticed from Figure 86 (a) an important increase of the Ga-O contribution of the Ga 3d peak after repeated immersions into H_2SO_4:H_2O_2. Furthermore, the peak shifted to 0.3 eV toward higher binding energies. However, no significant shift was observed for the N 1s peak (Figure 86 (b)). The shift of the Ga 3d peak toward higher binding energies and the diminution of its intensity could be related to a high amount of OH groups at the surface. Indeed, as shown in Figure 87, the O 1s spectra shifted toward higher binding energy. Furthermore, we can observe that the FWHM was smaller after the H_2SO_4:H_2O_2 treatments with 1.9 for the

treated sample versus 2.7 for the untreated one. Although the O 1s could not be deconvoluted, the shift and the reduction of the FWHM suggested the adsorption of an electronegative group, such as OH^- or the formation of Ga hydroxide. Furthermore, the peak was centred around 532.5 eV, which was reported to be related to the introduction of hydroxyl groups through the dissociative adsorption of water molecules [34, 94]. The adsorption of hydroxyl groups after H_2SO_4:H_2O_2 mixture has already been reported [48] and even used to functionalise the surface of GaN through hydroxylation reactions [96].

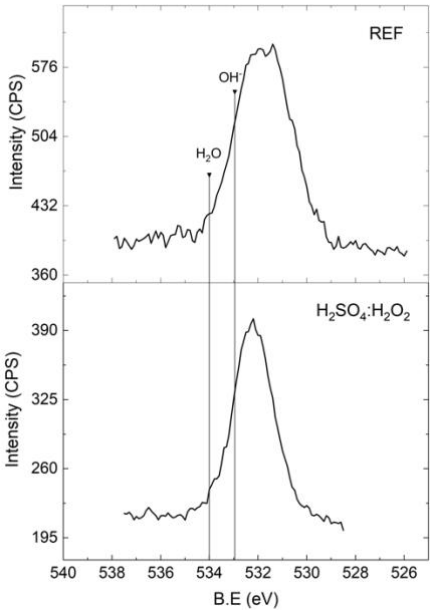

Figure 87. O 1s spectra before and after H_2SO_4:H_2O_2

We investigated the presence of hydroxyl groups by contact angle measurement, which is an effective measure to evaluate the hydrophilic or hydrophobic nature of a surface. We used the sessile drop technique shown in Figure 88. A water drop is deposited onto the surface with a syringe and is automatically measured by the Advance (Krüss) software.

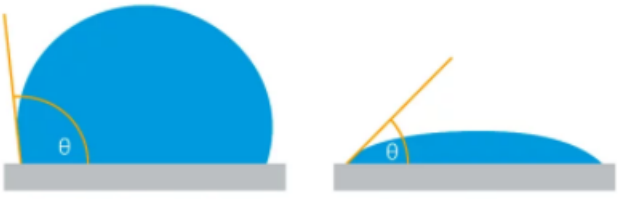

Figure 88. Contact angle measurement by the sessile drop technique (Krüss website)

The modification of the wettability can be attributed to the presence of OH species, oxidation [97] or also to the morphology [98]. In [97], the wettability was modified due to the

high electronegativity of the oxygen incorporated which increases the dipole moment of the surface and enables polar liquid like water to bond via hydrogen bonds or Van der Waals forces.

After the H_2SO_4:H_2O_2 treatments, the surface was hydrophilic, with a contact angle of 56° ($\theta < 90°$). However, the contact angle was increased compared to an untreated GaN surface for which the contact angle was 40°.

The increase of the carbon level might be responsible for the increase of the contact angle. As shown in Table 6, the total amount of carbon detected increased by 7.9 at.%. The total amount of oxygen only increased by 2.3 at. %, and the peak position of the O 1s peak indicated a change in the bonding state of oxygen that might be related to the formation of a Ga-OH layer on top of the GaN layer. Indeed, the Ga-O contribution increased about 3.3 at.% after the H_2SO_4:H_2O_2 treatments.

	Ga-N	Ga-O	N-Ga	N-Ga-O	O	C	Ga/N
REF	19.4	7.4	21.0	1.5	19.0	32.0	0.48
H_2SO_4:H_2O_2	11.3	10.7	14.2	2.6	21.3	39.9	0.44

Table 6. Atomic percentage (at. %) of GaN before and after H_2SO_4:H_2O_2 treatments

The decrease of the Ga/N ratio after H_2SO_4:H_2O_2 treatments suggested a loss of Ga-N bonds at the surface. The large contribution of OH species at the surface could have created gallium hydroxides, like $Ga(OH)_3$ that might have been dissolved in the liquid medium. However, the equivalent oxide thickness increased from 1.7 Å to 2.2 Å after treatments, which contradicts the putative etching of the surface by the formation of soluble gallium hydroxides. Therefore, the amount of gallium lost at the surface might be related to specific etching on defect points, which expose other faces than the c-plane that are more reactive towards etchants.

V.1.4 AFM and XRR measurements

The overall XPS investigations may suggest that the H_2SO_4:H_2O_2 mixture could have etch at defect points by forming gallium hydroxides, which were subsequently dissolved in the etching solution. Thus, we performed AFM measurements in order to evaluate the impact of the repeated H_2SO_4:H_2O_2 treatment on the surface morphology as shown in Figure 90.

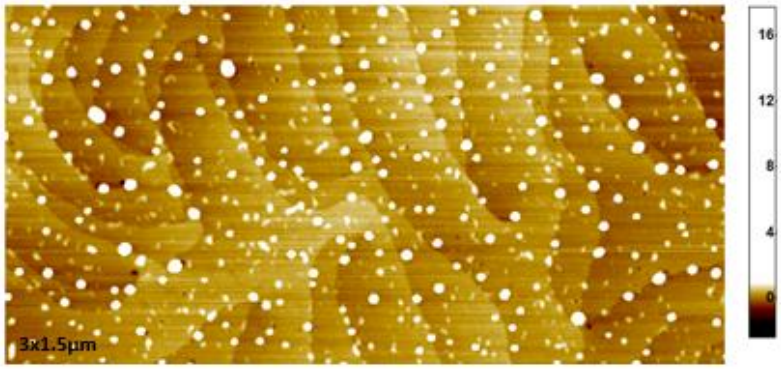

Figure 89. AFM image of the surface of GaN after several H_2SO_4:H_2O_2 treatments

We found white dots on the surface which may be linked to the presence of the OH species. Furthermore, some white dots were located next to dislocations and atomic steps, which could confirm our assumption, that the species of the H_2SO_4:H_2O_2 mixture attacked at defects points, here the dislocations or atomic steps, while no etching was observed at the c-plane.

It is important to keep in mind that the white dots represent interactions with the tips, and were thus not considered as oxide or hydroxide grains.

XRR measurements were also conducted in order to see if the wet treatments had etched the 17 nm GaN top layer. The measurements were performed at three different points, which were located at the centre, the mid-radius, and the edge of the wafer. The results are listed in Table 7.

	GaN/AlN cap thickness (nm)					
	Centre		Mid-radius (45 mm)		Edge (80 mm)	
	GaN	AlN	GaN	AlN	GaN	AlN
Untreated	17.1	2.7	16.0	2.6	14.2	1.8
H_2SO_4:H_2O_2	17.2	2.7	16.0	2.6	14.2	1.9

Table 7. Evolution of the GaN/AlN cap thickness after the H_2SO_4:H_2O_2 treatments

Again, no evidence of etching properties could be found, with no change in the thickness of the GaN/AlN remained the same after the H_2SO_4:H_2O_2 treatments. Therefore, one explanation of the gallium atoms loss could be their removal at the defects points where the surface is less stable.

V.1.5 Evolution of the surface morphology overtime

The XPS analysis revealed OH coverage over the surface. However, the XPS analyses were only performed four months after the H_2SO_4:H_2O_2 treatments. This paragraph intends to show the evolution of the surface morphology several months after the treatments. Figure 90 exhibits the surface morphology a few days after dipping the wafer into the solution. As we can see, no morphological changes could be observed after the H_2SO_4:H_2O_2 treatments.

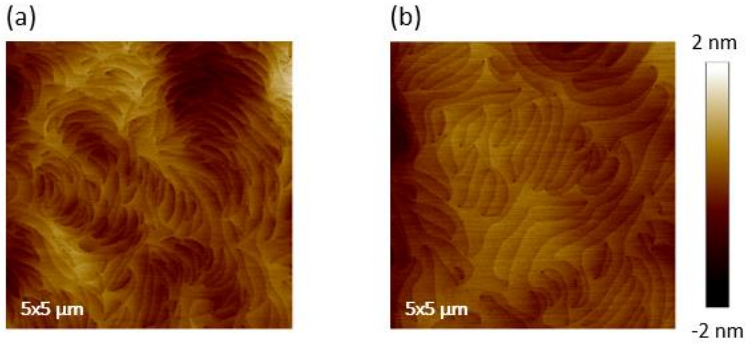

Figure 90. AFM images (a) before and (b) after H_2SO_4:H_2O_2 treatments

However, after performing new AFM measurements one month later (Figure 91), white dots started to appear all over the surface (Figure 91 (a) and (b)) and more specifically next to dislocations were visible (Figure 91 (b)). Two months later, the density of white dots had greatly increased (Figure 91 (c)).

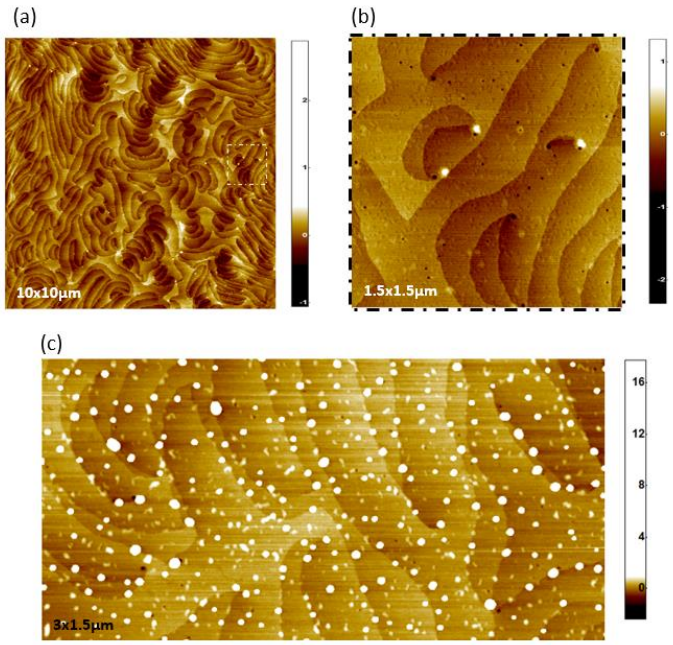

Figure 91. Evolution of the white dots after H_2SO_4:H_2O_2 treatments, (a) one month after the treatment (b) a zoom image of (a) showing the white dots near dislocations and (c) the evolution of the white dots 3 months after the treatments

The evolution of the white dots on the surface suggested that the modification of the surface chemistry started at dislocations then spread on the surface, perhaps through the atomic steps. This is similar to results in the literature, which suggest that oxidation starts at dislocations [87].

V.2. Hot phosphoric acid

V.2.1 Equipment and conditions of the wet treatments

Hot phosphoric acid (H_3PO_4) treatments were performed on a semi-automatic wet bench from SAPI. This equipment has the advantage to maintain the water in the solution while heating at high temperature, by adding periodically water which immediately mix with the acid to maintain the temperature. This way, the H_3PO_4 solution keeps its initial concentration, which was 85% (w/w).

The treatments were performed at 155°C and the immersion of the samples in H_3PO_4 was set for four different durations: 10, 20, 30 and 60 minutes. Then the samples were rinsed in deionised water and dried under N_2 flow.

V.2.2 Substrates

As mentioned in section I.4.2, for the transistor fabrication, a dry etching step is used to remove the AlGaN layer and thus depletes the 2DEG. Such energetic treatments induce surface damages and thus modify the surface. Therefore, for this study, we evaluated the impact of hot phosphoric acid (155 °C) on two kinds of GaN surfaces: as-grown and dry-etched surfaces, in order to be closer to the transistor manufacturing process. The standard dry etching process was an initial inductive coupled plasma reactive induced etching (ICP-RIE), which was a Cl_2/BCl_3-based plasma. The second step was an Atomic Layer Etching (ALE) Ar-based plasma, which is a less energetic etching step intended to remove the damaged layer. The ALE step was introduced because it has shown to improve electrical properties after ICP-RIE. For example, in a previous work [99], a final ALE step after ICP-RIE allowed the reduction of the sheet resistance of the 2DEG channel of the AlGaN/GaN heterojunction. Indeed, the plasma treatments are known to increase the resistance sheet which indicates electrical degradations.

During the transistor fabrication, the formation of the gate (and the contacts) of the transistor is performed with photolithography. A photoresist layer coating is deposited, exposed according to lithographical masks to define the gate, and then developed, thus defining the zone

to be etched. Then, the ICP-RIE takes place forming the gate. A stripping sequence is then required after etching in order to remove the remaining photoresist layer coating, as well as the etching residues. The stripping sequence consisted of an O_2 plasma followed by a wet cleaning step in DuPont™ PlasmaSolv® EKC 265™, which is a hydroxylamine-based commercial solution formulated to remove post-etch residue. For this study, and in order to keep the carbon contamination of the surface constant, no photoresist layer coatings were used.

The layer stack of the wafers was the same as those presented in section III.1.1, except that the GaN buffer was intentionally n-doped with silicon, with a carrier concentration of $5x10^{17}$ cm^{-3}. These layers allowed us to evaluate the impact of hot phosphoric acid on the electrical properties.

V.2.3 Influence of immersion time into H_3PO_4

V.2.3.1. Influence on the GaN surface chemistry

We investigated the effect of H_3PO_4 over time on both the as-grown and dry-etched surfaces and the Ga 3d spectra are shown in Figure 92. It can be noticed that, before H_3PO_4 treatment, the dry-etched sample did not exhibit a shift toward higher bonding energy compared the as-grown sample, unlike [99, 100]. This may be because, after plasma treatments, the samples were dipped into EKC265™, which had an etchant effect, removing the oxides created by the plasmas.

After the H_3PO_4 treatment, the Ga 3d peaks shifted towards higher binding energies, by about 0.7 eV and 0.5 eV for as-grown and dry-etched samples respectively. A shift toward higher binding energy typically revealed the adsorption of oxygen in $Ga\text{-}O^{2-}$ or $Ga\text{-}OH^{-}$ forms [3, 82].

Furthermore, a clear increase of the Ga-O component area could be noted when the samples were immersed for 30 and 60 minutes in H_3PO_4. However, no change in the Ga-O component was observed after 10 and 20 minutes. The contributions in percent of the Ga-O component are shown in Figure 93, with the formation of a gallium hydroxide starting from 30 minutes of treatment.

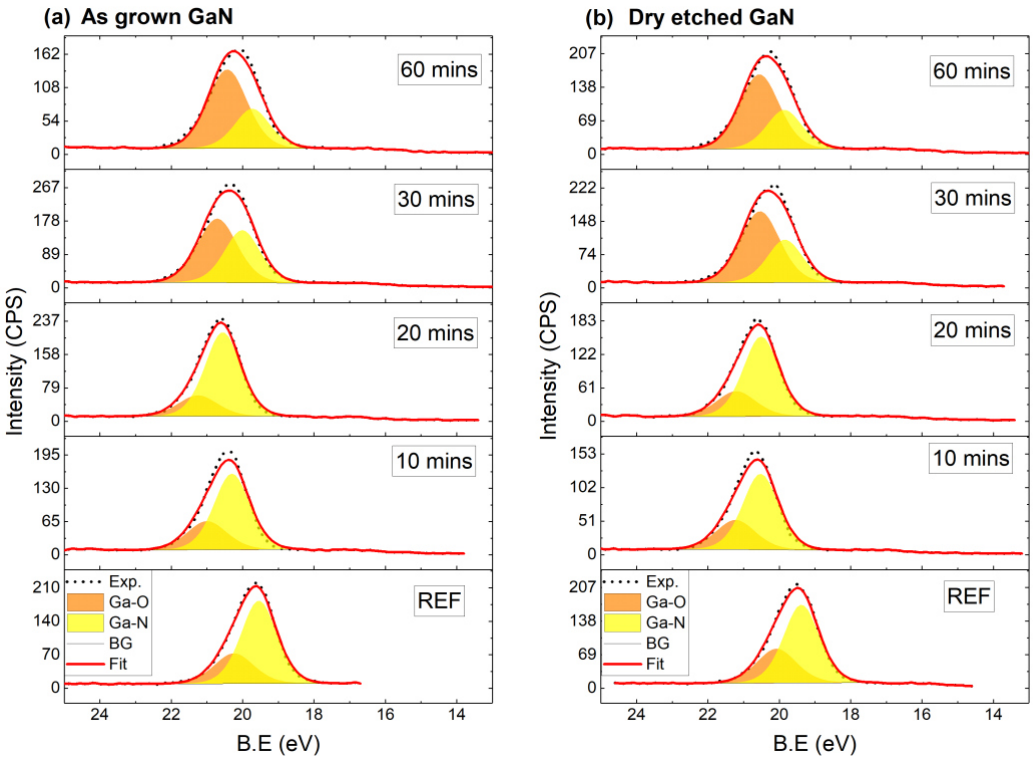

Figure 92. Evolution of the Ga 3d spectra of (a) as-grown GaN and (b) dry-etched GaN at different time of H_3PO_4 treatment

Dry-etched samples were slightly more oxidised than as-grown samples, in line with previous work [102]. We can also see from Figure 93 that the Ga-O amount of the dry-etched samples decreased and the difference between as-grown and dry-etched samples was reduced after 10 minutes in H_3PO_4. Thus, the decrease of the Ga-O component for the dry-etched sample was likely due to surface damage removal. We assume that the dry-etched GaN had initially more active sites that might be related to dangling bonds and vacancies, enabling the formation of Ga-O bonds, while for the as-grown GaN fewer active sites were initially present. However, the number of active sites significantly increased between 30 and 60 minutes. In addition, between 30 and 60 minutes of treatment, the as-grown sample gained almost 10% more of Ga-O contribution whereas the dry-etched sample barely gained 3%. This means that after 60 minutes, they both had around 70% of Ga-O.

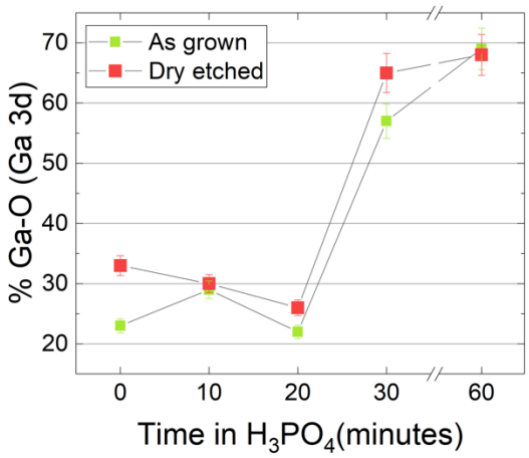

Figure 93. Evolution of the Ga-O component from the Ga 3d as a function of time in H_3PO_4

The analysis of the N 1s spectra led to a similar conclusion (Figure 94). After deconvolution, there was an increase of the N-Ga-O component at the expense of the N-Ga component. As for the Ga 3d spectra, the N-Ga-O contribution started to increase after 30 minutes of treatment and further increased with the H_3PO_4 treatment duration. However, no shifts toward higher binding energy was observed for 30 and 60 minutes after immersion in H_3PO_4 for both surfaces. However, shifts can be observed after 10 and 20 minutes of treatments, and the N 1s peaks of as-grown samples shifted by 0.38 eV and 0.68 eV for 10 and 20 minutes respectively. In the case of dry-etched samples, the N 1s peaks also shifted after 10 and 20-minutes treatments. In this case, the shifts were the same for both times, about 0.54-0.55 eV.

The shifts toward higher binding energies observed for the Ga 3d and the N 1s spectra after H_3PO_4 could be attributed to charge effects due to the adsorption of PO_4^{3-} and hydroxyl groups.

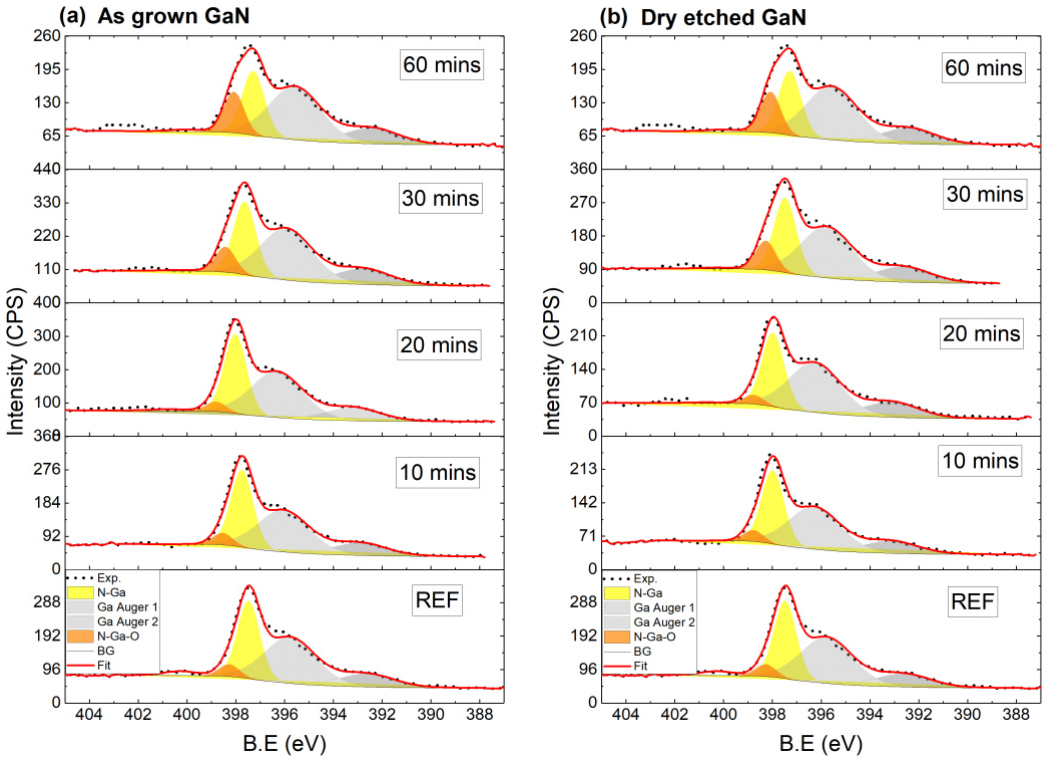

Figure 94. Evolution of N 1s spectra of (a) as-grown GaN and (b) dry-etched GaN at different times of treatment in H_3PO_4

The relative atomic percentage (at. %) of elements present at the surface are shown in Table 8 and Table 9, for the as-grown and dry-etched samples respectively.

Time in H_3PO_4 (min)	Total C % (C1s)	Total O % (O1s)	N-Ga % (N1s)	N-Ga-O % (N1s)	Total P % (P2p)	Ga-N% (Ga3d)	Ga-O % (Ga3d)
0	29	21	20	5	0	17	8
10	22	23	20	3	9	16	7
20	22	23	20	3	8	19	5
30	24	22	16	6	8	10	14
60	33	22	10	6	9	6	13

Table 8. Relative atomic percentage of elements present at the surface of the as-grown GaN samples

Time in H_3PO_4 (min)	Total C % (C1s)	Total O % (O1s)	N-Ga % (N1s)	N-Ga-O % (N1s)	Total P % (P2p)	Ga-N% (Ga3d)	Ga-O % (Ga3d)
0	24	19	23	5	0	21	8
10	22	26	18	3	9	16	6
20	20	27	16	3	11	17	6
30	24	22	16	6	8	9	15
60	27	22	13	7	8	8	15

Table 9. Relative atomic percentage of the elements present at the surface of the dry-etched GaN samples

The amount of PO_4^{3-} detected did not significantly change over time. Except for the dry-etched sample after 20 minutes of immersion, the atomic percentage (at. %) of P 2p was around 8 to 9 at. %. The amount of adsorbed phosphorus has been reported to be correlated with the treatment temperature [103], but we did not explore different temperatures in this study. Due to this relatively high amount of phosphorus, i.e. PO_4^{3-}, the O 1s spectra were difficult to deconvolute. Therefore, the amount of oxygen refers here to the total amount of O 1s detected which could include, Ga-O, PO_4^{3-}, C-O, etc.

The total amount of oxygen remained largely unchanged throughout the different treatment times. Although the O 1s spectra could not be deconvoluted (Figure 95) , the shifts of the peaks toward higher binding energy and the increase of intensity around 533 eV, indicated a relatively important adsorption of OH groups [104]. The adsorption of PO_4^{3-}could also be responsible for this increase and the shifts. The adsorption of OH groups at the surface explains the shifts of the Ga 3d spectra as well as of the N 1s for 10 and 20 minutes. Therefore, between 10 and 20 minutes, for both surfaces, a certain amount of OH groups may be present at the surface, leading to peak shifts. After 30 minutes, dangling bonds are created which are passivated with the OH groups present in the solution, promoting thereby the formation of some forms of gallium hydroxides. The formation of hydroxides at the surface is consistent with other works using H_3PO_4 based treatments [103, 104].

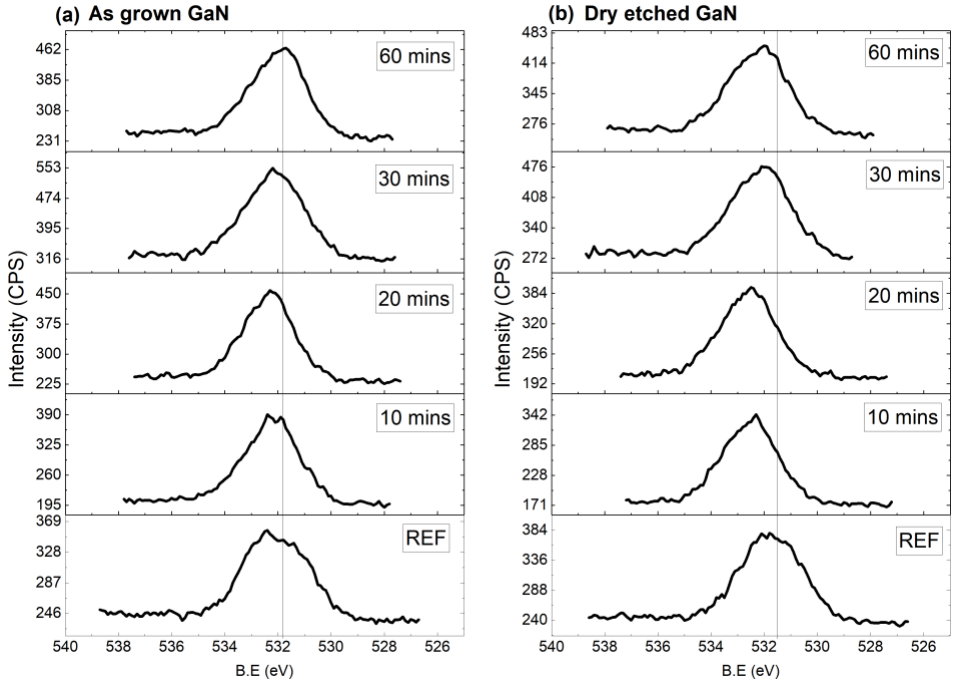

Figure 95. Evolution of the O 1s spectra of (a) as-grown GaN and (b) dry-etched GaN at different time of H_3PO_4 treatment

The evolution of the Ga/N ratio, which was calculated based on the Ga-N component of the Ga 3d and N 1s peaks is presented in Figure 96. A decrease was observed after 30 minutes of H_3PO_4 treatment for both surfaces. This result revealed a non-stoichiometric distribution of the gallium and nitrogen atoms at the surface, which was initially not far from Ga/N=0.5. After 30 minutes of treatment, the Ga/N ratio reached 0.40 and 0.35 for the as-grown GaN and the dry-etched GaN respectively. While the ratio did not change after 60 minutes for the dry-etched GaN, it was reduced to 0.37 for the as-grown GaN. Therefore, the Ga-N bonds at the surface were dissociated by the PO_x species, forming gallium hydroxide, in line with the work of Shintani *et al.* [53].

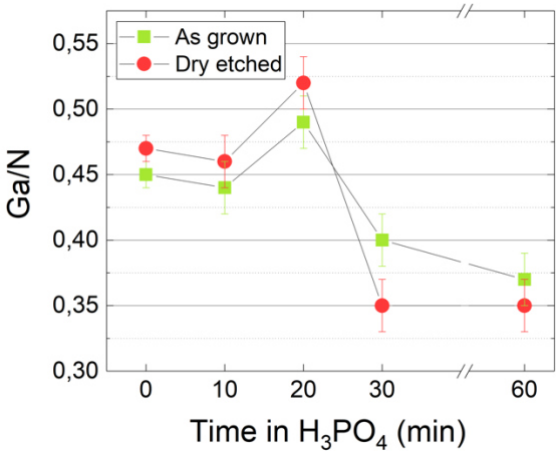

Figure 96. Evolution of the Ga/N surface ratio on as-grown and dry-etched GaN as a function of time in H_3PO_4

The dissociation of the Ga-N bonds might have resulted in the replacement of nitrogen atoms by oxygen atoms as illustrated in Figure 97.

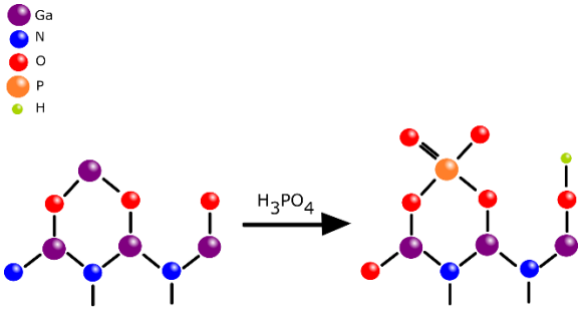

Figure 97. Scheme of the expected connections at the surface after H_3PO_4 treatment

The surface, which was initially covered by native oxide, was attacked at reactive sites, PO_4^{3-} dissociating the Ga-N bonds, as suggested by [53]. The treatment or the subsequent rinsing in deionised water, provided hydroxyl groups on the surface as well. Note that the exact nature of the Ga-OH and Ga-PO_x bonds are unclear.

V.2.3.2. Influence of H_3PO_4 on the morphology

The GaN surface morphological changes were examined by AFM as shown in Figure 98. We can see that, prior to H_3PO_4 treatment, the as-grown sample clearly exhibited defined rounded atomic steps, together with dark spots associated with threading dislocations having a screw type component. For the dry-etched sample, the surface was rougher because of the plasma treatment and it is difficult to clearly see atomic steps and dislocations.

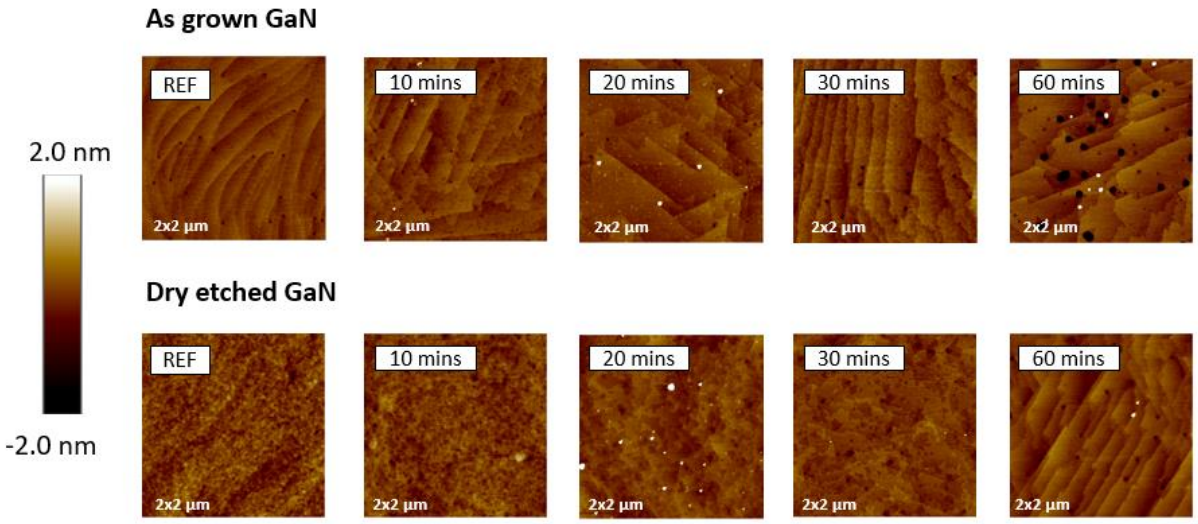

Figure 98. AFM images before and after hot H_3PO_4 treatment at different durations

For the as-grown sample, the atomic steps became straight and crystallographically aligned after 10 minutes of immersion in H_3PO_4. After 20 minutes, steps started to become triangular before becoming parallel after 30 minutes of immersion. Dark spots associated with threading dislocations on the as-grown sample evolved into well-defined hexagonal pits after 60 minutes in hot H_3PO_4 in line with the literature results on c-plane GaN [103–106]. In this case, there were 22 large pits after 60 minutes, compared with 21 pits on the surface of the as-grown sample without H_3PO_4 treatment. Larger holes were likely the emergence pits of dislocations with a screw component, while smaller ones could be pure edge type. The total density of threading dislocations was therefore of about 1.9×10^9 cm^{-2}, in line with the observations by Yon *et al.* [108] on similar samples. However, it is important to note that after 60 minutes, some of the large holes had hexagonal structures of different sizes, which is likely due to their overlapping making an accurate counting of dislocations difficult (Figure 99 (a)).

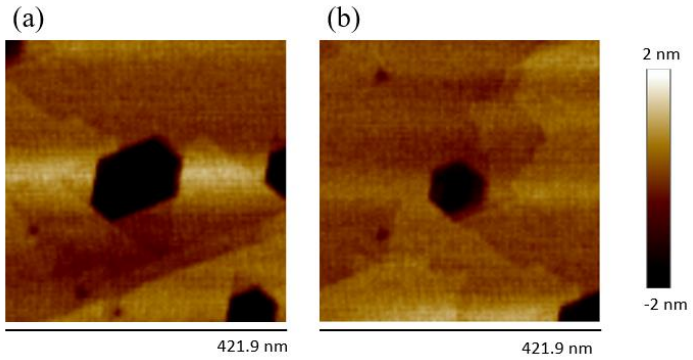

Figure 99. AFM images of (a) overlapping dislocations and (b) a single dislocation of the surface of an as-grown sample after 60 minutes in H_3PO_4

These AFM images indicated that etchant species attacked at defect points, i.e. dislocations or surface defects, in agreement with [55]. Indeed, the (0002) surface is very stable so the H_3PO_4 is not expected to attack everywhere. It is more likely that the attack occurred at non-equilibrium positions such as dislocations, atomic steps edges, or surface defects. Etching is reported to be dependent on the number of dangling bonds on the surface [28]. This is coherent with the opening of dislocations, which exposes inclined planes, with therefore different crystalline orientations on the surface, which can be attacked more easily. Atomic steps became aligned and straighter, in order to reduce their energy.

For the dry-etched sample, the surface started to show changes after 20 and 30 minutes, with the appearance of small triangular structures. After 60 minutes of immersion in H_3PO_4, the dry-etched surface exhibited straight atomic steps similar to those of the as-grown sample after 30 minutes in H_3PO_4. This evolution is shown schematically in Figure 100.

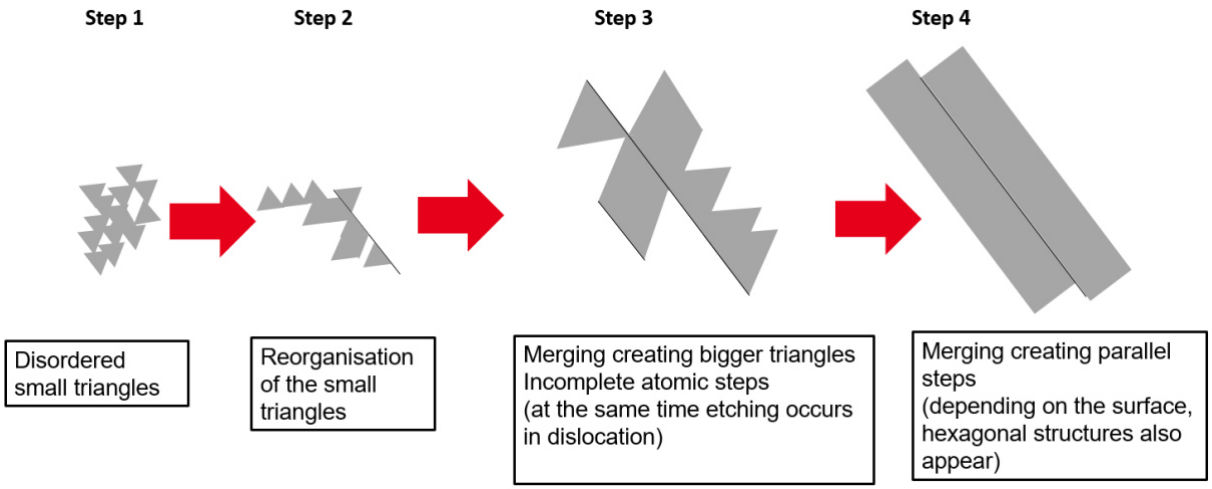

Figure 100. Evolution of the GaN surface for different durations in H_3PO_4. The black line is a visual guide to delimit the atomic steps

Based on these observations, we can thus suggest the following dry-etched recovery mechanism upon immersion in H_3PO_4. The use of a plasma treatment results in an amorphous surface where surface defects are not directly accessible. The kinetic migration of the wet etchant species toward active sites is therefore decreased. The H_3PO_4 wet etching starts first with the removal of the amorphous layer caused by the dry etching. Next, the re-organisation of the surface starts, with the emergence of small triangular structures (Figure 100, step 1). Small triangles merge overtime (Figure 100, step 2 and 3), leading to the appearance of parallel atomic steps oriented along the same crystallographic direction (Figure 100, step 4), as seen for the as-grown sample. During that stage, there is a progressive revelation of dislocations. Finally, based on the AFM image of the as-grown sample (Figure 98, top line), it is likely that dislocations will be further opened on GaN dry-etched surfaces for immersions longer than 60 minutes, with the same dislocations opening and merging [106].

V.2.3.3. XRR measurements

The AFM images clearly exhibited the etching properties of H_3PO_4 at non-equilibrium areas like atomic steps edges, dislocations and surface defects. Therefore, in order to see if the c-plane could be attacked as suggested in [109], we conducted XRR measurement on a GaN wafer capped with an additional GaN/AlN layers like presented in paragraph V.1.2, but with an initial thickness of about 26 nm and 2 nm for the GaN and AlN layers, respectively . The experiment was performed on an as-grown GaN immersed in H_3PO_4 for 60 minutes in the same conditions as those used before. We chose the duration time of 60 minutes because it exhibited the clear signs of over etching as presented in Figure 99. The results of the impact of H_3PO_4 on the GaN cap are shown in Table 10.

	GaN/AlN cap thickness (nm)	
	GaN	AlN
Untreated	25.9	2.0
H_3PO_4 60 minutes	25.0	2.0

Table 10. Evolution of the GaN/AlN cap after a 60 minutes H_3PO_4 treatment on as-grown GaN

The thickness of the GaN cap was slightly reduced by 0.9 nm. This is a significant result and not within the error of the measurement, as the XRR data showed a clear change in frequency between the two measurements (Figure 101).

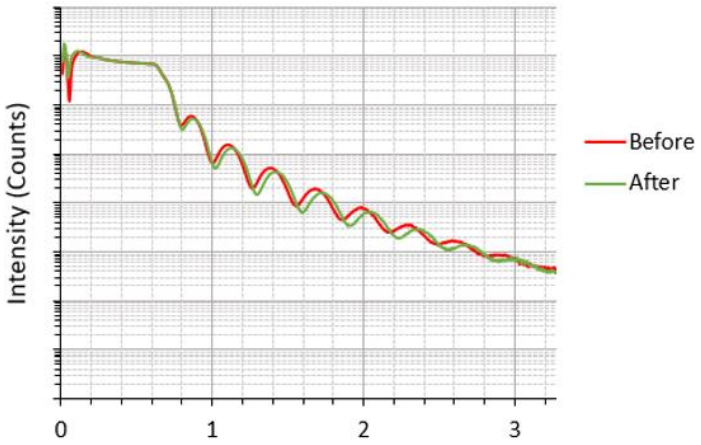

Figure 101. XRR scans before and after H_3PO_4 treatment (60 minutes)

Two possible scenarios might have occurred during the 60 minutes in H_3PO_4. The first possibility is that there was a vertical attack, i.e. c-plane that might have reduced the thickness. This case was suggested by Reiner *et al.* [109], where they used SEM and EDX analysis to propose a mechanism in which through dislocations, OH^- groups induced, steeper and more vertical etch rates. However, it seems unlikely that there would be an etch rate of 0.9 nm per hour, which is extremely slow. The second possibility is that the attack is only lateral, and due to etch back the atomic terraces, the overall thickness is reduced. Finally, a third scenario combines the two cases described before where both, vertical and lateral attacks occur, however, with a higher lateral etching rate than that of the vertical.

V.2.4 Influence of the ALE within the dry etching processes

V.2.4.1. Influence of H_3PO_4 on the surface chemistry

The delayed effect of H_3PO_4 on the dry-etched samples prompted us to investigate its effect at each step of this standard dry etching process. Table 11 summarises the dry etching steps of the studied samples. Samples A and B, which had been studied in the previous section, were used as references. Sample A stands for the as-grown GaN and sample B the standard dry-etched GaN.

	Etching steps prior to H_3PO_4			
	ICP-RIE	ALE	Strip. O_2	EKC 265™
Sample A				
Sample B	✓	✓	✓	✓
Sample C	✓		✓	✓
Sample D	✓	✓		

Table 11. Different dry etch treatment applied prior to H_3PO_4 wet etching

In particular, having shown the ability of H_3PO_4 to recover atomic steps after dry etching, this was also intended to examine whether the use of H_3PO_4 could avoid the need for expensive and time-consuming ALE.

The samples were immersed in H_3PO_4 for 30 minutes. This duration was chosen since it showed an impact on the surface chemistry without causing major degradations, such as wide dislocations opening, on both as-grown and dry-etched surfaces. This was also considered an acceptable time for industrial applications. The Ga 3d spectra before and after H_3PO_4 treatment are shown in Figure 102. Prior to H_3PO_4, the Ga 3d spectra of sample D exhibited a large contribution of the Ga-O component, whereas the sample C did not. Thus, the ALE probably allowed the formation of dangling bonds and vacancies leading the adsorption of oxygen, and forming some oxides at the surface. However, the stripping sequence did not exhibit the same amount of Ga-O and we suggest that the EKC 265™ step etched the oxides formed after the O_2 stripping. Therefore, all samples exhibited a different surface chemistry.

As a result, samples C and D did not exhibit the same evolution as the standard dry etched sample (sample B) nor the as-grown sample (sample A) after immersion in H_3PO_4. Indeed, no increase of the Ga-O component was observed on samples C and D. On the contrary, when the dry etching sequence stopped at the ALE step (sample D), a decrease of the Ga-O component was observed. Therefore, the H_3PO_4 enabled the removal of oxides formed after the ALE step. As discussed above, for a duration between 10 to 20 minutes, H_3PO_4 enabled the removal of some oxides as well for the standard dry etched GaN, sample B (Table 9 and Figure 93).

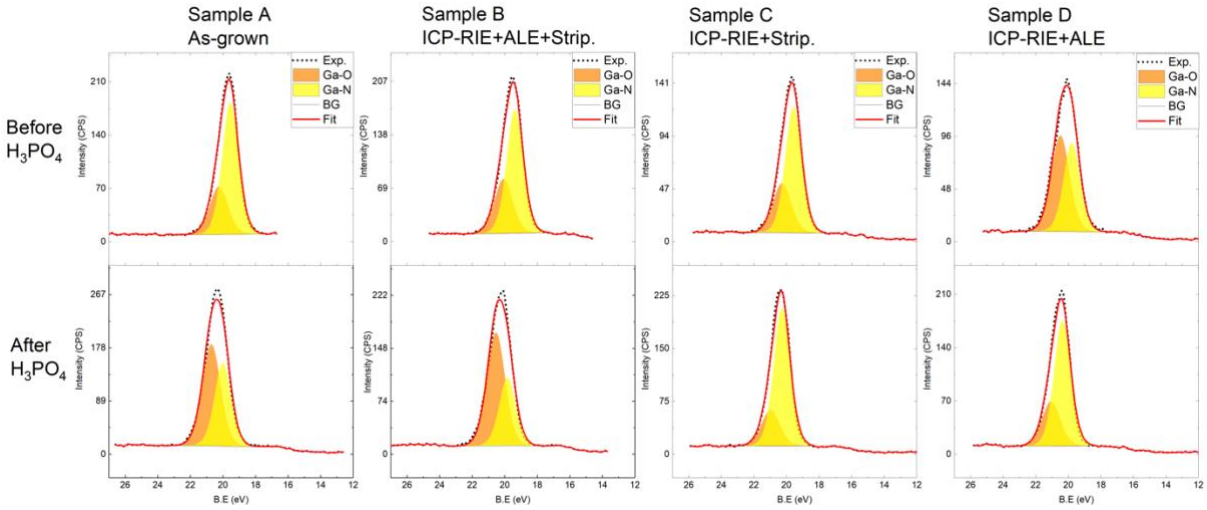

Figure 102. Evolution of the Ga 3d spectra for samples A to D before and after 30 minutes of H_3PO_4 treatment

The analysis of the N 1s spectra (Figure 103) showed the same trend that is the removal of some oxides. Indeed, before immersing the samples in H_3PO_4, the N 1s spectra of samples C and D needed a new contribution to fit the curve. This new contribution was positioned at 400 eV and could be assigned to Ga Auger because of the oxidised gallium. In the case of the sample C, this contribution (referred as Ga Auger in Figure 103) disappeared, since the final stripping was in EKC 265™, a hydroxylamine-based solution, which removed the oxide formed by the plasma treatments. This contribution also disappeared after H_3PO_4 treatment for samples C and D, which indicated the removal of some oxides.

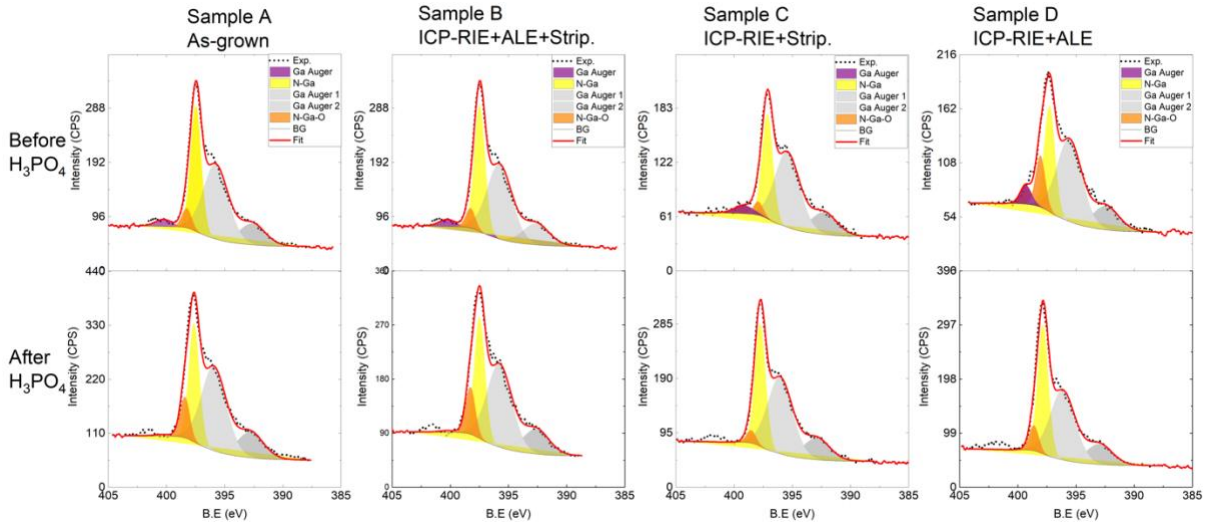

Figure 103. Evolution of the N 1s spectra for samples A to D before and after 30 minutes of H_3PO_4 treatment

The quantification of the elements before and after H_3PO_4, are presented in Table 12 and Table 13 for sample C and D respectively.

	Ga-N	Ga-O	N-Ga	N-Ga-O	O	C	P
Before H_3PO_4	15.0	6.5	13.6	1.6	21.0	42.4	0
After H_3PO_4	19.6	5.6	18.6	1.7	24.2	21.6	8.7

Table 12. Relative atomic % of surface species on sample C, i.e. ICP-RIE + Strip., before and after 30 min in H_3PO_4

	Ga-N	Ga-O	N-Ga	N-Ga-O	O	C	P
Before H_3PO_4	10.7	12.8	12.2	5.3	19.2	39.8	0
After H_3PO_4	16.7	6.6	20.8	3.6	24.2	18.0	10.1

Table 13. Relative atomic % of surface species on sample D, i.e. ICP-RIE + ALE, before and after 30 min in H_3PO_4

The dry etching processes did not seem to have an impact on the amount of phosphorus detected at the surface, which again is in good agreement with the result of Wilkins et al. [103] who only observed an influence of the temperature.

However, for the sample C, where the ALE step was removed, neither the Ga-O nor the N-Ga-O components increased. As stated before, the ICP-RIE induced considerable damage such as the creation of dangling bonds and vacancies, which make the surface somewhat amorphous. These induced defects can be found deep within the material. Therefore, the subsequent ALE step allowed the removal of the amorphous material resulting in a closer network more similar to the as-grown sample. In contrast, the surface of sample C, which is directly exposed to oxidative atmosphere right after the ICP-RIE plasma, was probably more damaged with the incorporation of oxygen, weakening the Ga-N bonds even more. The highest level of carbon was observed for sample C, due to the use of the EKC 265™ solution. As a consequence, fewer Ga atoms were accessible for bonding with hydroxyl groups. The H_3PO_4 treatment allowed the reduction of up to 50 % of the total amount of carbon, thus, we can assume that the reactions that first took place were the removal of some oxides and the carbon contamination.

V.2.4.2. Influence of H_3PO_4 on the morphology

The morphology of these samples was investigated by AFM before and after H_3PO_4 treatment as shown in Figure 104. The final morphology of the surface after H_3PO_4 immersion strongly differed from that obtained with the “standard dry etching” process including both ALE and the stripping sequence.

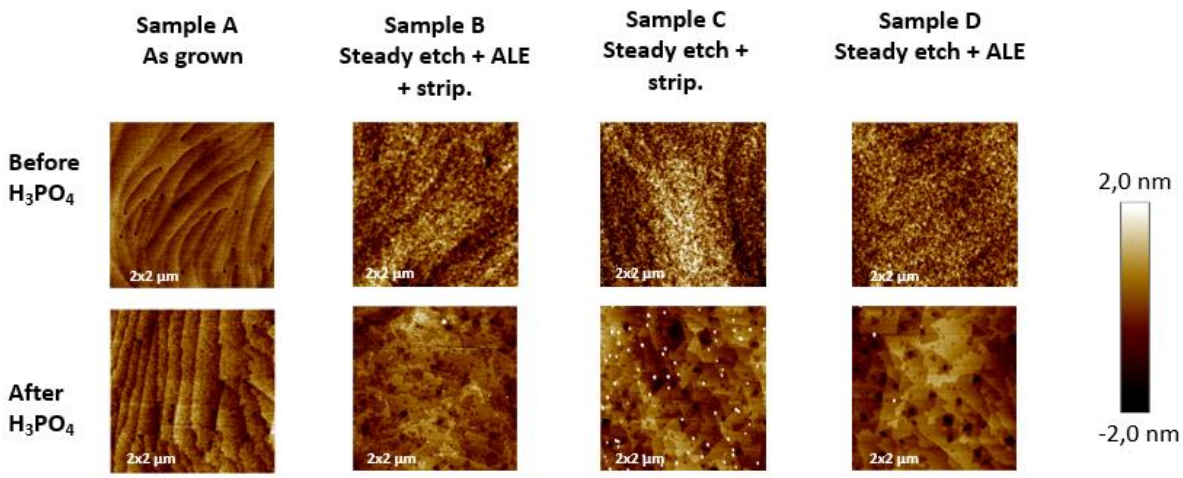

Figure 104. AFM images before and after 30 minutes in H_3PO_4 of sample A to D

The sample C without ALE appeared to exhibit a more organised surface after H_3PO_4 treatment than sample B, with ALE. Indeed, well-defined triangular structures appeared after immersion of sample C into H_3PO_4 whereas triangular structures of the "standard dry etching" process (sample B) were less distinguishable and smaller.

The sample D with ALE and without the stripping sequence exhibited larger triangular structures and atomic steps started to appear. Moreover, the dislocations turned into hexagonal structures, and some were overlapping, which is a sign of over etching. In the case of the as-grown sample (sample A), the over etching started after 60 minutes of treatment. Then we can see that the ALE without the stripping sequence tended to accelerate the etching of H_3PO_4. This could be explained by the strong possibility of residual chlorides adsorbed at the surface. In contrast, the standard dry etching process, which includes all the steps, seemed to delay the effect of H_3PO_4 for re-organising the surface. Then, in between, we have the sequence without ALE (sample C), where residual chlorides from the ICP-RIE might have been removed by the stripping sequence. Therefore, the effect, delayed or accelerated, observed on dry etched samples (B, C and D) strongly depends on the steps following the ICP-RIE process. These observations are consistent with the report of Tautz *et al.* [110] who reviewed the influence of surface damages induced by pre-processing on the etching rate of KOH. Depending on the damaging techniques conducted prior to wet etching, for example, it was reported that irradiation with Au+ ions at high energy combined with wet KOH treatment enhanced the formation of defect related etch pits.

Combining these observations with the pAR-XPS data showed that the amount of Ga-O was not directly responsible for the recovery of the surface. However, the effect of H_3PO_4 on

the surface may be related to sites that had been previously activated by the dry etching steps. We suggest that the accelerated etching process of sample D may be related to the presence of chloride residues coming from the plasma treatments. The presence of chloride then helped the removal of damaged material.

V.2.5 Influence of H_3PO_4 on the electrical properties

In order to understand the beneficial or detrimental impact of the H_3PO_4 treatment on the electrical properties, we performed C-V measurements at room temperature on the as-grown and standard dry-etched GaN surfaces before and after H_3PO_4 immersion. The elaboration of the MIS capacitors was presented in chapter II.6. First, we evaluated the impact of the H_3PO_4 treatment for a duration of 20, 30 and 60 minutes. The C-V curves are shown in Figure 105.

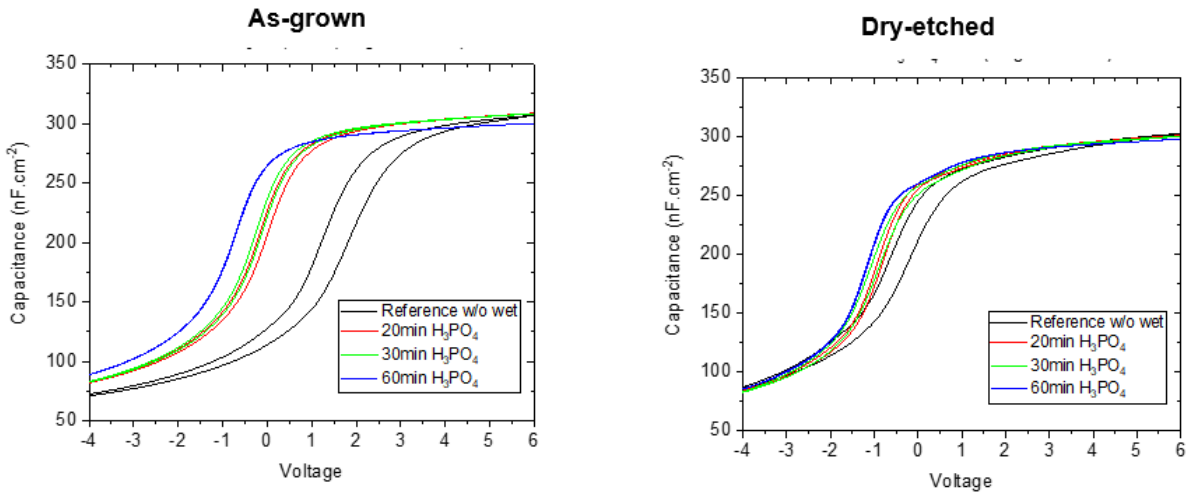

Figure 105. C-V curves before and after 20, 30 and 60 minutes in H3PO4 for as-grown (left) and dry-etched GaN (right)

For the untreated samples (as-grown and dry-etched samples), a hysteresis loop can be observed for both surfaces. Hysteresis is generally attributed to the presence of trapped charges at the interface or/and in the oxide. The immersion of GaN surfaces in H_3PO_4 allowed a clear reduction of this hysteresis loop for both surfaces which means that the wet treatment allowed the removal of impurities such as native oxides for example. Moreover, the reduction of the hysteresis also came with a negative shift of the curves for both GaN surfaces, which indicates probably a decrease of the D_{it} [111] and a reduction of the fixed charges. For the as-grown GaN, the shift towards negative voltage continues over time. However, for the dry-etched GaN, has no significant differences between the curves were seen for the variations in the duration of the

treatment. However, it should be noted that all of the curves show a negative voltage except the untreated sample of as-grown material.

To analyse the hysteresis behaviour of the capacitors Figure 106 represents the ΔV_{FB} of the as-grown GaN and the dry-etched GaN.

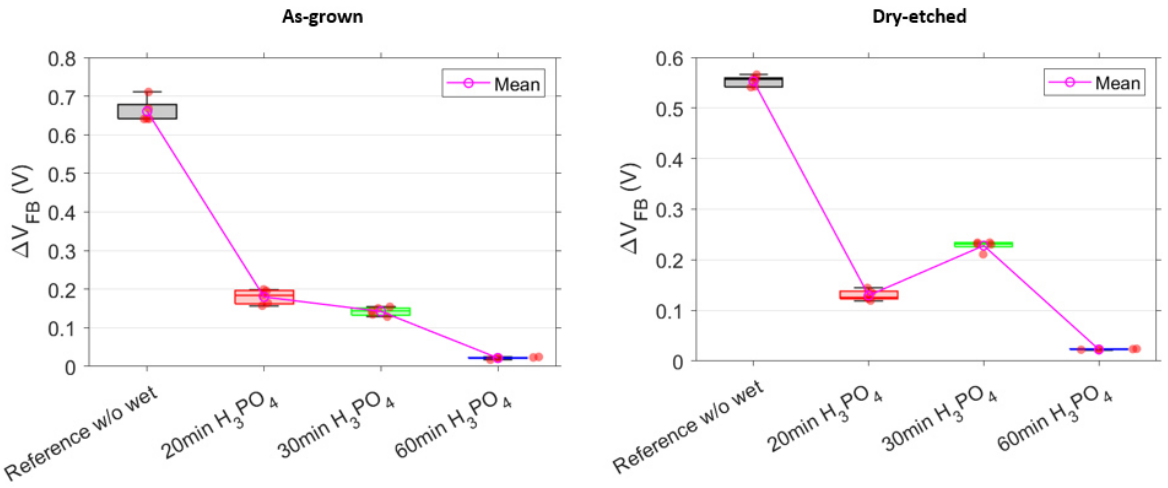

Figure 106. ΔV_{FB} before and after 20, 30 and 60 minutes in H_3PO_4 for the as-grown (left) and dry-etched GaN (right)

For the as-grown GaN, the ΔV_{FB} decreased with the increasing duration of treatment. The lowest ΔV_{FB} value obtained after 60 minutes in H_3PO_4 (mean value of 220 mV). The constant decrease of the hysteresis indicated a progressive reduction of the trapped charges. Therefore, neither the adsorbed species such as PO_x, or OH^-, nor the surface re-arrangement or the opening of the dislocations after 60 minutes had a negative impact on the density of surface trap.

For the dry-etched GaN, the lowest ΔV_{FB} was also recorded to be after 60 minutes in H_3PO_4, with a mean value similar to that obtained for the as-grown GaN sample (230 mV). However, an increase of the ΔV_{FB} was observed after 30 minutes of treatment, which may be due to the variations of the processes. According to the previous investigations done on the surface morphology, at this particular duration, the surface morphology started to re-organise into small atomic steps combined with de-organised small triangular structures, so this may also be playing a role. Concerning the surface chemistry, while the atomic % of Ga-O did not change, the level of N-Ga-O increased after 30 and 60 minutes of treatment, as shown in Figure 107 (a). The N-Ga-O contribution from the N 1s peak was attributed to the chemical environment of N atoms for which the nearest neighbours had been replaced by O atoms. We suggest the following mechanisms to explain the evolution of the N-Ga-O contribution and

ΔV_{FB}. If we attribute the decrease of the hysteresis for the 20 first minutes to oxide removal, this is coherent with both measurements. At 30 minutes, we suggest there is a simultaneous creation of N vacancies and the filling of the latter by O atoms, resulting in an increase in Ga-O. The filling of N vacancies by O was reported to act as a shallow donor, and to be energetically more favourable than N vacancies [112]. Finally, after 60 minutes, more created N vacancies were filled, decreasing the amount of trapped charges. Moreover, after 60 minutes, the surface morphology had been recovered, which could also explain a better ΔV_{FB}, as a well reconstructed surface should contain fewer trapped charges. The increase of the N-Ga-O contributions after 30 and 60 minutes was also observed for the as-grown GaN (Figure 107 (b)).

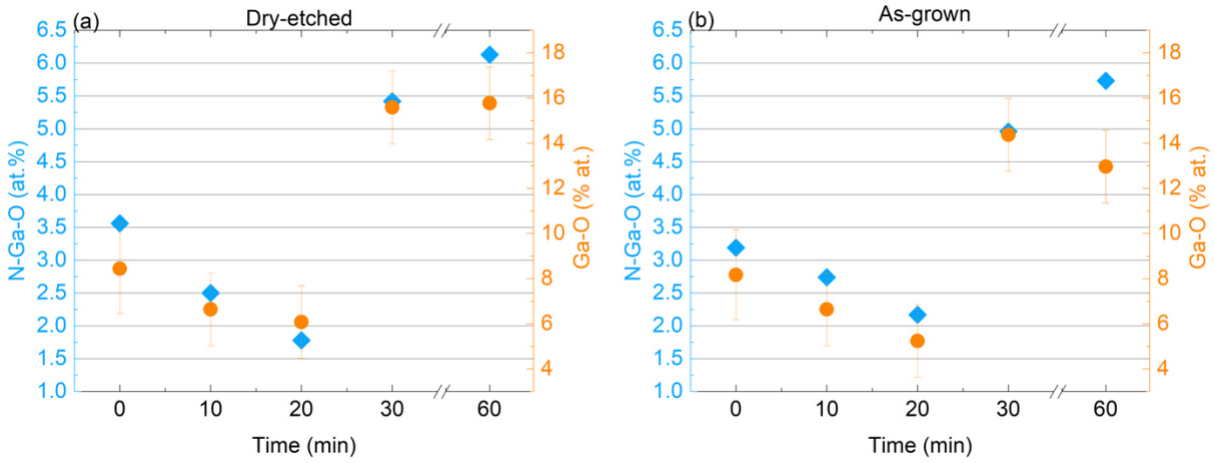

Figure 107. Evolution of the relative at. % of N-Ga-O and Ga-O contributions before and after H_3PO_4 treatment overtime of (a) dry-etched and (b) as-grown GaN

V.2.6 Conclusions

The C-V measurements, we showed that H_3PO_4 treatments lead to a decrease of trapped charges as suggested by the reduction of the hysteresis loop (or ΔV_{FB}). However, the MIS capacitors showed differences between as-grown GaN and dry-etched GaN. While the C-V curves of the as-grown GaN exhibited an increasing negative shift with increasing time of immersion, the evolution of the C-V curves of the dry-etched GaN did not show a particular impact of the treatment duration. Combining the pAR-XPS analyses with the C-V measurements showed that for both surfaces, the first 20 minutes of immersion enabled the decrease of the hysteresis loop, which was attributed to the native oxide removal. After 30 minutes in H_3PO_4, the surface was covered by OH^- and PO_x species, as suggested by the Ga 3d and the P 2p peaks and the position of the O 1s peak. Those species did not exhibit an impact on the electrical properties for the as-grown GaN. Furthermore, the surface morphology after 30 minutes was at an intermediate stage between the removal of some remaining amorphous

material and the recovery of the atomic steps. This was confirmed by the decrease of the ΔV_{FB} which was also the lowest and at the same time, the atomic steps were clearly defined along with the increase of the "N-Ga-O" contribution, revealing a more complete filling of the N vacancies compared to 30 minutes of treatment. The increase of the hysteresis loop after 30 minutes was also observed in the process flow experiments, which indicated that the state of the surface morphology and the surface chemistry after 30 minutes had an impact the electrical properties. After, 60 minutes in H_3PO_4, the opening of the treading dislocations observed on the as-grown GaN did not have a detrimental impact on the electrical properties.

General conclusion

In this PhD project, an initial work focused on a systematic review of commonly used wet etchants encountered in the microelectronic industry. This investigation was conducted on GaN wafers and GaN powders. From these experiments, we found that, in agreement with the literature, there was little impact of the wet etchants on the GaN wafers oriented (0001). The most effective treatment to reduce the surface oxygen content was obtained with high temperature solutions, HCl and H_3PO_4. The re-oxidation was hindered by adsorbates present on the surface, such as chloride and phosphate ions after HCl and H_3PO_4 treatments respectively. Although no XPS peak related to the presence of sulphur could be detected, sulphur-based treatments, particularly $(NH_4)_2S$, enabled a reduction of the oxide thickness and a reduction of the total amount of carbon, suggesting thus a very small amount of sulphur passivating the surface. The study on GaN powders made it possible to overcome the characterisation difficulties related to the heteroepitaxial material and to work under inert atmosphere (Argon), in order to gain better understanding of the mechanisms occurring during wet treatments. Due to the polycrystalline nature of the powders, the XPS analyses yielded opposite results from that obtained with GaN wafers. Indeed, most treatments found to have etching properties such as NH_4OH, HCl, and $(NH_4)_2S$ which exhibited oxidising properties. However, experiments performed with of 1-octanethiol on the GaN powders suggested that passivation might be possible with sulphur compounds which were more likely to be physisorbed on the GaN surface. Finally, the relatively low specific surface area of the powder limited the sensitivity of the measurements, meaning that it was not always easy to extract clear conclusions.

The overall observations done within the initial systematic review highlighted the inert characteristic of c-plane GaN. Therefore, the second part of this PhD project focused on the destabilisation of the Ga-N bonds at the surface, in order to initiate a more significant effect of the wet etchant, or to initiate oxidation, with the idea of moving towards digital etching. The first part of this study was dedicated to dry techniques that included nanosecond LASER and Rapid Thermal Processing (RTP). The nanosecond LASER first determined the melt point on as-grown and dry-etched GaN. SEM images revealed different behaviours between as-grown and dry-etched GaN, with the formation of droplets at the surface of the as-grown surface, which was attributed to gallium droplets, in agreement with the appearance of Ga-Ga contribution on the XPS Ga 3d peak. Furthermore, the as-grown GaN sample exhibited a

slightly lower melt point than the dry-etched GaN surface. In depth investigations highlighted this difference as well, in particular when the anneals were performed without N_2 flow. In this case, the as-grown surface adsorbed more oxygen than the dry-etched surface. The surface morphology investigated by AFM showed white areas or white dots when performing the anneals under N_2 or without N_2. These white areas/dots were attributed to oxide grains and their size increased with the number of shots. Their sizes were also larger on as-grown GaN, in agreement with the pAR-XPS analyses.

The RTP anneals performed under O_2 flow also allowed to examine the difference between the as-grown and the dry-etched GaN. AFM measurements revealed white dots on the dry-etched GaN while no particular structures appeared on the as-grown GaN. However, EDX and pAR-XPS analyses revealed the presence of a SiO_2 contamination layer that could have protected the GaN surface during the RTP anneals. The wet etching with HCl and $(NH_4)_2S$ performed in the same conditions as conducted in the initial systematic review revealed the efficiency of HCl as an etchant. Indeed, a total removal of the oxide grains observed on the annealed surfaces disappeared after HCl treatment, and the oxygen decreased and was found lower than before the RTP anneals for both surfaces. However, $(NH_4)_2S$ seemed to be less efficient on intentionally oxidised GaN. The wet etching performed with HCl treatment revealed larger dislocations on the as-grown surface while the dislocations were less visible on the dry-etched GaN but were still more distinguishable than before the wet etching treartment. This result showed that oxidation starts at surface defect points, such as at dislocations where crystallographic orientations other than (0001) are exposed, which is in agreement with the literature.

A second method for destabilising the GaN surface was investigated through wet etching performed at high temperature (155-160°C). Several short-time immersions into H_2SO_4:H_2O_2 solution led to the formation of white dots that appeared several months after the treatment. As a first step, the density of white dots corresponded to the density of dislocations known for GaN-on-Si and, as a second step, the density of the white dots spread all over the surface. Combining these observations with pAR-XPS analyses, those white dots were believed to be related to the formation of a Ga-OH layer on top of the GaN layer.

To get closer to the transistor process fabrication, the influence of the H_3PO_4, as destabilising treatment of the Ga-N bonds, was investigated on as-grown and dry-etched GaN. The investigations on the surface morphology showed a recovery of the atomic step on the dry-etched GaN. The re-organisation of the surface occurred with delay on the dry-etched surfaces

compared to as-grown GaN. This delayed effect was attributed to the less accessible reactive sites, which were believed to be the surface sites where alternative crystallographic orientations were exposed, such as atomic step edges and dislocations. A mechanism of the atomic step recovery was proposed. For both surfaces, the first 20 minutes of treatment revealed oxide removal, then after 30 minutes OH^- adsorption occurred. No relationship between the OH^- adsorption and the re-organisation of the surface was established. However, C-V measurements revealed a progressive reduction of the trapped charges as a function of the duration of treatment for both surfaces. The first 20 minutes were attributed to the removal of the native oxide, and after 30 minutes to the filling of the N vacancies by oxygen atoms. We also investigated the possibility of removing the ALE step from the standard dry-etching process. The results indicated that without ALE, the etching rate was accelerated and led to the opening of the dislocation within 30 minutes (versus 60 minutes for the as-grown surface). On the other hand, removing the stripping sequence led to an incomplete recovery of the surface.

This PhD project highlighted the challenge of etching and passivating the (0001) orientation. Despite these difficulties, we found that long treatment of H_3PO_4 led to a recovery of the surface atomic steps after dry etching, and to an improvement of the electrical properties.

Perspectives

As this study showed the complexity of treating GaN surfaces, there is a significant amount of work which could be done to further this work.

First, to complete the link between the initial GaN (0001) studies and the powder samples, it would be interesting to perform tests on powder samples with a higher specific surface area to generate more signal from the surface reactions. Furthermore, as the powder samples expose multiple orientations on their surface, a study of different planes such as m-plane, or a-plane could help to explain the different reactions occurring on powder and GaN on silicon samples.

Next, it would be useful to push the destabilisation experiments further. Although the RTP + HCl treatment revealed dislocations for the as-grown samples, this was not the case for dry-etched samples, and so it may be possible to combine an oxidation of samples after etching with chemical treatments, such as HCl or even H_3PO_4. Furthermore, surface investigations of

oxide removal after LASER anneal was not performed, and it would be interesting to compare the results to those after RTP annealing. LASER annealing could be easier to integrate into processing flows, due to its lower thermal budget for the same peak temperatures. These points could then also be integrated into electrical components, first as capacitors, and then as transistors, in order to understand their impact on the device properties.

Although this PhD examined temperature as a way of breaking down surface bonds, an alternative method would be to try to use various plasma treatments to damage the surface bonds. In combination with wet chemical treatments, this could also function as a "digital etching" mechanism, to allow surface contamination elements to be removed.

Another point which was not completely understood is the mechanism behind the H_3PO_4 etching. In particular, the fact that 9Å of GaN was etched during a H_3PO_4 treatment of 60 minutes is surprising. If this is an auto-limiting reaction, or if there is an attack taking place along the atomic steps, a better understanding would allow improved implementation of this wet treatment, perhaps in combination with annealing or oxidation steps.

Finally, at several points during this PhD, we observed evolution of the GaN surface over time, in particular in combination with annealing or oxidation steps. Due to the time-consuming nature of such a study, it was not possible to pursue this any further, but this is an important element of GaN surface understanding which would be important to examine.

References

[1] W. Bi, *Handbook of GaN semiconductor materials and devices*. Boca Raton: CRC Presss, Taylor & Francis Group, CRC Press is an imprint of the Taylor & Francis Group, an informa business, 2017.

[2] C. Zhou *et al.*, 'Review—The Current and Emerging Applications of the III-Nitrides', *ECS J. Solid State Sci. Technol.*, vol. 6, no. 12, p. Q149, Nov. 2017, doi: 10.1149/2.0101712jss.

[3] B. S. Eller, J. Yang, and R. J. Nemanich, 'Electronic surface and dielectric interface states on GaN and AlGaN', *J. Vac. Sci. Technol. Vac. Surf. Films*, vol. 31, no. 5, p. 050807, Sep. 2013, doi: 10.1116/1.4807904.

[4] Y. Niiyama, S. Ootomo, J. Li, T. Nomura, S. Kato, and T. P. Chow, 'Normally off operation GaN-based MOSFETs for power electronics applications', *Semicond. Sci. Technol.*, vol. 25, no. 12, p. 125006, Dec. 2010, doi: 10.1088/0268-1242/25/12/125006.

[5] E. A. Jones, F. F. Wang, and D. Costinett, 'Review of Commercial GaN Power Devices and GaN-Based Converter Design Challenges', *IEEE J. Emerg. Sel. Top. Power Electron.*, vol. 4, no. 3, pp. 707–719, Sep. 2016, doi: 10.1109/JESTPE.2016.2582685.

[6] E. Johnson, 'Physical limitations on frequency and power parameters of transistors', in *1958 IRE International Convention Record*, Mar. 1965, vol. 13, pp. 27–34. doi: 10.1109/IRECON.1965.1147520.

[7] B. J. Baliga, 'Power semiconductor device figure of merit for high-frequency applications', *IEEE Electron Device Lett.*, vol. 10, no. 10, pp. 455–457, Oct. 1989, doi: 10.1109/55.43098.

[8] S. J. Pearton, C. R. Abernathy, and F. Ren, *Gallium nitride processing for electronics, sensors, and spintronics*. New York: Springer, 2006.

[9] S. Hamady, 'New concepts for normally-off power Gallium Nitride (GaN) High Electron Mobility Transistor (HEMT)', Toulouse 3 Paul Sabatier, Toulouse, France, 2014. [Online]. Available: https://tel.archives-ouvertes.fr/tel-01132563/document

[10] J.-C. De Jaeger, 'Dispositifs HEMT à base de GaN - Matériaux et épitaxie', août 2017.

[11] J.-C. DE JAEGER, 'Dispositifs HEMT à base de GaN Technologie et caractérisation',

no. ref. article : e1996, 2017, [Online]. Available: https://www.techniques-ingenieur.fr/base-documentaire/electronique-photonique-th13/technologies-des-dispositifs-actifs-42286210/dispositifs-hemt-a-base-de-gan-e1996/

[12] W. Utsumi, H. Saitoh, H. Kaneko, T. Watanuki, K. Aoki, and O. Shimomura, 'Congruent melting of gallium nitride at 6 GPa and its application to single-crystal growth', *Nat. Mater.*, vol. 2, no. 11, pp. 735–738, Nov. 2003, doi: 10.1038/nmat1003.

[13] H. Amano, N. Sawaki, I. Akasaki, and Y. Toyoda, 'Metalorganic vapor phase epitaxial growth of a high quality GaN film using an AlN buffer layer', *Appl. Phys. Lett.*, vol. 48, no. 5, pp. 353–355, Feb. 1986, doi: 10.1063/1.96549.

[14] W. C. Johnson, J. B. Parson, and M. C. Crew, 'Nitrogen Compounds of Gallium. III', *J. Phys. Chem.*, vol. 36, no. 10, pp. 2651–2654, Oct. 1932, doi: 10.1021/j150340a015.

[15] E. Ejder, 'Growth and morphology of GaN', *J. Cryst. Growth*, vol. 22, no. 1, pp. 44–46, Mar. 1974, doi: 10.1016/0022-0248(74)90057-8.

[16] H. M. Manasevit, F. M. Erdmann, and W. I. Simpson, 'The Use of Metalorganics in the Preparation of Semiconductor Materials', *J. Electrochem. Soc.*, vol. 118, no. 11, pp. 1864–1867, 1971.

[17] S. Nakamura, 'GaN Growth Using GaN Buffer Layer', *Jpn. J. Appl. Phys.*, vol. 30, no. Part 2, No. 10A, pp. L1705–L1707, Oct. 1991, doi: 10.1143/JJAP.30.L1705.

[18] M. Charles *et al.*, '(Invited) Epitaxy of GaN on Si (111) for Power Electronics, RF and LEDs', *ECS Trans.*, vol. 86, no. 7, p. 233, Jul. 2018, doi: 10.1149/08607.0233ecst.

[19] R. J. Shul *et al.*, 'Inductively coupled high-density plasma-induced etch damage of GaN MESFETs', *Solid-State Electron.*, vol. 45, no. 1, pp. 13–17, Jan. 2001, doi: 10.1016/S0038-1101(00)00164-7.

[20] T. Hashizume and R. Nakasaki, 'Discrete surface state related to nitrogen-vacancy defect on plasma-treated GaN surfaces', *Appl. Phys. Lett.*, vol. 80, no. 24, pp. 4564–4566, Jun. 2002, doi: 10.1063/1.1485309.

[21] T. Hashizume and H. Hasegawa, 'Effects of nitrogen deficiency on electronic properties of AlGaN surfaces subjected to thermal and plasma processes', *Appl. Surf. Sci.*, vol. 234, no. 1, pp. 387–394, Jul. 2004, doi: 10.1016/j.apsusc.2004.05.091.

[22] M. E. Lin, Z. F. Fan, Z. Ma, L. H. Allen, and H. Morkoç, ‘Reactive ion etching of GaN using BCl3’, *Appl. Phys. Lett.*, vol. 64, no. 7, pp. 887–888, Feb. 1994, doi: 10.1063/1.110985.

[23] B. Molnar, C. R. Eddy, and K. Doverspike, ‘The influence of CH_4 /H_2 /Ar plasma etching on the conductivity of *n* -type gallium nitride’, *J. Appl. Phys.*, vol. 78, no. 10, pp. 6132–6134, Nov. 1995, doi: 10.1063/1.360555.

[24] C. B. Vartuli *et al.*, ‘Wet chemical etching survey of III-nitrides’, *Solid-State Electron.*, vol. 41, no. 12, pp. 1947–1951, Dec. 1997, doi: 10.1016/S0038-1101(97)00173-1.

[25] S. J. Pearton, J. C. Zolper, R. J. Shul, and F. Ren, ‘GaN: Processing, defects, and devices’, *J. Appl. Phys.*, vol. 86, no. 1, pp. 1–78, Jul. 1999, doi: 10.1063/1.371145.

[26] M.-S. Chung, W.-T. Lin, and J. R. Gong, ‘Formation of Hf ohmic contacts by surface treatment of n-GaN in KOH solutions’, *J. Vac. Sci. Technol. B Microelectron. Nanometer Struct. Process. Meas. Phenom.*, vol. 19, no. 5, pp. 1976–1980, Sep. 2001, doi: 10.1116/1.1406157.

[27] P. B. Shah, I. Batyrev, M. A. Derenge, U. Lee, C. Nyguen, and K. A. Jones, ‘Schottky metal-GaN interface KOH pretreatment for improved device performance’, *J. Vac. Sci. Technol. A*, vol. 28, no. 4, pp. 684–688, Jul. 2010, doi: 10.1116/1.3299253.

[28] D. Li *et al.*, ‘Selective etching of GaN polar surface in potassium hydroxide solution studied by x-ray photoelectron spectroscopy’, *J. Appl. Phys.*, vol. 90, no. 8, pp. 4219–4223, Oct. 2001, doi: 10.1063/1.1402966.

[29] D. A. Stocker, E. F. Schubert, and J. M. Redwing, ‘Crystallographic wet chemical etching of GaN’, *Appl. Phys. Lett.*, vol. 73, no. 18, pp. 2654–2656, Nov. 1998, doi: 10.1063/1.122543.

[30] J. Zhou *et al.*, ‘Surface morphologies of MOCVD-grown GaN films on sapphire studied by scanning tunneling microscopy’, *Appl. Surf. Sci.*, vol. 202, no. 3, pp. 131–138, Dec. 2002, doi: 10.1016/S0169-4332(02)00889-9.

[31] K. Prabhakaran, T. G. Andersson, and K. Nozawa, ‘Nature of native oxide on GaN surface and its reaction with Al’, *Appl. Phys. Lett.*, vol. 69, no. 21, pp. 3212–3214, Nov. 1996, doi: 10.1063/1.117964.

[32] T. Hashizume, S. Ootomo, T. Inagaki, and H. Hasegawa, ‘Surface passivation of GaN and GaN/AlGaN heterostructures by dielectric films and its application to insulated-gate

heterostructure transistors', *J. Vac. Sci. Technol. B Microelectron. Nanometer Struct.*, vol. 21, no. 4, p. 1828, 2003, doi: 10.1116/1.1585077.

[33] Y. Koyama, T. Hashizume, and H. Hasegawa, 'Formation processes and properties of Schottky and ohmic contacts on n-type GaN for field effect transistor applications', *Solid-State Electron.*, vol. 43, no. 8, pp. 1483–1488, Aug. 1999, doi: 10.1016/S0038-1101(99)00093-3.

[34] S. W. King *et al.*, 'Cleaning of AlN and GaN surfaces', *J. Appl. Phys.*, vol. 84, no. 9, pp. 5248–5260, Nov. 1998, doi: 10.1063/1.368814.

[35] C. J. Sandroff, M. S. Hegde, L. A. Farrow, C. C. Chang, and J. P. Harbison, 'Electronic passivation of GaAs surfaces through the formation of arsenic—sulfur bonds', *Appl. Phys. Lett.*, vol. 54, no. 4, pp. 362–364, Jan. 1989, doi: 10.1063/1.101451.

[36] T. Maruyama *et al.*, 'Surface treatment of GaN and InN using (NH4)2Sx', *Phys. Status Solidi C*, vol. 0, no. 7, pp. 2031–2034, Dec. 2003, doi: 10.1002/pssc.200303489.

[37] C. Huh, S.-W. Kim, H.-S. Kim, I.-H. Lee, and S.-J. Park, 'Effective sulfur passivation of an n-type GaN surface by an alcohol-based sulfide solution', *J. Appl. Phys.*, vol. 87, no. 9, pp. 4591–4593, May 2000, doi: 10.1063/1.373107.

[38] A. Kumar, T. Singh, M. Kumar, and R. Singh, 'Sulphide passivation of GaN based Schottky diodes', *Curr. Appl. Phys.*, vol. 14, no. 3, pp. 491–495, Mar. 2014, doi: 10.1016/j.cap.2013.12.021.

[39] H. H. Han *et al.*, 'Suppressed charge trapping characteristics of (NH4)2Sx passivated GaN MOS device with atomic layer deposited HfAlOx gate dielectric', *Microelectron. Eng.*, vol. 178, pp. 240–244, Jun. 2017, doi: 10.1016/j.mee.2017.05.027.

[40] L. L. Smith, S. W. King, R. J. Nemanich, and R. F. Davis, 'Cleaning of GaN surfaces', *J. Electron. Mater.*, vol. 25, no. 5, pp. 805–810, May 1996, doi: 10.1007/BF02666640.

[41] S.-C. Liu *et al.*, 'Effective surface treatment for GaN metal–insulator–semiconductor high-electron-mobility transistors using HF plus N2 plasma prior to SiN passivation', *Jpn. J. Appl. Phys.*, vol. 55, no. 1S, p. 01AD06, Nov. 2015, doi: 10.7567/JJAP.55.01AD06.

[42] H. Okada, M. Shinohara, Y. Kondo, H. Sekiguchi, K. Yamane, and A. Wakahara, 'Investigation of HCl-based surface treatment for GaN devices', Bali, Indonesia, 2016, p. 020011. doi: 10.1063/1.4941210.

[43] J. J. Uhlrich, L. C. Grabow, M. Mavrikakis, and T. F. Kuech, ‘Practical Surface Treatments and Surface Chemistry of n-Type and p-Type GaN’, *J. Electron. Mater.*, vol. 37, no. 4, pp. 439–447, Apr. 2008, doi: 10.1007/s11664-007-0348-5.

[44] F. Machuca, Z. Liu, Y. Sun, P. Pianetta, W. E. Spicer, and R. F. W. Pease, ‘Simple method for cleaning gallium nitride (0001)’, *J. Vac. Sci. Technol. A*, vol. 20, no. 5, pp. 1784–1786, Sep. 2002, doi: 10.1116/1.1503782.

[45] C. R. English *et al.*, ‘Impact of surface treatments on high-κ dielectric integration with Ga-polar and N-polar GaN’, *J. Vac. Sci. Technol. B Nanotechnol. Microelectron. Mater. Process. Meas. Phenom.*, vol. 32, no. 3, p. 03D106, May 2014, doi: 10.1116/1.4831875.

[46] T. Hossain *et al.*, ‘Effect of GaN surface treatment on Al2O3/n-GaN MOS capacitors’, *J. Vac. Sci. Technol. B*, vol. 33, no. 6, p. 061201, Sep. 2015, doi: 10.1116/1.4931793.

[47] N. Nepal, N. Y. Garces, D. J. Meyer, J. K. Hite, M. A. Mastro, and J. Charles R. Eddy, ‘Assessment of GaN Surface Pretreatment for Atomic Layer Deposited High-k Dielectrics’, *Appl. Phys. Express*, vol. 4, no. 5, p. 055802, May 2011, doi: 10.1143/APEX.4.055802.

[48] H. Wang, H. Zhang, J. Liu, D. Xue, H. Liang, and X. Xia, ‘Hydroxyl Group Adsorption on GaN (0001) Surface: First Principles and XPS Studies’, *J. Electron. Mater.*, vol. 48, no. 4, pp. 2430–2437, Apr. 2019, doi: 10.1007/s11664-019-07011-1.

[49] Y. Tsuji *et al.*, ‘XPS analysis of the terminated-bonding states at GaN surface after chemical and plasma treatments’, *Phys. Status Solidi C*, vol. 10, no. 11, pp. 1557–1560, Nov. 2013, doi: 10.1002/pssc.201300225.

[50] C.-Y. Lee, C. Chang, W.-P. Shih, and C.-L. Dai, ‘Wet etching rates of InGaZnO for the fabrication of transparent thin-film transistors on plastic substrates’, *Thin Solid Films*, vol. 518, no. 14, pp. 3992–3998, May 2010, doi: 10.1016/j.tsf.2009.12.010.

[51] H.-C. Cheng, ‘Wet Etching’, in *Handbook of Visual Display Technology*, J. Chen, W. Cranton, and M. Fihn, Eds. Berlin, Heidelberg: Springer, 2012, pp. 861–870. doi: 10.1007/978-3-540-79567-4_59.

[52] H. M. Ng, W. Parz, N. G. Weimann, and A. Chowdhury, ‘Patterning GaN Microstructures by Polarity-Selective Chemical Etching’, *Jpn. J. Appl. Phys.*, vol. 42, no. Part 2, No. 12A, pp. L1405–L1407, Dec. 2003, doi: 10.1143/JJAP.42.L1405.

[53] A. Shintani and S. Minagawa, ‘Etching of GaN Using Phosphoric Acid’, *J.*

Electrochem. Soc., vol. 123, no. 5, pp. 706–713, 1979, doi: 10.1149/1.2132914.

[54] P. Visconti, K. M. Jones, M. A. Reshchikov, R. Cingolani, H. Morkoç, and R. J. Molnar, 'Dislocation density in GaN determined by photoelectrochemical and hot-wet etching', *Appl. Phys. Lett.*, vol. 77, no. 22, pp. 3532–3534, Nov. 2000, doi: 10.1063/1.1329330.

[55] P. Visconti *et al.*, 'Investigation of defects and surface polarity in GaN using hot wet etching together with microscopy and diffraction techniques', *Mater. Sci. Eng. B*, vol. 93, no. 1, pp. 229–233, May 2002, doi: 10.1016/S0921-5107(02)00011-9.

[56] X. Xu, R. P. Vaudo, J. Flynn, and G. R. Brandes, 'Acid etching for accurate determination of dislocation density in GaN', *J. Electron. Mater.*, vol. 31, no. 5, pp. 402–405, May 2002, doi: 10.1007/s11664-002-0091-x.

[57] G. C. DeSalvo *et al.*, 'Wet Chemical Digital Etching of GaAs at Room Temperature', *J. Electrochem. Soc.*, vol. 143, no. 11, p. 3652, Nov. 1996, doi: 10.1149/1.1837266.

[58] J. Lin, X. Zhao, D. A. Antoniadis, and J. A. del Alamo, 'A Novel Digital Etch Technique for Deeply Scaled III-V MOSFETs', *IEEE Electron Device Lett.*, vol. 35, no. 4, pp. 440–442, Apr. 2014, doi: 10.1109/LED.2014.2305668.

[59] H.-C. Chiu *et al.*, 'High Uniformity Normally-OFF p-GaN Gate HEMT Using Self-Terminated Digital Etching Technique', *IEEE Trans. Electron Devices*, vol. 65, no. 11, pp. 4820–4825, Nov. 2018, doi: 10.1109/TED.2018.2871689.

[60] T. Meguro, M. Ishii, K. Kodama, Y. Yamamoto, K. Gamo, and Y. Aoyagi, 'Surface processes in digital etching of GaAs', *Thin Solid Films*, vol. 225, no. 1, pp. 136–139, Mar. 1993, doi: 10.1016/0040-6090(93)90142-C.

[61] M. Ishii, T. Meguro, H. Kodama, Y. Yamamoto, and Y. Aoyagi, 'Study of Surface Processes in the Digital Etching of GaAs', *Jpn. J. Appl. Phys.*, vol. 31, no. Part 1, No. 7, pp. 2212–2215, Jul. 1992, doi: 10.1143/JJAP.31.2212.

[62] T. Meguro *et al.*, 'Layer-By-Layer Controlled Digital Etching by Means of an Electron-Beam-Excited Plasma System', *Jpn. J. Appl. Phys.*, vol. 29, no. 10R, p. 2216, Oct. 1990, doi: 10.1143/JJAP.29.2216.

[63] F. Djamdji and R. Blunt, 'Hall mobility profiling in high electron mobility transistor structures', *Mater. Sci. Eng. B*, vol. 20, no. 1, pp. 77–81, Jun. 1993, doi: 10.1016/0921-5107(93)90401-8.

[64] D. Buttari, S. Heikman, S. Keller, and U. K. Mishra, 'Digital etching for highly reproducible low damage gate recessing on AlGaN/GaN HEMTs', in *Proceedings. IEEE Lester Eastman Conference on High Performance Devices*, Aug. 2002, pp. 461–469. doi: 10.1109/LECHPD.2002.1146788.

[65] N.-H. Lee *et al.*, 'Effects of various surface treatments on gate leakage, subthreshold slope, and current collapse in AlGaN/GaN high-electron-mobility transistors', *Jpn. J. Appl. Phys.*, vol. 53, no. 4S, p. 04EF10, Mar. 2014, doi: 10.7567/JJAP.53.04EF10.

[66] R. T. Haasch, 'X-Ray Photoelectron Spectroscopy (XPS) and Auger Electron Spectroscopy (AES)', in *Practical Materials Characterization*, M. Sardela, Ed. New York, NY: Springer New York, 2014, pp. 93–132. doi: 10.1007/978-1-4614-9281-8_3.

[67] S. Evans, 'Energy calibration secondary standards for X-ray photoelectron spectrometers', *Surf. Interface Anal.*, vol. 7, no. 6, pp. 299–302, 1985, doi: 10.1002/sia.740070609.

[68] B. L. Pearce, S. J. Wilkins, M. S. Rahn, and A. Ivanisevic, 'In situ functionalization of gallium nitride powder with a porphyrin dye', *J. Mater. Res.*, vol. 30, no. 19, pp. 2910–2918, Oct. 2015, doi: 10.1557/jmr.2015.152.

[69] M. K. Khan, Q. Y. Wang, and M. E. Fitzpatrick, '1 - Atomic force microscopy (AFM) for materials characterization', in *Materials Characterization Using Nondestructive Evaluation (NDE) Methods*, G. Hübschen, I. Altpeter, R. Tschuncky, and H.-G. Herrmann, Eds. Woodhead Publishing, 2016, pp. 1–16. doi: 10.1016/B978-0-08-100040-3.00001-8.

[70] M. Yasaka, 'X-ray thin-film measurement techniques', p. 9, 2010.

[71] L. E. Black, *New Perspectives on Surface Passivation: Understanding the Si-Al2O3 Interface*. Cham: Springer International Publishing, 2016. doi: 10.1007/978-3-319-32521-7.

[72] T. Alphazan *et al.*, 'Shallow Heavily Doped n++ Germanium by Organo-Antimony Monolayer Doping', *ACS Appl. Mater. Interfaces*, vol. 9, no. 23, pp. 20179–20187, Jun. 2017, doi: 10.1021/acsami.7b02645.

[73] M. Diale, F. D. Auret, N. G. van der Berg, R. Q. Odendaal, and W. D. Roos, 'Analysis of GaN cleaning procedures', *Appl. Surf. Sci.*, vol. 246, no. 1–3, pp. 279–289, Jun. 2005, doi: 10.1016/j.apsusc.2004.11.024.

[74] A. Cruz-López *et al.*, 'Synthesis and characterization of gallium nitride nanoparticles

by using solvothermal-soft-chemical methodology', *Mater. Sci. Semicond. Process.*, vol. 30, pp. 435–441, Feb. 2015, doi: 10.1016/j.mssp.2014.10.028.

[75] H. Qiu, C. Cao, and H. Zhu, 'Synthesis of nanocrystalline GaN by the sol–gel method', *Mater. Sci. Eng. B*, vol. 136, no. 1, pp. 33–36, Jan. 2007, doi: 10.1016/j.mseb.2006.08.062.

[76] S. Cho, J. Lee, I. Y. Park, and S. Kim, 'New simple synthesis route of GaN powders from gallium oxyhydroxide', *Mater. Sci. Eng. B*, vol. 95, no. 3, pp. 275–278, Sep. 2002, doi: 10.1016/S0921-5107(02)00264-7.

[77] H.-D. Xiao *et al.*, 'Thermal oxidation behaviors of GaN powders', *Mater. Lett.*, vol. 59, no. 29–30, pp. 4041–4043, Dec. 2005, doi: 10.1016/j.matlet.2005.07.061.

[78] H.-D. Xiao *et al.*, 'Synthesis and properties of GaO2H nanorods', *Mater. Lett.*, vol. 58, no. 30, pp. 3925–3928, Dec. 2004, doi: 10.1016/j.matlet.2004.08.020.

[79] M. Musiał, J. Gosk, A. Twardowski, J. F. Janik, and M. Drygaś, 'Nanopowders of gallium nitride GaN surface functionalized with manganese', *J. Mater. Sci.*, vol. 52, no. 1, pp. 145–161, Jan. 2017, doi: 10.1007/s10853-016-0317-6.

[80] D. B. Mawhinney, J. A. Glass, and J. T. Yates, 'FTIR Study of the Oxidation of Porous Silicon', *J. Phys. Chem. B*, vol. 101, no. 7, pp. 1202–1206, Feb. 1997, doi: 10.1021/jp963322r.

[81] M. Karyaoui, A. Bardaoui, M. Ben Rabha, J. C. Harmand, and M. Amlouk, 'Effect of rapid oxidation on optical and electrical properties of silicon nanowires obtained by chemical etching', *Eur. Phys. J. Appl. Phys.*, vol. 58, no. 2, p. 20103, May 2012, doi: 10.1051/epjap/2012120099.

[82] J. (Jeanne) Yang, Y. Zhao, and R. L. Frost, 'Infrared and infrared emission spectroscopy of gallium oxide α-GaO(OH) nanostructures', *Spectrochim. Acta. A. Mol. Biomol. Spectrosc.*, vol. 74, no. 2, pp. 398–403, Oct. 2009, doi: 10.1016/j.saa.2009.06.032.

[83] V. M. Bermudez, 'Study of oxygen chemisorption on the GaN(0001)-(1×1) surface', *J. Appl. Phys.*, vol. 80, no. 2, pp. 1190–1200, Jul. 1996, doi: 10.1063/1.362924.

[84] G. Testa, L. Fontana, I. Venditti, and I. Fratoddi, 'Functionalized platinum nanoparticles with surface charge trigged by pH: synthesis, characterization and stability studies', *Beilstein J. Nanotechnol.*, vol. 7, no. 1, pp. 1822–1828, Nov. 2016, doi: 10.3762/bjnano.7.175.

[85] W. Sui, W. Zhao, X. Zhang, S. Peng, Z. Zeng, and Q. Xue, 'Comparative anti-corrosion

properties of alkylthiols SAMs and mercapto functional silica sol–gel coatings on copper surface in sodium chloride solution', *J. Sol-Gel Sci. Technol.*, vol. 80, no. 2, pp. 567–578, Nov. 2016, doi: 10.1007/s10971-016-4108-y.

[86] L. Dagault, 'Investigation of SiGe epilayers behaviour upon Ultraviolet Nanosecond Laser Annealing', Toulouse 3 Paul Sabatier, 2021.

[87] T. Yamada *et al.*, 'Comprehensive study on initial thermal oxidation of GaN(0001) surface and subsequent oxide growth in dry oxygen ambient', *J. Appl. Phys.*, vol. 121, no. 3, p. 035303, Jan. 2017, doi: 10.1063/1.4974458.

[88] E. G. Seebauer, P. Gorai, and G. K. Sujan, 'Formation of Ultra-Shallow Junctions', in *Reference Module in Materials Science and Materials Engineering*, Elsevier, 2016. doi: 10.1016/B978-0-12-803581-8.09402-9.

[89] H. Kim, S.-J. Park, and H. Hwang, 'Thermally oxidized GaN film for use as gate insulators', *J. Vac. Sci. Technol. B Microelectron. Nanometer Struct. Process. Meas. Phenom.*, vol. 19, no. 2, pp. 579–581, Mar. 2001, doi: 10.1116/1.1349733.

[90] Y. Nakano, T. Kachi, and T. Jimbo, 'Inversion behavior in thermally oxidized p-GaN metal–oxide–semiconductor capacitors', *J. Vac. Sci. Technol. B Microelectron. Nanometer Struct. Process. Meas. Phenom.*, vol. 21, no. 5, pp. 2220–2222, Sep. 2003, doi: 10.1116/1.1612937.

[91] Y. Zhou *et al.*, 'Formation, etching and electrical characterization of a thermally grown gallium oxide on the Ga-face of a bulk GaN substrate', *Solid-State Electron.*, vol. 52, no. 5, pp. 756–764, May 2008, doi: 10.1016/j.sse.2007.10.045.

[92] E. D. Readinger *et al.*, 'Wet thermal oxidation of GaN', *J. Electron. Mater.*, vol. 28, no. 3, pp. 257–260, Mar. 1999, doi: 10.1007/s11664-999-0024-z.

[93] S. D. Wolter, B. P. Luther, D. L. Waltemyer, C. Önneby, S. E. Mohney, and R. J. Molnar, 'X-ray photoelectron spectroscopy and x-ray diffraction study of the thermal oxide on gallium nitride', *Appl. Phys. Lett.*, vol. 70, no. 16, pp. 2156–2158, Apr. 1997, doi: 10.1063/1.118944.

[94] H. Sun *et al.*, 'HCl Flow-Induced Phase Change of α-, β-, and ε-Ga_2O_3 Films Grown by MOCVD', *Cryst. Growth Des.*, vol. 18, no. 4, pp. 2370–2376, Apr. 2018, doi: 10.1021/acs.cgd.7b01791.

[95] R. Jia *et al.*, 'Distinct Photoinduced Wetting Transitions of Differently Doped GaN: An Indication of Collective Behavior', *J. Phys. Chem. C*, vol. 122, no. 43, pp. 24818–24822, Nov. 2018, doi: 10.1021/acs.jpcc.8b08050.

[96] A. Arranz, C. Palacio, D. García-Fresnadillo, G. Orellana, A. Navarro, and E. Muñoz, 'Influence of Surface Hydroxylation on 3-Aminopropyltriethoxysilane Growth Mode during Chemical Functionalization of GaN Surfaces: An Angle-Resolved X-ray Photoelectron Spectroscopy Study', *Langmuir*, vol. 24, no. 16, pp. 8667–8671, Aug. 2008, doi: 10.1021/la801259n.

[97] C. Buchheim *et al.*, 'Tuning of Surface Properties of AlGaN/GaN Sensors for Nanodroplets and Picodroplets', *IEEE Sens. J.*, vol. 6, no. 4, pp. 881–886, Aug. 2006, doi: 10.1109/JSEN.2006.877984.

[98] I. Dzięcielewski, J. L. Weyher, and W. Dzwolak, 'On the hydrophobicity of modified Ga-polar GaN surfaces', *Appl. Phys. Lett.*, vol. 102, no. 4, p. 043704, Jan. 2013, doi: 10.1063/1.4790435.

[99] S. Ruel *et al.*, 'Atomic layer etching of GaN using Cl2 and He or Ar plasma', *J. Vac. Sci. Technol. A*, vol. 39, no. 2, p. 022601, Feb. 2021, doi: 10.1116/6.0000830.

[100] Y. Zhong, 'Self-terminated etching of GaN with a high selectivity over AlGaN under inductively coupled Cl2/N2/O2 plasma with a low-energy ion bombardment', *Appl. Surf. Sci.*, p. 8, 2017.

[101] M. Grodzicki, P. Mazur, and A. Ciszewski, 'Changes of electronic properties of p-GaN(0 0 0 1) surface after low-energy N+-ion bombardment', *Appl. Surf. Sci.*, vol. 440, pp. 547–552, May 2018, doi: 10.1016/j.apsusc.2018.01.097.

[102] L. Vauche *et al.*, 'Study of an Al_2O_3/GaN Interface for Normally Off MOS-Channel High-Electron-Mobility Transistors Using XPS Characterization: The Impact of Wet Surface Treatment on Threshold Voltage V_{TH}', *ACS Appl. Electron. Mater.*, vol. 3, no. 3, pp. 1170–1177, Mar. 2021, doi: 10.1021/acsaelm.0c01023.

[103] S. J. Wilkins, T. Paskova, and A. Ivanisevic, 'Effect of etching with cysteamine assisted phosphoric acid on gallium nitride surface oxide formation', *J. Appl. Phys.*, vol. 114, no. 6, p. 064907, Aug. 2013, doi: 10.1063/1.4817899.

[104] M. Mishra *et al.*, 'Wet chemical etching induced stress relaxed nanostructures on polar

& non-polar epitaxial GaN films', *Phys. Chem. Chem. Phys.*, vol. 19, no. 13, pp. 8787–8801, Mar. 2017, doi: 10.1039/C7CP00380C.

[105] S. J. Wilkins, T. Paskova, C. L. Reynolds, and A. Ivanisevic, 'Comparison of the Stability of Functionalized GaN and GaP', *ChemPhysChem*, vol. 16, no. 8, pp. 1687–1694, 2015, doi: 10.1002/cphc.201500105.

[106] S.-C. Han *et al.*, 'Formation of Hexagonal Pyramids and Pits on V-/VI-Polar and III-/II-Polar GaN/ZnO Surfaces by Wet Etching', *J. Electrochem. Soc.*, vol. 157, no. 1, p. D60, 2010, doi: 10.1149/1.3253564.

[107] S. K. Hong, B. J. Kim, H. S. Park, Y. Park, S. Y. Yoon, and T. I. Kim, 'Evaluation of nanopipes in MOCVD grown (0001) GaN/Al2O3 by wet chemical etching', *J. Cryst. Growth*, vol. 191, no. 1–2, pp. 275–278, Jul. 1998, doi: 10.1016/S0022-0248(98)00366-2.

[108] V. Yon, N. Rochat, M. Charles, E. Nolot, and P. Gergaud, 'X-Ray Diffraction Microstrain Analysis for Extraction of Threading Dislocation Density of GaN Films Grown on Silicon, Sapphire, and SiC Substrates', *Phys. Status Solidi B*, vol. 257, no. 4, p. 1900579, 2020, doi: https://doi.org/10.1002/pssb.201900579.

[109] M. Reiner, M. Reiss, T. Brünig, L. Knuuttila, R. Pietschnig, and C. Ostermaier, 'Chemical understanding and utility of H3PO4 etching of group-III- nitrides', *Phys. Status Solidi B*, vol. 252, no. 5, pp. 1121–1126, 2015, doi: https://doi.org/10.1002/pssb.201451504.

[110] M. Tautz and D. Díaz Díaz, 'Wet-Chemical Etching of GaN: Underlying Mechanism of a Key Step in Blue and White LED Production', *ChemistrySelect*, vol. 3, no. 5, pp. 1480–1494, 2018, doi: https://doi.org/10.1002/slct.201702267.

[111] M. A. Mahjoub *et al.*, 'Impact of wet treatments on the electrical performance of Ge0.9Sn0.1 based p-MOS capacitors', p. 27.

[112] T. Mattila and R. M. Nieminen, '*Ab initio* study of oxygen point defects in GaAs, GaN, and AlN', *Phys. Rev. B*, vol. 54, no. 23, pp. 16676–16682, Dec. 1996, doi: 10.1103/PhysRevB.54.16676.

Appendix

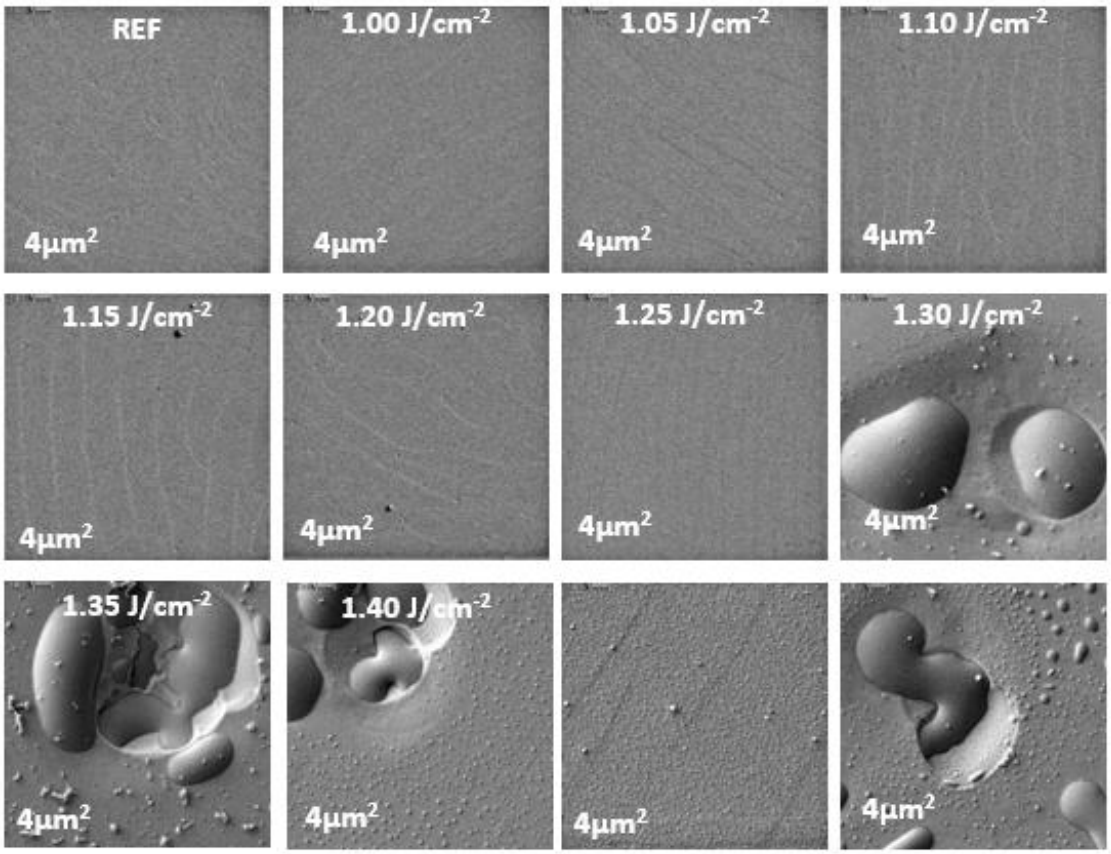

A- 1 SEM images of as-grown GaN before and after a single LASER shot of at different energies from 1.0 to 1.5 J.cm^{-2}. REF stands for the surface prior to LASER anneal

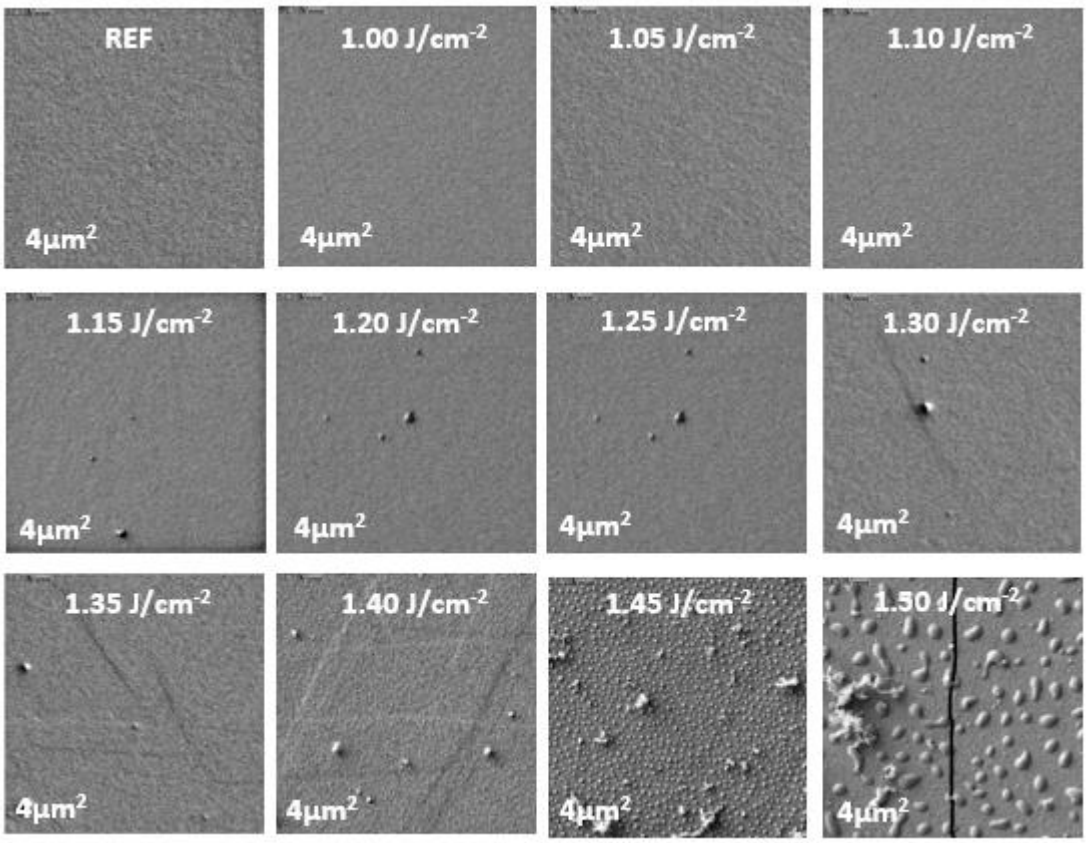

A- 2 SEM images of dry-etched GaN before and after a single LASER shot of at different energies from 1.0 to 1.5 $J.cm^{-2}$. REF stands for the surface prior to LASER anneal